



Western Washington University  
Western CEDAR

---

WWU Graduate School Collection

WWU Graduate and Undergraduate Scholarship

---

Fall 2021

## Structural and Mutational Characterization of the Blood Coagulation Factor VIII C Domain Lipid Binding Interface

Shaun C. Peters

Western Washington University, shaunpeters8080@gmail.com

Follow this and additional works at: <https://cedar.wwu.edu/wwuet>

 Part of the [Chemistry Commons](#)

---

### Recommended Citation

Peters, Shaun C., "Structural and Mutational Characterization of the Blood Coagulation Factor VIII C Domain Lipid Binding Interface" (2021). *WWU Graduate School Collection*. 1068.  
<https://cedar.wwu.edu/wwuet/1068>

This Masters Thesis is brought to you for free and open access by the WWU Graduate and Undergraduate Scholarship at Western CEDAR. It has been accepted for inclusion in WWU Graduate School Collection by an authorized administrator of Western CEDAR. For more information, please contact [westerncedar@wwu.edu](mailto:westerncedar@wwu.edu).

**Structural and Mutational Characterization of the Blood Coagulation Factor VIII C  
Domain Lipid Binding Interface**

By

Shaun C. Peters

Accepted in Partial Completion  
of the Requirements for the Degree  
Master of Science

ADVISORY COMMITTEE

Chair, Dr. P. Clint Spiegel

Dr. Jeanine Amacher

Dr. John Antos

GRADUATE SCHOOL

David L. Patrick, Dean

## **Master's Thesis**

In presenting this thesis in partial fulfillment of the requirements for a master's degree at Western Washington University, I grant to Western Washington University the non-exclusive royalty-free right to archive, reproduce, distribute, and display the thesis in any and all forms, including electronic format, via any digital library mechanisms maintained by WWU.

I represent and warrant this is my original work and does not infringe or violate any rights of others. I warrant that I have obtained written permissions from the owner of any third party copyrighted material included in these files.

I acknowledge that I retain ownership rights to the copyright of this work, including but not limited to the right to use all or part of this work in future works, such as articles or books.

Library users are granted permission for individual, research and non-commercial reproduction of this work for educational purposes only. Any further digital posting of this document requires specific permission from the author.

Any copying or publication of this thesis for commercial purposes, or for financial gain, is not allowed without my written permission.

Signature: *Shaun C. Peters*

Date: 11/24/2021

**Structural and Mutational Characterization of the Blood Coagulation Factor VIII C  
Domain Lipid Binding Interface**

A Thesis  
Presented to  
The Faculty of  
Western Washington University

In Partial Fulfillment  
Of the Requirements for the Degree  
Master of Science

By  
Shaun C. Peters  
November 2021

## Abstract

---

Blood coagulation factor VIII (fVIII) functions as a cofactor in the blood coagulation cascade for proteolytic activation of factor X by factor IXa. During coagulation, fVIII is activated and subsequently binds to activated platelet surfaces by coordination of the fVIII C1 and C2 domains to the exposed phosphatidylserine of activated platelet membranes. Structural and mutational studies have suggested that both hydrophobic and electrostatic interactions occur between the two tandem C domains and activated lipid surfaces, but models of C domain phospholipid binding propose conflicting regions that directly interact with the membrane surface.

This thesis reports the determination of the molecular structure of an isolated fVIII porcine C2 domain in the presence of the phosphatidylserine headgroup (OPLS) at 1.3 Å. The OPLS molecule makes direct contact with Q2213, N2217, S2289, and R2320. This structure represents the first deposited structure of fVIII C domains in the presence of a lipid headgroup moiety. Furthermore, phospholipid binding characteristics of basic residues within the proposed phospholipid binding regions were investigated by mutagenesis. Specifically, mutations at R2163, R2320, and a double mutant of R2163/R2320 caused almost complete abrogation of lipid binding to soluble lipid nanodiscs. Using these findings, an updated model of fVIII lipid binding is proposed using structural information from C2 domain inhibitors, previous literature, and newly defined interactions between C2 and OPLS. Together, this study proposes that R2163 and R2320 are the center of a conserved phospholipid binding motif that extends across homologous blood clotting proteins.

## Acknowledgements

---

The work described here was accomplished in the Spiegel lab at Western Washington University from the spring of 2017 to the fall of 2021. I extend my appreciation and thanks to Dr. P. Clint Spiegel for the opportunity to join his research lab as a sophomore in Biological Anthropology, allowing me to continue my studies in a master's program, and providing an academic bridge for me to pursue research in. I additionally wish to thank previous graduate students Ian Smith, Serena Wo, Joseph Gish, and Chris Swanson for the mentorship they provided throughout my undergraduate studies as well as A.P Wang and Micah Nakao for emotional and mental support during graduate studies within the Spiegel lab.

I owe a great deal of gratitude to former and present lab members of the Spiegel lab. Specifically, Junior Reese and Cris Mitchel helped provide the initial groundwork for the C1C2 domain aspect of this project and helped perform the sedimentation assays. I sincerely thank Corbin Mitchell for working side by side to troubleshoot hybridoma and mutant expression and Dr. Kenneth Childers, who was a pivotal influence and mentor within the lab during my graduate school studies. I honestly could not have accomplished this work without the support I received. I would also like to thank my committee members, Dr. P. Clint Spiegel, Dr. Jeanine Amacher, and Dr. John Antos for their thoughtful and supportive advice in preparation of this thesis.

Finally, I extend my utmost appreciation to Amanda Rennie for her motivation, sacrifice, and support during my graduate studies.

## Table of Contents

Abstract.....	iv
Acknowledgements.....	v
List of Figures.....	vii
List of Tables.....	ix
Abbreviations.....	x
Introduction.....	1
Chapter 1.....	2
Chapter 2.....	27
Chapter 3.....	37
Chapter 4.....	57
Works Cited.....	68
Appendix.....	75

## List of Figures

Figure 1. TEM image of a platelet .....	2
Figure 2. Activated platelet morphology .....	3
Figure 3. Activated membrane phospholipid composition .....	4
Figure 4. Extrinsic blood coagulation cascade .....	7
Figure 5. Intrinsic blood coagulation cascade.....	8
Figure 6. Molecular details of fVIII.....	9
Figure 7. Flexibility of the fVIII C2 domain .....	11
Figure 8. C domain homology modeling .....	12
Figure 9. Structure of ET3i .....	16
Figure 10. Anti-C2 domain inhibitors.....	18
Figure 11. Initial activated platelet binding model .....	20
Figure 12. Anti-C2 domain PS binding ELISA .....	21
Figure 13. Current activated platelet binding model .....	23
Figure 14. C2 domain sequence and structure homology .....	26
Figure 15. Functionality of SHuffle cells .....	29
Figure 16. Purification of fVIII C domain constructs.....	38
Figure 17. FPLC secondary removal of contaminants.....	39
Figure 18. Enterokinase cleavage and purification.....	40
Figure 19. Visual change in antibody expression .....	41

Figure 20. Hybridoma cells and Protein G purification.....	42
Figure 21. Phospholipid ELISA experiments of C domain constructs.....	43
Figure 22. Wild-type C domain sedimentation assays.....	44
Figure 23. Sedimentation assay of C domains bound to inhibitors .....	45
Figure 24. C2 domain mutational sedimentation assays.....	46
Figure 25. MSP1D1 protein to lipid molar ratio optimizations .....	47
Figure 26. MSP1D1 lipid composition optimizations .....	48
Figure 27. Binding verification of cleaved nanodiscs to ET3i .....	49
Figure 28. BLI measurement of C1C2 constructs to cleaved nanodiscs .....	51
Figure 29. Porcine C2:OPLS crystal structure.....	54
Figure 30. Flexibility of hydrophobic loops in the porcine C2:OPLS structure.....	55
Figure 31. OPLS density and molecular contacts.....	56
Figure 32. Current model of activated platelet binding .....	58
Figure 33. ELISA of WT C2 and R2320S phospholipid binding.....	59
Figure 34. Planar modeling of C2 domain conformations.....	63
Figure 35. Structural modeling of fVIII bound to C2 inhibitor .....	64
Figure 36. C2 mutational modeling within the planer phospholipid model .....	65
Figure 37. fIX epitope mapping on planar fVIII phospholipid model.....	67

## List of Tables

Table 1. Nomenclature of blood clotting factors .....	5
Table 2. Characterization of hemophilia A severity .....	13
Table 3. Protein expression yield for C domain constructs .....	37
Table 4. Binding kinetics of E3ti to MSP1D1 samples .....	47
Table 5. Binding kinetics of nanodiscs lipid composition experiments .....	48
Table 6. Apparent affinities of C1C2 constructs to nanodiscs.....	50
Table 7. X-ray data collection and model refinement statistics.....	53

## List of Abbreviations

<b>ABTS</b>	2,2'-Azinobis (3-ethylbenzthiazoline-6-sulfonic acid)
<b>AMC</b>	Anti-mouse antibody capture biosensors
<b>a1, a2, a3</b>	Acidic regions of the blood coagulation factor A domains
<b>BCC</b>	Blood coagulation cascade
<b>BDD-fVIII</b>	B domain deleted blood coagulation factor VIII
<b>BME</b>	$\beta$ -mercaptoethanol
<b>BSA</b>	Bovine serum albumin
<b>BU</b>	Bethesda unit
<b>CDR</b>	Complementarity determining regions
<b>cND</b>	Cleaved nanodiscs
<b>C1</b>	First carboxy-terminal domain of fVIII
<b>C2</b>	Second carboxy-terminal domain of fVIII
<b>DMSO</b>	Dimethyl sulfoxide
<b>DOPC</b>	1,2- dioleoyl-sn-glycero-3-phosphocholine
<b>DOPS</b>	1,2-dioleoyl-sn-glycero-3-phospho-L-serine sodium salt
<b>F<sub>AB</sub></b>	Fragment of antigen binding
<b>FBS</b>	Fetal bovine serum
<b>fI</b>	Fibrinogen
<b>fIa</b>	Fibrin
<b>fII</b>	Prothrombin
<b>fIIa</b>	Thrombin
<b>FPLC</b>	Fast protein liquid chromatography
<b>FRET</b>	Fluorescent resonance energy transfer
<b>fV</b>	Blood coagulation factor V

<b>fVa</b>	Activated blood coagulation factor V
<b>fVII</b>	Blood coagulation factor VII
<b>fVIII</b>	Blood coagulation factor VIII
<b>fVIIIa</b>	Activated blood coagulation factor VIII
<b>fXa</b>	Activated blood coagulation factor X
<b>fXIIa</b>	Hageman factor
<b>HA</b>	Hemophilia A
<b>hC1</b>	Human first carboxy-terminal domain of fVIII
<b>hC2</b>	Human second carboxy-terminal domain of fVIII
<b>HEPES</b>	N-(2-Hydroxyethyl) piperazine-N'-2-ethanesulfonic Acid
<b>IgSF</b>	Immunoglobulin super family
<b>IMAC</b>	Immobilized metal affinity chromatography
<b>IPTG</b>	Isopropyl B-D-thiogalactopyranoside
<b>ITI</b>	Immune tolerance induction
<b>K<sub>d</sub></b>	Equilibrium dissociation constant
<b>LB</b>	Lysogeny Broth
<b>LB<sub>50</sub></b>	Lysogeny Broth supplemented with Ampicillin
<b>mAb</b>	Monoclonal antibody
<b>MedE</b>	Hybridoma Medium E
<b>MES</b>	2-(N-morpholino) ethane sulfonic acid
<b>ND</b>	Nanodiscs
<b>OPDS</b>	O-phospho-D-serine
<b>OPLS</b>	O-phospho-L-serine
<b>PC</b>	Phosphatidylcholine
<b>PE</b>	Phosphatidylethanolamine

<b>pI</b>	Isoelectric point
<b>PMSF</b>	Phenylmethanesulphonyl fluoride
<b>PS</b>	Phosphatidylserine
<b>pC2</b>	Porcine second carboxy-terminal domain of fVIII
<b>rEK</b>	Recombinant enterokinase
<b>rfVIIa</b>	Recombinant activated blood coagulation factor VII
<b>rfVIII</b>	Recombinant blood coagulation factor VIII
<b>S column</b>	Strong ion-exchange chromatography column
<b>TF</b>	Tissue factor
<b>UV's</b>	Unilamellar vesicles
<b>VWD</b>	von Willebrand disease
<b>vWF</b>	Von Willebrand factor
<b>Xase</b>	Tenase complex

## Introduction

Hemostasis is a multi-faceted, essential process that prevents extended bleeding episodes during vascular injury through formation of stable blood clots. The processes that encompass blood clot formation are intricate, positive-feedback loops comprised of protein complexes formed between serine proteases and subsequent cofactors. These complexes are essential to hemostasis, as dysregulation or mutations to the blood factors complexes leads to bleeding disorders. Our area of interest stems from the bleeding disorder hemophilia A, which is caused by deficient or absent blood coagulation factor VIII within the circulatory system. During vascular injury, fVIII functions in the secondary arm of the coagulation cascade, binding in tandem with blood coagulation factor IX to activated platelet surfaces to amplify the production of terminal blood coagulation thrombin. The activity of fVIII is dependent on its ability to bind to activated platelet surfaces in which binding occurs through two carboxy-terminal (C) domains. Mutations to fVIII C domains have been shown to prevent fVIII activity in hemophilia A patients, which can potentially result in life-threatening bleeding. Although studies have demonstrated that the main interactions of fVIII to phospholipids are centered on the C domains, the molecular basis of the interactions is still debated. The putative binding interactions consist of hydrophobic contacts between C2 and the anhydrous tails of lipid molecules and charge-charge interactions between basic residues grouped within the C domains to acidic phospholipid head groups present on activated membrane surfaces. We investigated the specific association of both C domains to activated platelet-mimicking surfaces to explain the components of fVIII phospholipid binding and inform the role of mutations in causing hemophilia A.

## Chapter 1: Hemostasis and FVIII

### Introduction to the Hemostasis

Hemostasis is a highly regulated and localized physiological process that seals vascular injuries while maintaining normal blood flow within the circulatory system. This physiological process relies on the interplay between smooth muscles, platelets, blood clotting proteins, and feedback loops to control hemorrhages.<sup>2</sup> During a normal hemostatic response, three major events occur in the formation of a blood clot: vasoconstriction, primary hemostasis, and secondary hemostasis.<sup>2</sup> Vasoconstriction, or otherwise known as vascular spasm, is an autonomic reflex occurring immediately after vascular injury to minimize blood loss at the site of injury.<sup>3</sup> This constriction of the blood vessel reduces the diameter and exposes collagen fibers from the underlying connective tissue to initiate primary hemostasis.<sup>2</sup>

### Primary Hemostasis (platelet plug formation)

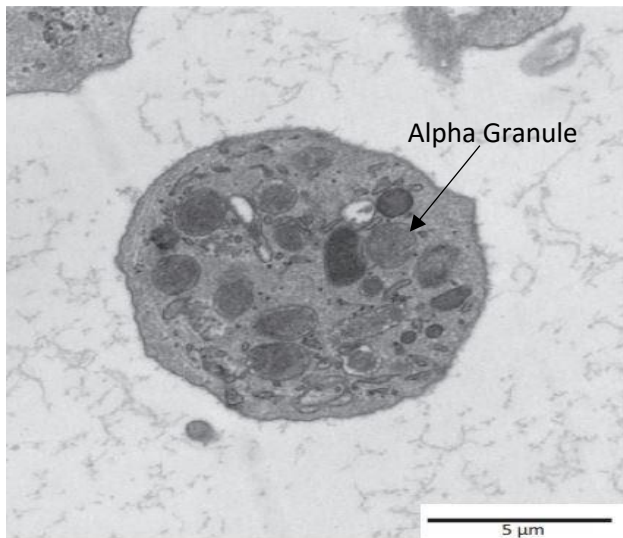


**Figure 1.** Transmission electron microscopy image of a non-activated platelet containing alpha granules (arrow).<sup>81</sup>

Primary hemostasis involves the localized activation and aggregation of platelets at the site of injury.<sup>4</sup> Platelets are small non-nuclear cell fragments produced from megakaryocytes found in bone marrow.<sup>5</sup> Platelets contain two distinct types of granular bodies, alpha and dense, which release their contents during platelet activation. Alpha granules (Figure 1) contain numerous clotting factors such as fVIII,

factor V (fV), and von Willebrand factor (vWF), which function throughout the secondary stage of hemostasis.<sup>5</sup> Dense granules contain smaller signaling molecules and hormones including histamine, calcium, and epinephrine which attract immune cells for protection from foreign particles. In healthy blood vessels, circulating platelets do not adhere to the surface or self-aggregate due to antithrombotic factors that line blood vessels.<sup>4</sup> But, upon vascular injury, the exposed sub-endothelial collagen acts as a scaffold for platelet adhesion.<sup>6</sup>

The adhesion process is mediated by numerous receptors on platelet surfaces, notably GPIb-IX-V, which binds to vWF.<sup>4</sup> vWF is a large multimeric glycoprotein composed of three A domains, three B domains, two C domains, and four D domains that circulates in plasma, resides in the sub-endothelial layer, and is released from platelets during activation.<sup>7</sup> During hemostasis, the A3 domain of vWF associates to the exposed collagen from the interstitial fluid.<sup>8</sup> Concurrently, binding of the vWF A3 domain to collagen spatially orients the vWF A1 domain near GPIb-IX-V receptors on platelets.<sup>4,8</sup> Once adhered to the site of vascular injury, the platelet undergoes a morphological change and releases the contents of the granules into the surrounding vessel in a process called activation (Figure 2).<sup>6</sup> During this activation, platelets become irregular in shape, promoting platelet-platelet interactions through self-aggregation.<sup>9</sup> In addition to macroscopic changes in platelet morphology, the membrane composition of platelet surfaces undergoes a

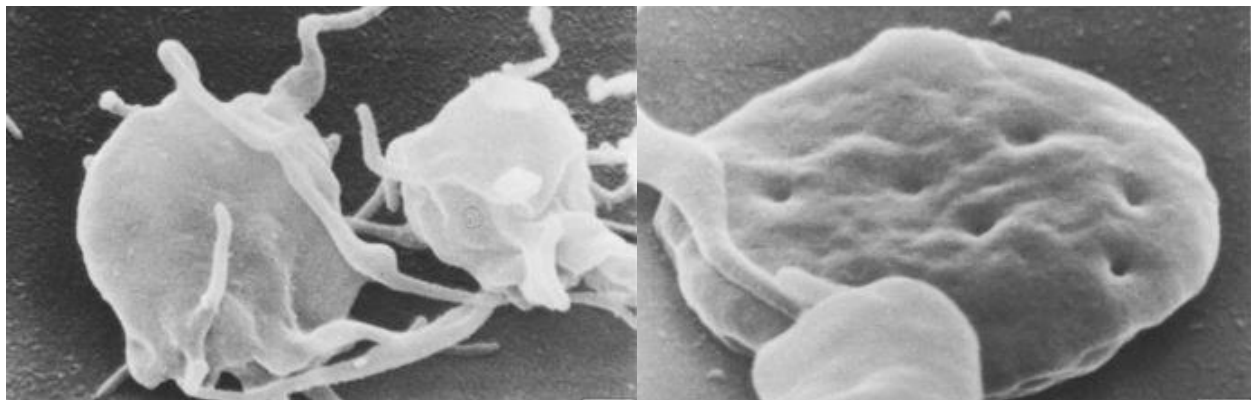


**Figure 2.** Morphological change of activated (left) and unactivated (right) platelets.<sup>9</sup>

procoagulant change due to redistribution of negatively charged phosphatidylserine (PS) and phosphatidylethanolamine (PE) to the membrane surface (Figure 3).<sup>6</sup> An enzyme, scramblase, nonspecifically flips the negatively charged PS or PE residing in the cytosolic side of platelet membranes with positively charged phosphatidylcholine (PC) on the extracellular side.<sup>6,10</sup> Activated platelets contain approximately 5-fold higher PS composition compared to circulating platelets. The increase of negatively charged phospholipid headgroups on the outside of platelets provides a surface for released coagulation factors to bind during secondary hemostasis and stabilize the initial platelet plug.

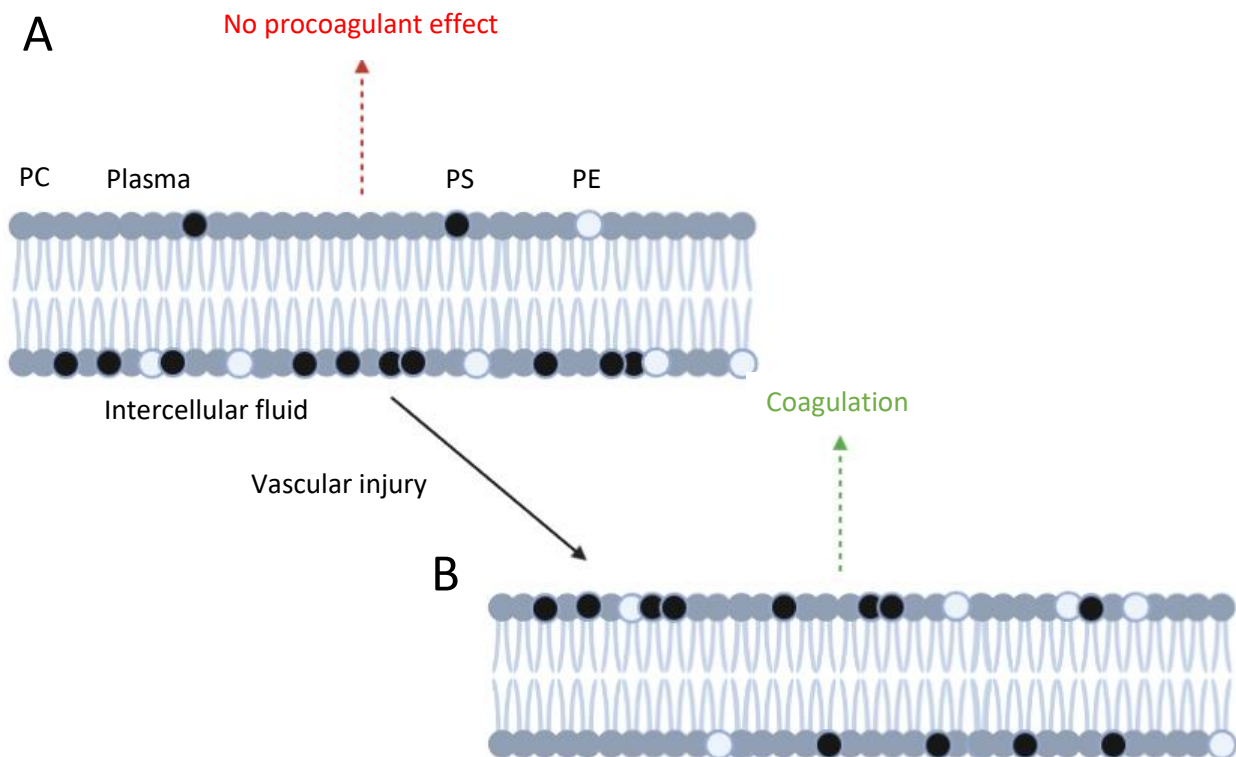


**Figure 3.** A. Typical membrane composition of non-activated platelets with PS and PE concentrated in the inner leaflet. B. Extracellular leaflet redistribution post-vascular injury. Scramblase, activated by influx of calcium, nonspecifically switches PC lipid heads with PS or PE. Adapted from Lhermusier et al.<sup>82</sup>

## Secondary Hemostasis (thrombin generation)

After formation of the initial unstable clot, the secondary pathway of hemostasis begins, involving a cascade of proteolytically activated clotting factors to produce a stable fibrin clot (Table 1). Secondary hemostasis is generally referred to as the Blood Coagulation Cascade (BCC) and functions in two separate, yet intimately connected, pathways: the extrinsic and intrinsic pathways.

**Table 1.** Nomenclature of Pertinent Coagulation factors involved in the BCC.<sup>5</sup>

<b>Clotting factor Abbreviation</b>	<b>Clotting Factor Name</b>	<b>Function</b>
I	Fibrinogen	Stable clot formation
II	Prothrombin	Activation of I, V, VII, VIII, XI, XIII, and platelets
TF (III)	Tissue Factor	Co-factor to VIIa
V	Proaccelerin	Cofactor to Xa
VII	Proconvertin	Activates IX, X
VIII	Antihaemophilic factor A	Cofactor to IXa
IX	Antihaemophilic factor B	Activates X, forms X-ase complex with VIIIa
X	Stuart-Prower factor	Activates II, forms prothrombinase complex with Va
XI	Plasma Thromboplastin antecedent	Activates IX
XII	Hageman factor	Activates XI, VII
XIII	Fibrin-stabilizing factor	Cross-links fibrin

## Extrinsic Pathway

The extrinsic pathway is initiated immediately upon blood vessel damage (Figure 4). Along with collagen, tissue factor (TF), an integral membrane protein, is exposed to the plasma at the site of injury and acts as a cofactor to factor VII (fVII), promoting activation of fVII and formation of the extrinsic tenase (Xase) complex (TF:FVIIa).<sup>11</sup> Formation of the extrinsic Xase complex catalyzes the generation of fXa which associates with cofactor fVa to negatively charged platelet surfaces.<sup>1</sup> The complex of fXa:fVa:PS:Ca<sup>2+</sup> forms the prothrombinase complex and catalyzes the cleavage of prothrombin (fII) to thrombin (fIIa). Thrombin, as the terminal coagulation factor, catalyzes the formation of fibrin (Ia) from fibrinogen (I). Thrombin additionally catalyzes the activation of transglutaminase fXIII to form cross-linked fibrin, yielding an elastic and stable clot.<sup>1</sup> The generation of a cross-linked fibrin clot through the prothrombinase complex is called the “common pathway”. Although the extrinsic pathway forms a stable clot, the rate of blood clot formation is low and insufficient to effectively stop hemorrhage. The intrinsic pathway, however, is a positive feedback loop initiated by thrombin, the extrinsic pathway, and collagen to amplify the level of activated coagulation factors, setting the stage for large scale thrombin production.<sup>5</sup>

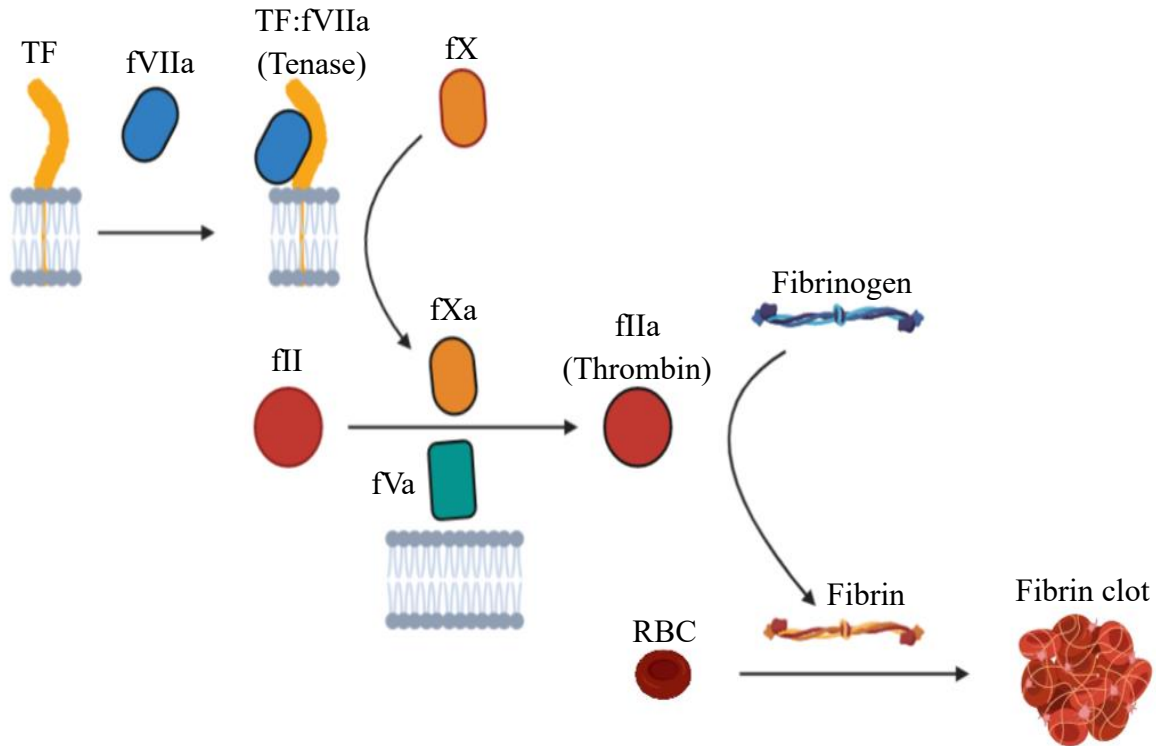


**Figure 4.** Extrinsic arm of the blood coagulation cascade. Tissue factor (TF) is exposed to the interstitial fluid prior to vessel hemorrhage. Upon hemorrhage, TF is exposed to fVIIa containing plasma and activates small amounts of fX by forming the extrinsic tenase complex (fXa:fVa:PS:Ca<sup>2+</sup>). This generation of fXa allows coordination with fVa to form the prothrombinase complex, producing a small influx of thrombin for use in the second arm of secondary hemostasis.

### **Intrinsic Pathway (amplification of thrombin generation).**

The intrinsic pathway is activated by two separate proteins. The first is collagen, which activates Hageman factor (fXIIa).<sup>1</sup> FXIIa proteolytically activates fXI, which can also be activated by thrombin.<sup>11</sup> Following activation, fXIa converts fIX to fIXa. The second protein, Thrombin (IIa), also proteolytically activates fVIII (fVIIIa) and causes fVIIIa dissociation from its carrier protein, vWF.<sup>12</sup> FVIIIa binds to activated platelets, functioning as a cofactor for fIXa and together form the intrinsic Xase complex.<sup>1</sup> Subsequently, the Xase complex activates fX (fXa) and the association of fXa to fVa on platelet surfaces forms the prothrombinase complex, producing large-

scale thrombin generation through the common pathway. The initial formation of thrombin from the extrinsic pathway becomes amplified by the intrinsic pathway, increasing the downstream generation of insoluble fibrin and stable blood clots.<sup>1</sup> Dysregulation of the intrinsic arm of the pathway is associated with numerous blood clotting deficiencies; namely hemophilia A (fVIII), hemophilia B (fIX), Hemophilia C (fXI), and factor X deficiency. Specifically, fIXa in the absence of fVIII has a catalytic efficiency 200,000-fold lower than in the presence of fVIII and hinders the functionality of the intrinsic arm of the cascade. It is for this reason that fVIII is of principle concern within this study.

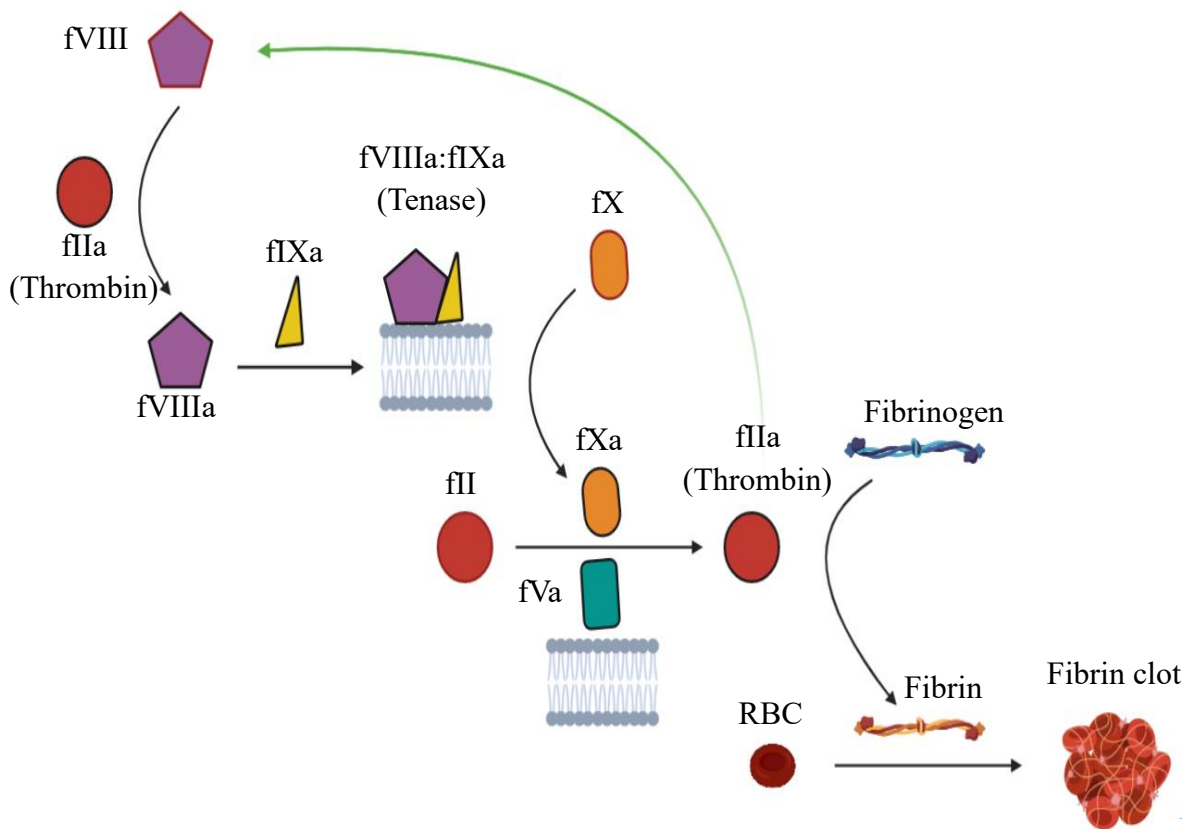


**Figure 5.** Intrinsic (amplification) arm of the blood coagulation cascade. Thrombin generated in the extrinsic arm activates fVIII. Dissociation of fVIII from vWF allows interaction with fIXa on activated platelet surfaces. Formation of fVIIIa:fIXa:Ca<sup>2+</sup>:PS (intrinsic tenase complex) generates large scale thrombin product, which in a positive feedback loop, functions to generate a cascade of fVIIIa. This positive feedback loop is inactivated by active protein C when hemostasis is reached.<sup>83</sup>

## Factor VIII and Hemophilia A

Blood coagulation factor VIII (fVIII) is a 2,332 residue glycoprotein secreted from endothelial cells and activated platelets, functioning as an essential cofactor in the intrinsic aspect of the blood coagulation cascade.<sup>13,14</sup> Factor VIII is synthesized with the domain structure A1-a1-A2-a2-B-a3-A3-C1-C2 with each A domain containing a highly acid region (a1, a2, and a3) heavily clustered with aspartate and glutamate residues (Figure 6).<sup>14</sup> The three A domains of fVIII retain 40% sequence similarity to one another and have sequence homology to both factor V (fV) and the copper binding protein, ceruloplasmin.<sup>14,15</sup> Between differing species, the B domain has high sequence divergence and offers little physiological benefit, as removing the B domain retains procoagulant activity.<sup>16</sup> Initial processing of fVIII cleaves away approximately 300 residues of the B domain, generating a heterodimer that circulates bound with its carrier protein, vWF.<sup>17</sup>

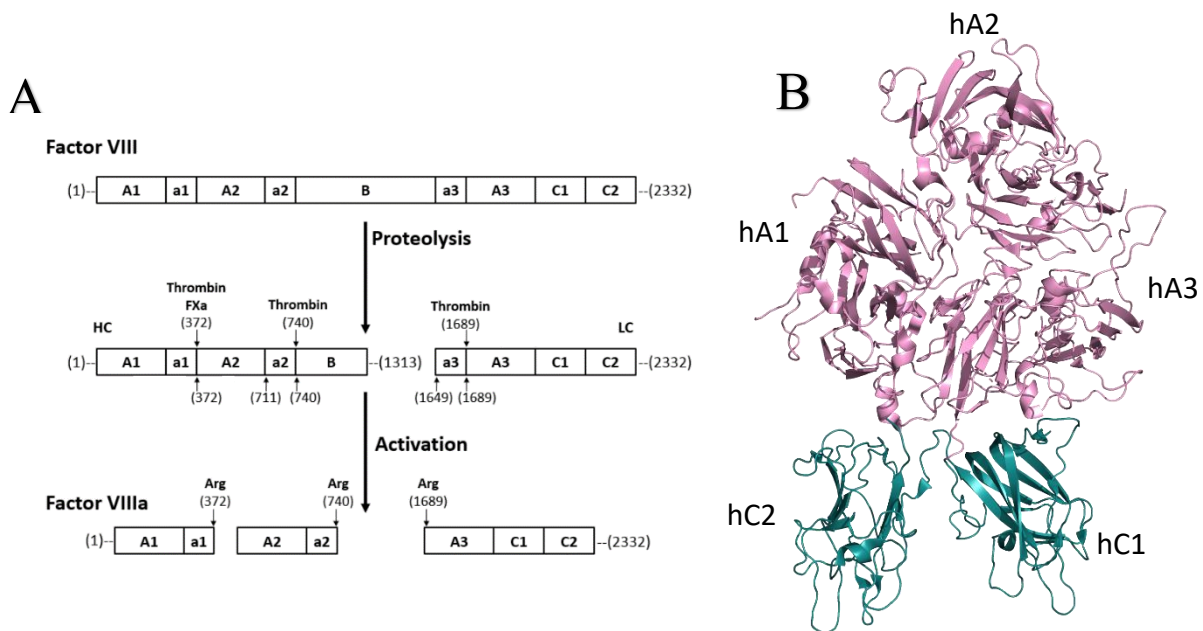


**Figure 6.** Molecular details of fVIII. A) Activation schematic of fVIII. Thrombin activates fVIII by cleaving between A1-A2, A2-B, and A2-A3 domains, generating heterotrimeric fVIIIa at highly acidic regions (denoted a1, a2, a3). Schema is modified from Mazurkiewicz-Pisarek et al 2016. B) Current human model of fVIII at 3.7 Å. The three A domains are clustered above the two platelet binding C domains. Derived from PDB: 6MF2.

Heterodimeric fVIII consists of a heavy chain (A1-a1-A2-a2-B) with differing lengths of the B domain due to limited proteolysis, and a light chain (A3-a3-C1-C2) containing the phospholipid binding region.<sup>15</sup> VWF interacts with the fVIII light chain to protect fVIII from premature inactivation during normal hemostasis, but the exact binding interaction between fVIII and VWF is not completely understood.<sup>18</sup> During vascular injury, thrombin proteolytically activates fVIII by cleaving fVIII at residues R372 (A1-A2), R740 (A2-B), and R1689 (A3 N-terminal).<sup>19</sup> Thrombin activation cleaves away the remaining segment of the B domain, separates the A1 and A2 domains, and removes the acidic region from the A3 domain.<sup>15</sup> Post-activation, fVIIIa is released from vWF as a heterotrimer of A1/A2/A3-C1-C2 and binds to activated platelet surfaces with fIXa to form the intrinsic Xase complex.<sup>20</sup>

An X-ray crystallographic structure of B domain-deleted recombinant fVIII was first reported in 2008 at a resolution of 3.7 Å.<sup>14</sup> The structure of fVIII highlighted slight differences between the fluidity of the two C domains. The C2 domain loosely packs to the C1 and A3 domains, maintaining a 400 Å<sup>2</sup> and 200 Å<sup>2</sup> hydrophobic interface, respectively, between the domains.<sup>14</sup> In contrast, the C1 domain is tightly associated with the A3 domain, creating a 1200 Å<sup>2</sup> hydrophobic interface.<sup>14</sup> This inherent flexibility of the C2 domain was suggested to play a role in platelet association. In 2020, the high-resolution structure of a fVIII gene therapeutic candidate ET3i was crystallized with two molecules of ET3i in the same space group, allowing comparative analysis between local conformational changes. Specifically, the fVIII C2 domains in each of the models were in different conformations. Model A adopted a conformation previously described in literature whereas model B underwent a central axis rotation of ~35-45 degrees in relation to previously described structures (Figure 7).

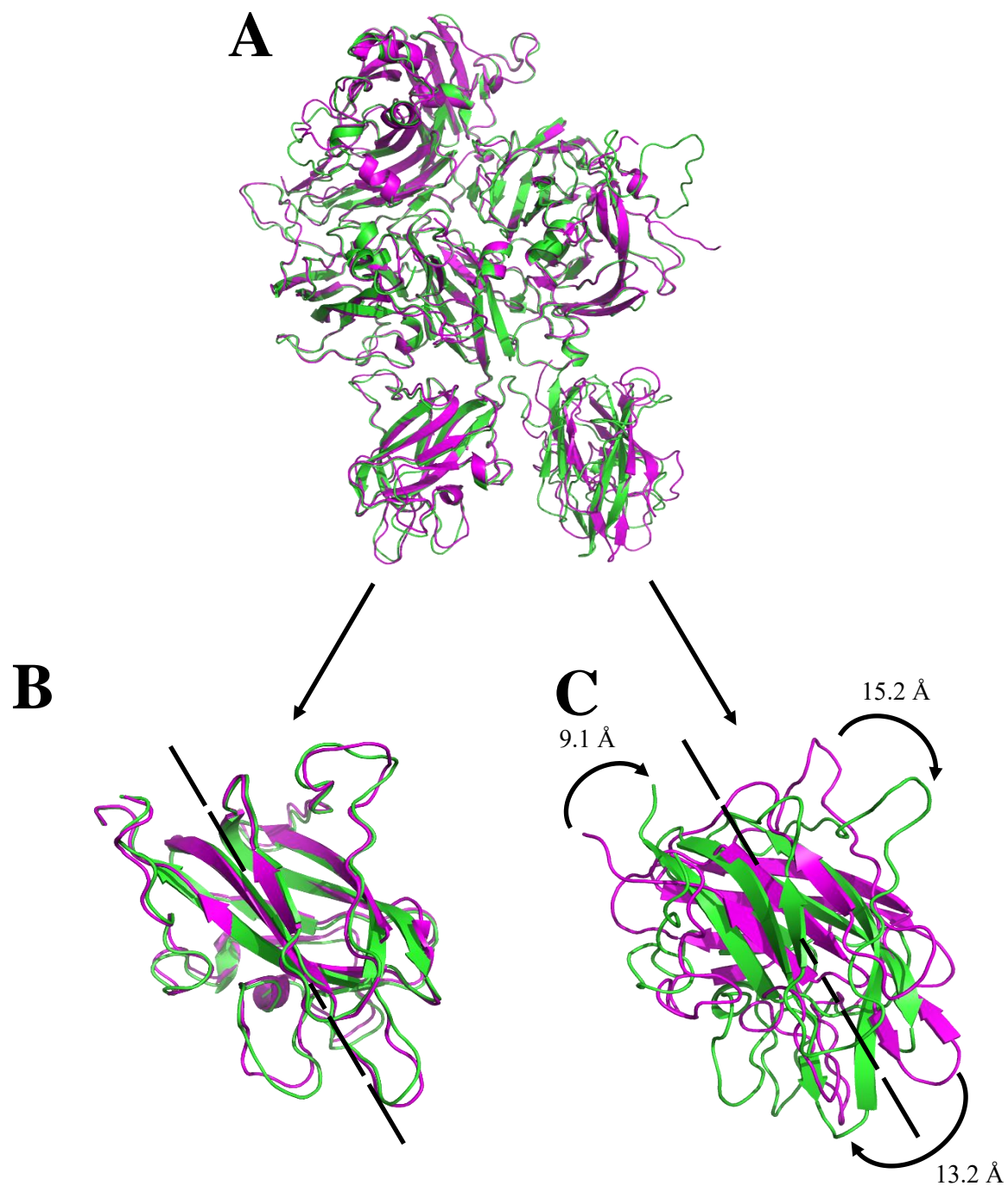


**Figure 7.** Flexibility of the fVIII C2 domain. A.) fVIII gene therapeutic candidate ET3i model A (green) aligned with ET3ia model B (purple). B.) Alignment of ET3i model A and B C1 domain. Black line represents a central axis orientation. C.) C2 domain alignment of ET3i model A and B. Model B adopts a unique conformation previously not published in literature. The entire C2 domain rotates about the central axis, causing the hydrophobic loops to swing and rotate away from the C1 domain.

This flexibility of the C2 domain compared to the C1 domain, presumably due to the differences in hydrophobic contacts with the A domains, may allow two distinct motifs of fVIII, one upon which platelet binding occurs and the other where the fVIII C2 domain is rotated away during binding to vWF. Structural analysis of fVIII bound to lipids would provide insight into the

C2 domain ligand bound conformational state compared to known native conditions.

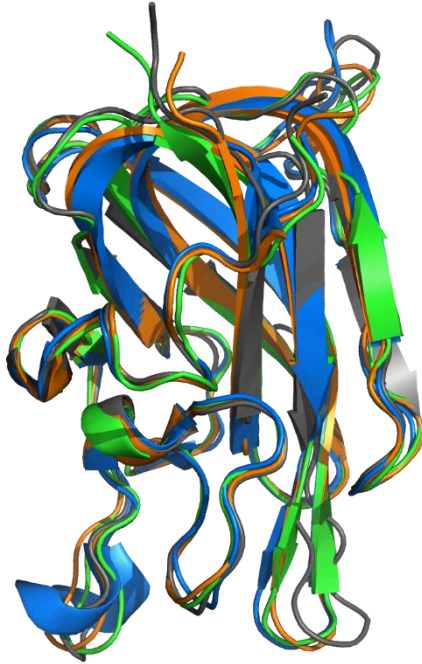


**Figure 8.** Structural alignment of C2 domains from various C domain containing molecules. Lactadherin (PDB: 3BN6, blue), factor V (PDB: 1CZS, cyan), human fVIII (PDB: 6MF2, red), porcine fVIII (PDB: 4MO3, orange).

The C domains of fVIII are contiguous across other clotting factors, originate from the discoidin class of lectins, and share unique properties that facilitate binding to phospholipid surfaces. The two fVIII C domains are structurally homologous to one another and contain two beta hairpin loops that extend beyond the overall globular fold.<sup>14</sup> High resolution structures of the C2 domain from fVIII and fV demonstrate high structural homology with

common features such as the two hydrophobic protrusions on the bottom portion of the protein domain (Figure 8).<sup>21</sup> The affinity of recombinant C2 to phospholipids is 5-100 fold lower than fVIII, suggesting that both C domains must be present for optimal binding.

Disruption of functional fVIII is essential for effective clotting as absence of or mutations to fVIII can lead to the development of the bleeding disorder, hemophilia A.

## Hemophilia A

Hemophilia A is a recessive, X-linked bleeding disorder resulting from mutations to the F8 gene in which hemostasis is interrupted due to deficient or inactive fVIII. Approximately 1 in 5,000 males worldwide are affected by these gene mutations and one third of hemophiliacs are the result of spontaneous mutation with no prior family history.<sup>22,23</sup> Individuals with hemophilia A are unable to form effective blood clots, causing extended or spontaneous bleeding episodes (Table 2).<sup>23</sup> Severity of Hemophilia A is characterized as severe (<1% of normal fVIII activity), moderate (1-5% of normal fVIII activity), and mild (5-40% of normal fVIII activity).<sup>23</sup>

Treatment for hemophilia A includes prophylaxis: injections of fVIII concentrates to prevent anticipated bleeding episodes.<sup>23</sup> Although the available treatment is generally successful, previously untreated patients are vulnerable to developing inhibitors to fVIII therapy and approximately 30% of severe hemophiliacs develop an inhibitory response to treatment.<sup>22,24</sup> Development of inhibitory antibodies (inhibitors) can reduce treatment efficacy, increase bleeding episodes, and increase hemophilia severity.<sup>25,26</sup> Treatments for fVIII inhibitors includes non-replacement therapy or immune tolerance induction (ITI). Non-replacement therapy universally applies to either small molecule therapy or bypassing agents. Small molecule therapies utilize low

**Table 2.** Classification of bleeding phenotype with severity of hemophilia A.

<b>Severity</b>	<b>Factor VIII Level</b>	<b>Bleeding phenotype</b>
Mild	5-40 % of normal	Severe bleeding during surgery or traumatic incident
Moderate	1-5 % of normal	Occasional spontaneous bleeding, severe bleeding during surgery or traumatic incident
Severe	<1 % of normal	Spontaneous bleeding into muscle and joints, predominately in the absence of hemostatic challenge

molecular weight compounds that increase fVIII levels without offering fVIII replacement. One of these small molecule treatments, Desmopressin acetate (1-deamino-8-D-arginine vasopressin, DDAVP), is an analog of Vasopressin and is used to treat von Willebrand disease (VWD) or Hemophilia A.<sup>27</sup> Bypassing agents amplify the blood clotting cascade without utilizing fVIII. Addition of recombinant activated fVII (rfVIIa), activated prothrombin complex (FEIBA), or anti-tissue factor pathway inhibitor antibody (TFPI, Concizumab) increase clotting through amplification of the common or extrinsic pathway of blood coagulation.<sup>28-30</sup> One promising bypassing agent is an anti-fIX-fX bispecific antibody manufactured by Roche called Hemlibra. By binding both fIX and fX, Hemlibra replaces fVIII's coordinating role in the intrinsic tenase complex, allowing effective downstream thrombin production. One caveat to this treatment is the FDA has assigned a black box label, alluding to major risks associated with the drug. Whereas small molecule therapy and bypassing agents aim to promote hemostasis without fVIII, ITI involves overwhelming the immune system with large quantities of fVIII, eliminating the inhibitory response, and allowing resumption of fVIII replacement therapy.<sup>24</sup> Low-responding inhibitors can generally be overcome with small, increased doses of fVIII concentrates, but only 30% of inhibitor-possessing patients have low-responding inhibitors.<sup>25</sup> For the 70% of patients with high-responding inhibitors, treatments must utilize bypassing agents or ITI. Reversal of inhibitors by ITI permits the resumption of fVIII replacement therapy and is generally considered the best treatment option to date.<sup>24,31</sup> Although ITI is effective in reversing the immunological response to fVIII replacement therapy, the cost and quantity of fVIII required for treatment poses a substantial obstacle to most patients.<sup>22</sup>

One avenue for current fVIII therapeutics entails producing a more effective fVIII replacement product that minimizes immune response generated during replacement therapy and the financial

burden of replacement therapy. The financial burden stems from shortage of fVIII concentrates due to low fVIII *in vitro* and *in vivo* expression.<sup>32</sup> *In vitro* expression of fVIII occurs by cloning the fVIII gene into eukaryotic cells, producing recombinant fVIII (rfVIII). Many of these rfVIII product are expressed and recovered at low yields, however, and have ignited significant research efforts into increased fVIII expression and half-life.<sup>32</sup> Research from the Loller lab in 2002 compared the expression of human rfVIII (rh-fVIII) to porcine (pig) rfVIII (rp-fVIII).<sup>32</sup> Rp-fVIII expressed 10- to 14-fold higher than rh-fVIII. One next-generation therapeutic approach that could become more effective than replacement therapy is gene therapy, which involves correcting the defective or absent gene within the affected patients' cells. Gene therapy would prevent the weekly injections patients incur with replacement therapy and minimize cost but may still cause an unwanted immune response since the immune system doesn't recognize fVIII as a non-foreign entity. Although still in animal model testing, development of a bioengineered human/porcine chimeric fVIII construct ET3i (Figure 9) with porcine A1 and A3 (pA1, pA3) domains and human A2, C1, and C2 (hA2, hC1, hC2) domains may offer a solution to both financial and inhibitor problems.<sup>33</sup> ET3i expresses  $5.3 \pm 0.75$ -fold greater than rh-fVIII in COS-7 cells and maintains slightly higher activity than rh-fVIII.<sup>34</sup> Immunogenicity studies demonstrate porcine fVIII elicits a lower immune response than human fVIII with ET3i studies demonstrating similar results. This next generation therapeutic may offer a future less immunogenic, higher expressing fVIII molecule that can minimize frequent injections and prevent development of neutralizing inhibitors.

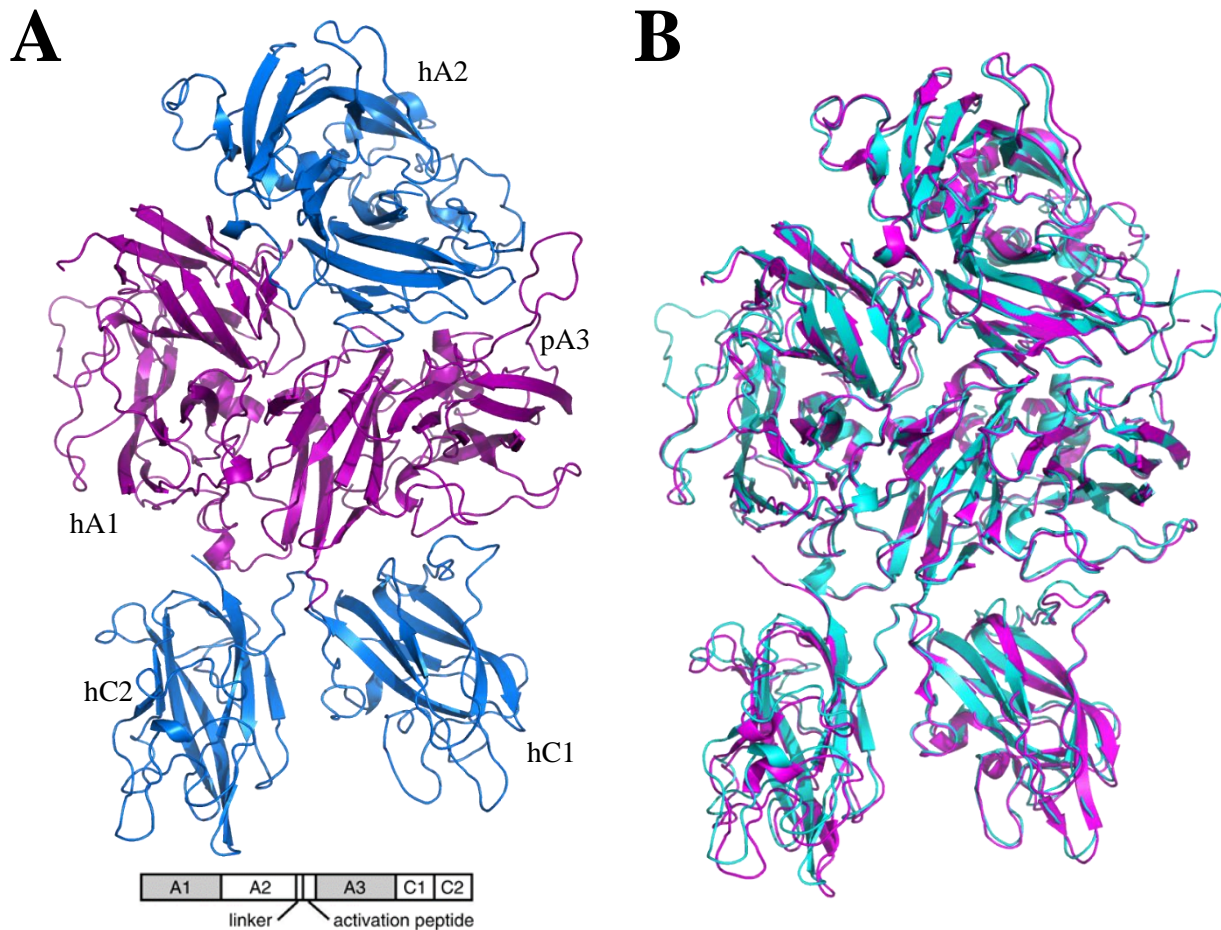


**Figure 9.** Structure of Bioengineered ET3i. A) Ribbon diagram representing ET3i model A (PDB: 6MF0), blue: human A2, C1, and C2 domains, purple: porcine A1 and A3 domains. Domain structure of ET3i (shaded regions represent porcine swapped domains, unshaded represent human domains). B) Structural alignment of human/porcine chimeric fVIII construct ET3i (cyan) and high resolution human fVIII (magenta) (PDB: 6MF2).

### FVIII inhibitors

As previously mentioned, the most serious complication to fVIII replacement therapy is the development of pathogenic inhibitory antibodies.<sup>25</sup> Inhibitors significantly reduce the efficacy of fVIII replacement therapy, increase the severity of bleeding symptoms, and increase morbidity from 12% to 43%.<sup>26</sup> Approximately 30% of patients with severe hemophilia A develop inhibitors,

normally developing within the first 10-20 exposures to fVIII treatment.<sup>25</sup> To quantify the anamnestic response of a patient, the concentration of titer is defined as a Bethesda unit (BU), the inverse dilution factor. In a Bethesda assay, inhibitor containing plasma is diluted with pooled normal plasma until 50% of fVIII activity in the mixture is recovered.<sup>25</sup> Plasma samples requiring more extensive dilutions (high-responding inhibitors) record values of 5 BU or higher, with low-responding inhibitors generally showing less than 5 BU.<sup>25</sup>

Antibodies are immunoglobulins produced by white blood cells. These glycoproteins belong to the immunoglobulin super family (IgSF) and are comprised of two heavy and two light chains.<sup>35</sup> Each immunoglobulin chain contains a single NH<sub>2</sub>-terminal variable IgSF domain and a constant COOH-terminal domain, both connected by a disulfide bridge.<sup>35</sup> Within each variable domain, three hypervariable complementarity determining regions (CDR) constitute the antigen binding region of each immunoglobulin, also known as the paratope.<sup>35</sup> Each paratope binds to a specific region (epitope) of the target substrate (antigen).<sup>35</sup> Inhibitors for fVIII are categorically organized by specific domain recognition and sub-classified for effects on fVIII function. The two most common targets of fVIII inhibitors are the A2 and C2 domains.<sup>36</sup> Anti-A2 inhibitors are known to inhibit fVIIIa through preventing Xase activation of fX, but still allow binding to fX.<sup>37</sup> These antibodies are presumed to bind between residues 373-606, yet specific epitopes are not yet structurally defined.<sup>37</sup> While A2 antibodies have been isolated to one functional disruption and one structural epitope, anti-C2 antibodies are sub-classified as non-classical or classical inhibitors. It was first suggested in 1989 by Morio Aria et al. that anti-C2 antibodies prevent effective interaction of fVIII with phospholipids.<sup>36</sup> These “classical” anti-C2 antibodies differ from “non-classical” anti-C2 domain antibodies as non-classical anti-C2 antibodies do not interfere with phospholipid interactions. Non-Classical anti-C2 domain antibodies disrupt the activation of fVIII

by fXa or thrombin, regardless of whether fVIII is protected by vWF or not.<sup>38,39</sup> Over 30 anti-C2 domain antibodies have been characterized today, binding to 5 different epitopes on the C2 domain (A, AB, B, BC, and C).<sup>40</sup> Three anti-C2 domain inhibitors of interest are BO2C11, G99, and 3E6. (Figure 10). BO2C11 and 3E6 are functionally defined as classical antibodies, but structurally bind to epitopes AB and A, respectively.<sup>40</sup> Although 3E6 and BO2C11 are both potent inhibitors *in vitro* for vWF ( $IC_{50} = 0.6 \mu\text{g/mL}$  and  $0.007 \mu\text{g/mL}$ , respectively) and phospholipid binding ( $IC_{50} = 0.4 \mu\text{g/mL}$  and  $0.01 \mu\text{g/mL}$ , respectively), BO2C11 requires a significant dilution factor (20,000 BU/mg) compared to 3E6 (41 BU/mg).<sup>40</sup> G99 is a group BC antibody and is classified as non-classical inhibitor, but is a powerful inhibitor *in vitro* (15,000 BU/mg).<sup>40</sup>

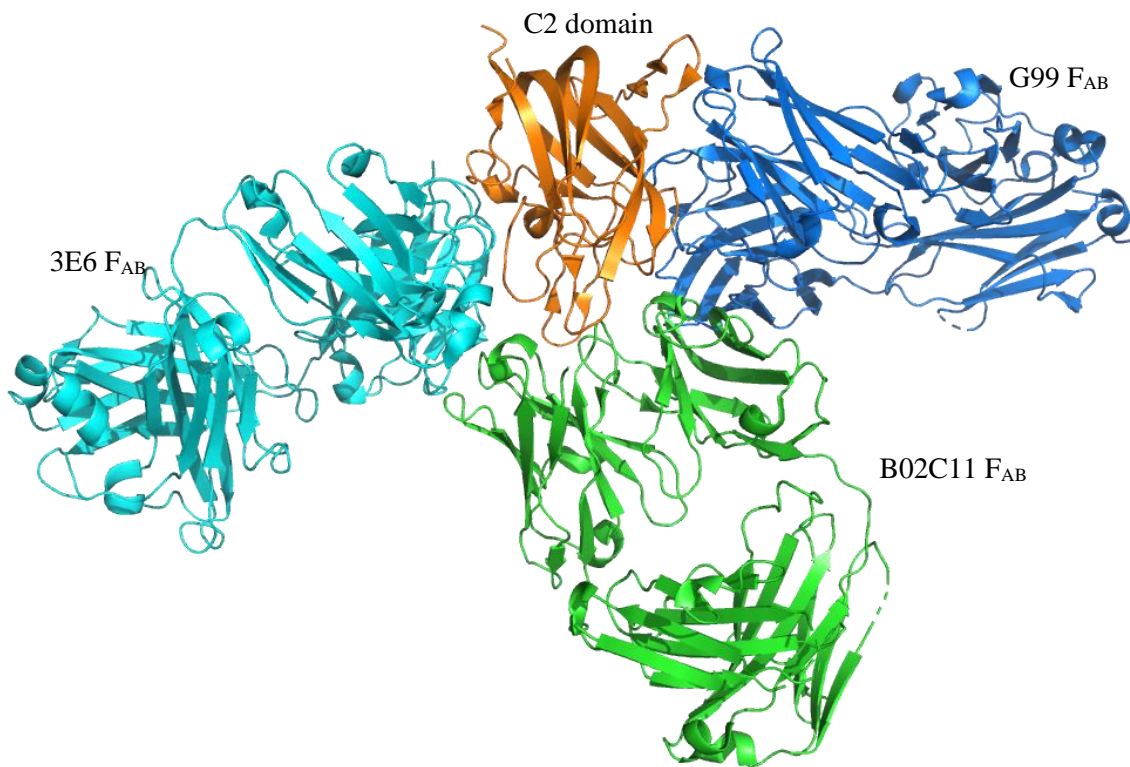


**Figure 10.** Anti-C2 domain inhibitors bound to isolated fVIII C2 domain.

Recent publications have highlighted the significance of anti-C1 domain antibodies in patients with acquired and congenital hemophilia A.<sup>41</sup> 78% of patients with acquired hemophilia A (AHA) and 57% of patients with congenital hemophilia A (HA) in this population were found to have inhibitory antibodies targeting the C1 domain of fVIII.<sup>41</sup> Type I inhibitory human antibodies targeting the C1 domain were found to disrupt fVIII cofactor activity and binding to vWF.<sup>42</sup> Later, type II antibodies recognizing the C1 domain were connected to increased fVIII clearance due to disruption of the fVIII:vWF interaction.<sup>43</sup> One such type II inhibitor is monoclonal antibody (mAb) 2A9. Epitope mapping by HDX-MS detailed 2A9 as a group A inhibitor.<sup>44</sup> The group A inhibitor epitope includes residues 2063-2071 and 2129-2136, resulting in a vWF IC<sub>50</sub> of 1.1 µg/mL and phospholipid binding IC<sub>50</sub> of 0.9 µg/mL.<sup>44</sup> Within the same study, a group B inhibitor (B136) was isolated and determined to be more potent, with a 700 BU/mg of IgG versus 23 BU/mg for 2A9.<sup>44</sup> Moreover, the IC<sub>50</sub> of vWF binding for B136 was 2.75-fold lower and 22.5-fold lower for phospholipid binding, requiring less inhibitor to reach 50% inhibition of fVIII function.<sup>44</sup> The residues of interaction on the C1 epitope for B136 appear to consist of 2077-2084, and overlap with human derived group A/B antibody KM33 at residues 2036-2044, 2091-2092, and 2157-2164.<sup>44</sup> Structural characterization for these anti-C1 domain inhibitors is ongoing and may provide insight on fVIII phospholipid binding interactions within the C1 domain and may shed insight into the conserved nature between the two C domains. Although antibodies cause difficulties within replacement therapy, therapeutic induced antibodies offer invaluable insight into the structure/function relationship of regions of fVIII and have been the epicenter of C2 domain phospholipid binding models.

## Inhibitor-based binding phospholipid binding models

The C2 domain of fVIII has historically attracted the most interest due to the multitude of interactions including vWF, antibody inhibitors, and platelet surfaces. During activation, the acidic A3 region is cleaved, promoting fVIIIa dissociation from vWF. With vWF tethered to platelets through the A1 domain, dissociation of fVIII occurs in close proximity to activated platelet surfaces. The exact platelet surface binding motif for the fVIII C domains is currently controversial as there are two models proposed, but both current fVIII binding models rely exclusively on the biochemical interplay between the hydrophobic and electrostatic interactions of the C2 domain.<sup>14</sup>

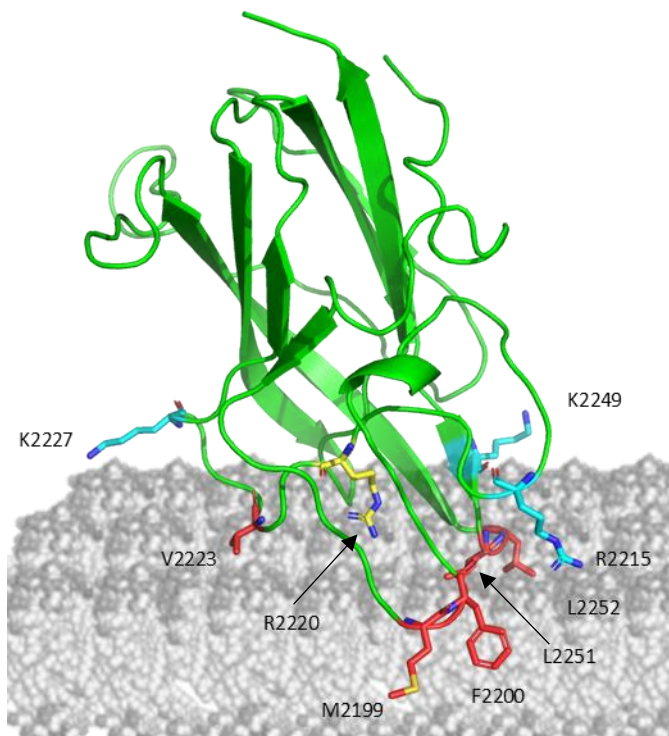


**Figure 11.** Initial activated platelet binding model of the fVIII C2 domain. Hydrophobic residues (red) comprise two hydrophobic loops that insert into the anhydrous leaflet of platelets. Basic residues (red) interact with negatively charged PS headgroups on activated platelet surfaces. The model was centered around R2220 (yellow) as the principal residue. PDB: 6MF0.

The first crystal structure of isolated fVIII C2 domain was published in 1999 and revealed two hydrophobic beta-hairpin loops. These loops were proposed to extend into the anhydrous interior of the phospholipid bilayer (M2199, F2200, V2223, L2251, and L2252) and are surrounded by basic residues (R2215, K2227, K2249) (Figure 11).<sup>45</sup> Positioning the hydrophobic beta-hairpin loops into the anhydrous interior of a platelet bilayer oriented R2220 directly above the lipid surface, suggesting that this residue was the center of the phospholipid binding motif. In support of this binding model, a 2-

dimensional (2D) crystal structure of B-domain deleted fVIII (BDD-fVIII) bound to a negatively charged lipid bilayer was solved to 1.5 nm.<sup>46</sup> Within this structure, the two previously described loops were corroborated and an additional loop was proposed for W2313-H2315.<sup>46</sup> Mutagenesis studies targeting the hydrophobic loops demonstrate that M2199/F2200, L2251-L2255, W2313-H2315 play a role in phospholipid binding. A crystallographic structure of classical inhibitory antibody BO2C11 further supports the model of C2 association to lipid surfaces via hydrophobic loops as both hydrophobic loops are sequestered in the BO2C11 paratope, completely blocking phospholipid binding. Although no isolated high resolution structure exists for the isolated C1 domain, mutational data suggests that mutations to K2092 and F2093 contribute to a 3-fold reduction in affinity for membrane-binding sites.<sup>47</sup> Residues L2092 and F2093 are synonymous to the L2252/2253 sequestered in the BO2C11 epitope on the C2 domain. Collectively, the preliminary model was based on the incorporation of both hydrophobic loops protruding into the anhydrous leaflet of platelets and complemented by a collection of basic residues surrounding the hydrophobic loops.

This initial lipid binding model for the C2 domain of fVIII has since been challenged by structural epitope analysis of the crystal structure of isolated human C2 domain ternary complex with two pathogenic antibody inhibitor fragments (G99 and 3E6) from the Spiegel Lab.<sup>48</sup> 3E6 is a classical inhibitor, completely disrupting the ability of C2 to bind to phospholipids, whereas G99 is a non-classical inhibitor and allows C2 to bind phospholipids (Figure 12).<sup>38,40,49</sup> Epitope mapping of the

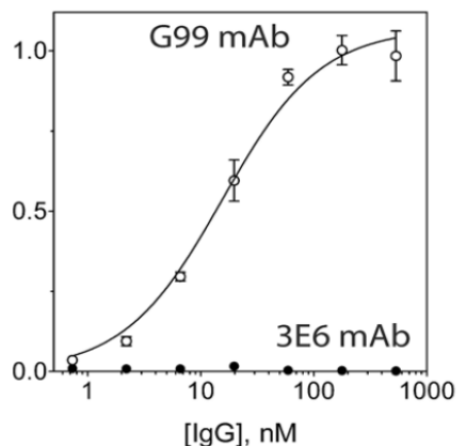


**Figure 12.** ELISA of C2 lipid binding with non-classical and classical inhibitors. FVIII C2 domain immobilized to PS was able to bind to G99 and not 3E6, demonstrating that PS binding occurs at the 3E6:C2 interface. Adapted from Brison et al.

G99 fragment of antigen binding (F<sub>AB</sub>) overlaps with K2227, which was postulated to be positioned towards the membrane in tandem with R2220 in the preliminary model.<sup>50</sup> Since G99 has little to no effect on the phospholipid binding capabilities, it seems implausible that K2227 is positioned towards the phospholipid membrane. Additionally, the porcine fVIII C2 domain consists of a glutamic acid at position 2227, which carries the opposite charge as a lysine, and further suggests that K2227 is not directly involved in phospholipid binding. The 3E6 F<sub>AB</sub> encompasses loops consisting of residues E2181-A2188 and T2202-R2215.<sup>48</sup> Specifically, the 3E6 F<sub>AB</sub> associates to K2183, D2187, R2209, H2211, Q2213, G2214, and R2215.<sup>48</sup> Uniquely, the 3E6 F<sub>AB</sub> completely disrupted phospholipid binding but the two previously proposed hydrophobic loops (Met2199/Phe2200 and Leu2251/Lue2252) were not within the 3E6 epitope, suggesting the C2 domain hydrophobic and electrostatic interactions function in a cooperative manner, rather than a complimentary role. Given the inhibition of phospholipid binding by blocking electrostatics and the fact that K2227 must not be involved in phospholipid binding, a new model was proposed utilizing all three anti-C2 epitopes (Figure 13). By overlaying the B02C11, 3E6 and G99 F<sub>AB</sub> with a high resolution of isolated C2 domain, the hydrophobic loops bound to B02C11, and basic residues involved in binding to 3E6 can be positioned at the interactive surface of lipid membranes while the G99 epitope is faced away.

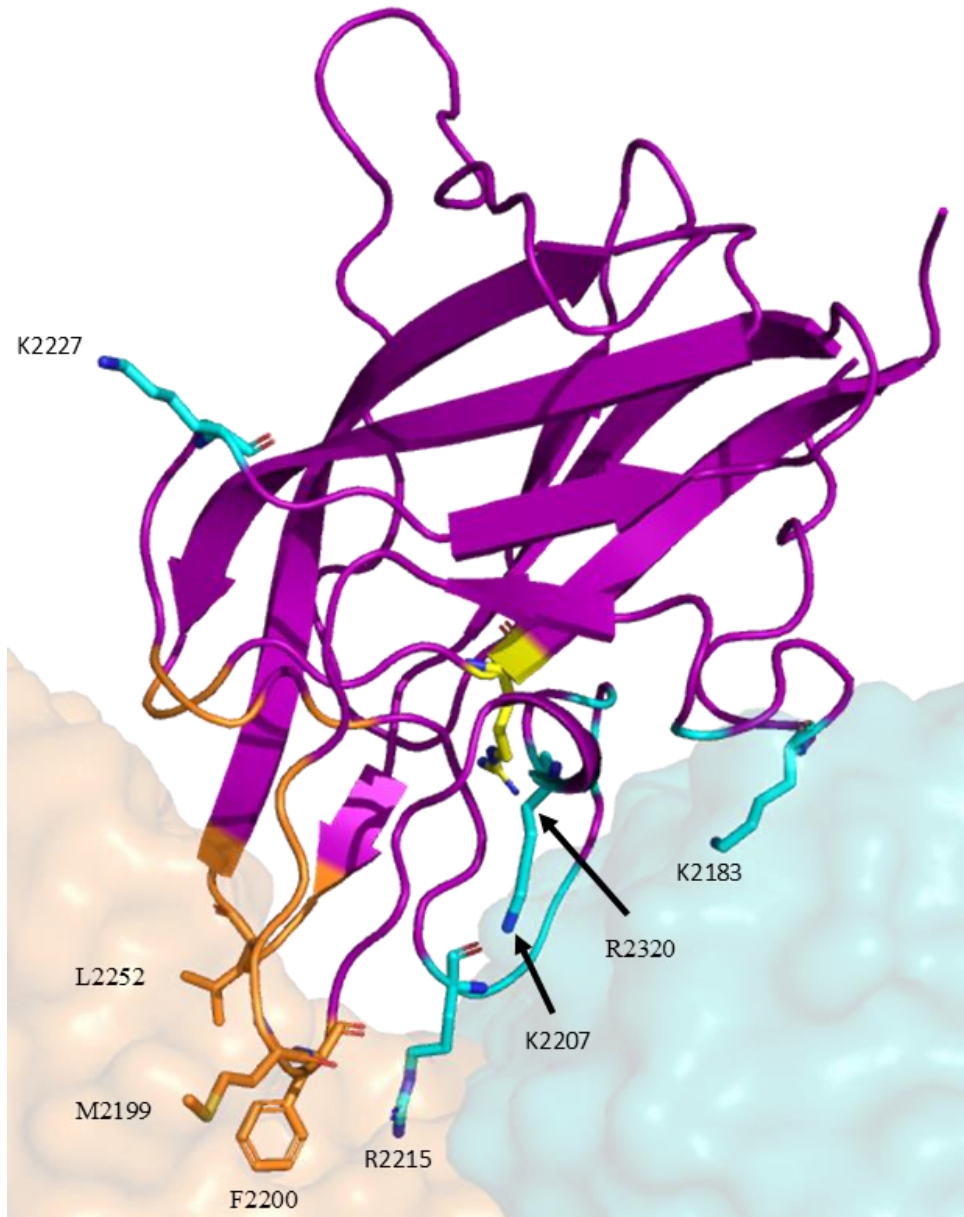


**Figure 13.** Revised activated platelet binding model of the fVIII C2 domain. Hydrophobic residues (orange) comprise two hydrophobic loops that insert into the anhydrous leaflet of platelets. Basic residues (blue) interact with negatively charged PS headgroups on activated platelet surfaces. The model was centered on R2320 (yellow) as the principal residue. Surface maps of 3E6 and Bo2C11 (blue and orange, respectively), represent the phospholipid surface. PDB: 6MF0.

## **Electrostatic interactions of fVIII C domains and lipid membranes.**

Mutational assays for the C2 domain based on hemophilia A mutations and proposed phospholipid binding models have demonstrated that mutations to hydrophobic residues M2199/F2200, L2251-L2255, and W2313-H2315 are required for optimal membrane binding and procoagulant activity. However, these studies barely touch on the important role of phosphatidylserine in platelet binding. During platelet activation, lipid composition of the lipid bilayer is perturbed, with an increase of negatively charged phospholipids redistributed to the extracellular environment.<sup>6,10</sup> Without this charge distribution change, fVIII has negligible affinity to these phospholipid surfaces.<sup>51,52</sup> Studies have shown that fVIII specifically binds to the L-isomer of phosphatidylserine (OPLS) and that >95% of fVIII activity is lost in the presence of the D-isomer (OPDS).<sup>53</sup> This implies that there is at least one essential binding motif for phosphatidylserine that exists within the light chain of fVIII. Given that the fVIII light chain has two C domains with very high sequence and structural homology, it is more plausible that a conserved motifs exist within each of the C domains. Previous literature of alanine scanning mutations on basic residues within the C2 domain have indicated that Q2213, N2217, and R2220 had no effect on the relative specific activity of fVIII for lipid membranes.<sup>54</sup> Inhibitor peptides spanning residues 2313-2323 results in >90% inhibition of the C2 domain to phospholipids, suggesting the lipid binding moiety resides in this region.<sup>55</sup> Although the W2315-H2315 have since been reported to disrupt phospholipid binding in low (4%) PS containing lipid vesicles *in vitro*, but *in vivo* assays have demonstrated WT effector function, suggesting this region functions in a complementary fashion rather than essential and most likely forms interaction in the anhydrous interior rather than with the OPLS headgroups of phosphatidylserine.<sup>56</sup> Homology modeling and membrane binding predictions have suggested that three arginine residues within the C1 and C2

domain may form mutually exclusive interactions with phospholipids.<sup>57</sup> These residues, R2163 (C1), R2220 (C2), and R2320 (C2) are buried within the hydrophobic core of the beta-barrel motif and extend towards the exterior of the molecule. R2220 has been previously shown to have no effect on lipid membrane binding and thus disagree with simulation data.<sup>54</sup> With limited mutational data on the C1 domain, functional insights can only be inferred from the C2 mutational data available. Characterization of hemophilia A-related missense mutations amongst the C2 domain revealed a 5% relative activity of a R2320T mutation compared to wild-type, insinuating the potential of R2320 as an essential residue for phospholipid membrane binding.<sup>58</sup> Moreover, the conservation of this R2320 across species and between homologous clotting fV suggest that this residue might lie within a conserved binding motif. Electrostatic surface mapping of the R2320 residue within the C2 domain demonstrates that this residue carries the most basic electrostatic potential and thus may make direct contact with the negatively charged phosphatidylserine containing lipid surfaces (Figure 14).

Collectively, the fVIII binding mechanism to PS containing platelet membranes is proposed to orient around the facilitation of hydrophobic contacts between solvent exposed hydrophobic loops of the C domains and an undetermined number of basic residues positioned above these hydrophobic loops. The main goal of this study was to elucidate which of the basic residues surrounding the hydrophobic loops is essential of phospholipid binding. A detailed understanding of the phospholipid binding interactions would inform the advancement of hemophilia A therapeutics.

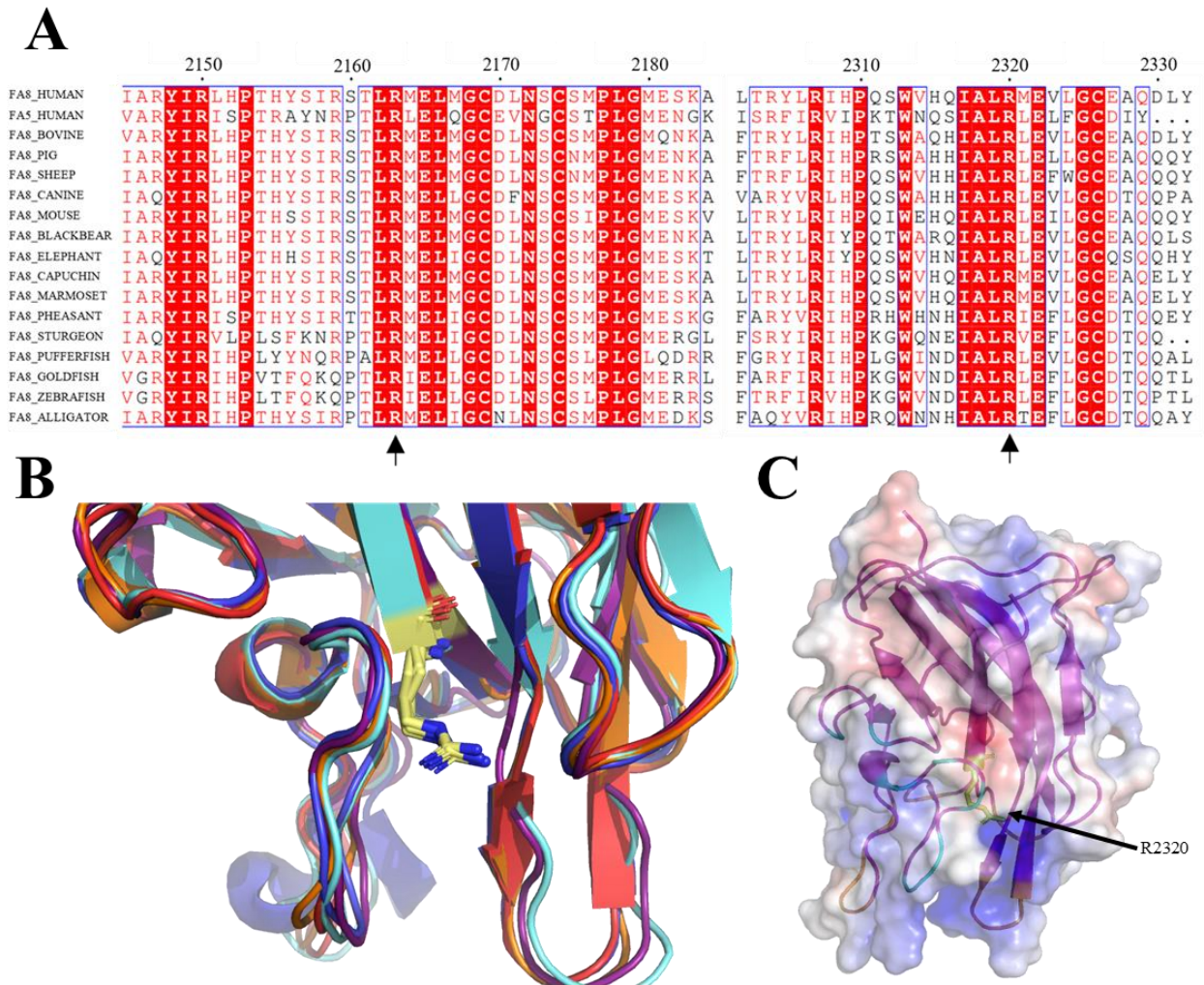


**Figure 14. FVIII C2 domain sequence and structural alignment** A.) Sequence alignment of fVIII among various species and fV. Red columns indicate complete sequence conservation across species. R2320 and R2163, the sequence homolog of the C2 domain, are completely conserved across species and clotting factors (Arrows). B.) Ribbon diagram representation of the structural alignment of Lactadherin (PDB: 3BN6, blue), factor V C2 domain (PDB: 1CZS, cyan), human fVIII (PDB: 6MF2, red), porcine fVIII C2 domain (PDB: 4MO3, orange), and fVIII C1 domain (PDB: 6MF2, purple). The conserved fVIII C2 R2320 residue is shown as sticks in yellow from all aligned C domain homologs. C.) Surface electrostatic mapping of the C2 domain positions R2320 in the most basic cleft of the C2 domain. The surface potential calculation was performed with APBS with surface potential value of  $\pm 5$  kT/e, and were generated with PyMol (blue: positive charge, red: negative).

## Chapter 2: Materials and Methods

### **Site directed mutagenesis of human C2 domain:**

The gene for wild type human C2 domain (residues 2171-2332) was prepared previously in a pET15b plasmid (Spiegel 2004). Human C2 mutations (R2320S, R2215A, K2183A, D2187A, A2201P, K2227A, and R2215A) were manufactured using the Agilent Technologies QuikChange Lightning Site-Directed Mutagenesis Kit with pEt32a (+)/6his-thioredoxin-S-fVIII C2 plasmid templates. DNA from the plasmids containing C2 domain mutations were extracted using QIAquick PCR purification kit from Qiagen and sequencing was performed at Nevada Genomics. Verified C2 mutant DNA was transformed into chemically competent SHuffle T7 B *E. coli* cells purchased from New England Biolabs Inc. Approximately 100 ng of mutant DNA was incubated with the competent cells and plated on Lysogeny Broth (LB) (1% tryptone (w/v), 1% NaCl (w/v), 0.5% yeast extract (w/v)) ampicillin 50 mg/ml (LB<sub>50</sub>) agar plates. A single colony was selected for sell stock preparations and cell stocks were stored at -80 °C in 20% (v/v) glycerol.

### **Over expression of C2 WT and Mutant proteins:**

Overnight cultures were grown from single colony cell stocks in 10 mL LB<sub>50</sub> while shaking at 30 °C and then added to 1 L of LB<sub>50</sub> shaking at 180 rpm, 30 °C until the absorbance at 600 nm reached a value of 0.6-0.8. Protein growth was induced by the addition of isopropyl B-D-thiogalactopyranoside (IPTG) to 500 µM and the temperature was adjusted to 15 °C and left overnight for 18-20 hours. Cells were pelleted by centrifugation at 6371x g for 10 min at 4 °C (FIBERLite F10-6x500y rotor, Thermo Fisher Scientific, Waltham, MA) and resuspended in Lysis buffer (300 mM NaCl, 20 mM Tris-HCl pH 7.5, 10 mM imidazole pH 8.0, 10.0% (v/v) glycerol, and 0.5% (v/v) Triton X-100) with addition of lysozyme and phenylmethylsulphonyl fluoride

(PMSF). Cells were mechanically lysed using a Branson Sonifier 450 probe at power output 5 and duty cycle 50% for 30 seconds repeated three times with 60 second pauses in-between cycles. Cell debris were removed by centrifugation at 16,000 rpm for 30 min at 4 °C (FIBERLite F21- 8x50y rotor, Thermo Fisher Scientific), followed by filtration with 0.45-um cellulose sterile syringe filters. TALON cobalt immobilized cobalt affinity resin (TAKARA Bio) was equilibrated in lysis buffer at 1 mL settled resin/ 2 L bacterial growth and incubated with filtered lysate for 30 minutes at 4 °C. Settled resin was rinsed with 30 CV of lysis buffer; with 30 CV of wash buffer (150 mM NaCl, 20 mM Tris-HCl pH 7.5, 10 mM imidazole pH 8.0, and 10% (v/v) glycerol); and eluted with elution buffer (150 mM NaCl, 20 mM Tris-HCl pH 8.0, 150 mM imidazole pH 8.0, and 10% (v/v) glycerol) following a 10-minute incubation time. Eluted protein was dialyzed in storage buffer containing 150 mM NaCl, 25 mM Tris-HCl pH 8.0, and 10% (v/v) glycerol at a concentration between 2-4 mg/mL.

### **Transformation of FVIII C1 and C1C2 domain containing plasmids:**

FVIII residues (2048-2332) were ordered from Genscript in a pET32a+ vector using *BamHI* and *XhoI* restriction sites. FVIII C1C2 residues were transformed into C3029J Shuffle K12 *E. coli* cells following New England Biolabs (NEB) protocol and additional mutations (R2320S, R2215A, A2201P, R2163S, and R2163S/R2320S) were transformed in an identical manner (Figure 15). Isolated fVIII C1 domain and corresponding mutations R2163S and R2163C were transformed as per above. Transformed cells were plated on ampicillin treated agar and left to grow at 30 °C overnight. Single colonies of transformed cells were further expanded in 10 mL's of LB<sub>50</sub> inside a New Brunswick Scientific Excella E25 at 30 °C, 225 rpm, for 16-18 hours. Expanded cultures were stored at -80 °C in 20 % (v/v) glycerol.

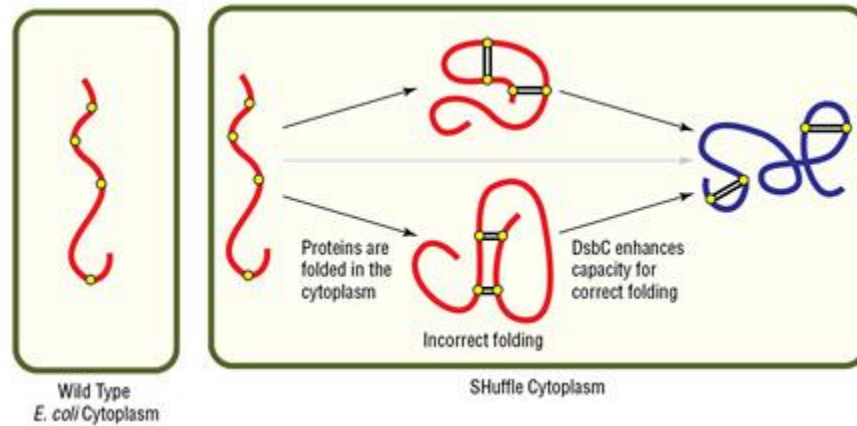


**Figure 15. Functionality of SHuffle cell lines.** *E. coli* cytoplasm is a reducing environment and prevents the formation of disulfide bonds during protein folding. SHuffle cell lines are engineered to have enhanced folding and disulfide formation due to removal of reductive enzymes. Adapted from NEB protocol.

### **Growth and expression of FVIII C1C2 domain constructs:**

LB media was prepared and autoclaved in-house. Overnight cultures with 10 mL of *E. coli* K12 cells containing fVIII C domain constructs were added to 1 L of LB and grown until an OD<sub>600</sub> of 0.3 was reached, where flasks were quickly cooled on ice. When cooled cells reached an O.D<sub>600</sub> of 0.4, 0.4 mL of 1M IPTG was added and protein was left at 180 rpm, 15 °C for 18 hours. Expressed cells were pelleted and resuspended in 30-35 ml of cold lysis buffer (20 mM N-(2-Hydroxyethyl) piperazine-N'-2-ethanesulfonic Acid (HEPES) pH 7.4, 500 mM NaCl, 10 mM Imidazole, 10% (v/v) glycerol, 0.1% v/v triton, 10 mM MgCl<sub>2</sub>) with the addition of 350 µL of 100 mM PMSF and 700 µL of 50 mg/ml lysozyme. Enzymatic lysis occurred for 30 minutes on ice with intermittent mixing. Cells were further lysed with mechanical sonication as described above. Cell debris and insoluble proteins were separated from soluble fraction through a 45-minute centrifugation at 17,000 rpm, 4 °C. High-speed cell supernatant was filtered through 5.0 µm and 0.45 µm filters before batch binding for 30 minutes with 1 mL of TALON resin per 2 liters of LB

prep. Immobilized metal affinity chromatography (IMAC) was performed by collecting the batch flow through, a lysis buffer rinse, 20 CV Wash (20 mM HEPES pH 7.2, 500 mM NaCl, 15 mM Imidazole, 10% (v/v) glycerol), and 20 CV Elution (20 mM HEPES pH 6.8, 300 mM NaCl, 150 mM Imidazole, 10% (v/v) glycerol) steps. IMAC elution was diluted with HBS (50 mM HEPES pH 7.4, 300 mM NaCl) to a final imidazole concentration of 5 mM and loaded onto a Capto His-Trap 5 mL column for subsequent purification. A 100 CV ATP wash in HBS supplemented with 20 mM MgCl<sub>2</sub> and 10 mM ATP was performed and rinsed with 1X HBS until absorbance flattened. Elution was achieved using an imidazole gradient from 0 mM Imidazole to 500 mM Imidazole and collected in 4 mL fractions. Eluent fractions containing >95% pure C1 or C1C2 (assayed by SDS-PAGE) were buffer exchanged into low pH HBS (20 mM HEPES pH 6.8, 150 mM NaCl, 10% (v/v) glycerol) and concentrated using a 30,000-cutoff concentrator to 0.3-0.4 mg/mL. Samples were stored at -80 °C. Protein purity and yield was verified via SDS-PAGE using 12.5% bis-acrylamide gels. Fractions containing expressed protein of interest were dialyzed in Dialysis buffer (20 mM HEPES pH 6.0, 150 mM NaCl, and 10% (v/v) glycerol). Precipitates were removed post-dialysis via centrifugation at 4000xg for 5 minutes.

### **Cation Exchange chromatography:**

Co-elutants from IMAC required subsequent purification via cation exchange. Due to the instability of C1 containing constructs, post-IMAC elution samples were diluted 1/6 to a final concentration of 150 NaCl and were injected into the Hi-trap Capto S 5 mL cation exchange column attached to a fast protein liquid chromatography (FPLC) device (AKTA prime Plus manufactured by GE Healthcare Life Sciences). Protein loading buffer contained 20 mM 2-(*N*-morpholino) ethane sulfonic acid (MES) pH 6.0, 150 mM NaCl. Protein was eluted using a 30-40 mL gradient elution to 100% B solution containing 20mM MES pH 6.0, 500 mM NaCl. Protein

peaks were collected in 0.5 mL Fractions and analyzed for purity on 12.5% SDS-PAGE gels. Eluted protein was concentrated with a 30,000 MWCO Amicon 15-mL spin filters. The column was cleaned with 1 M NaOH between subsequent runs and stored in 20% ethanol with 200 mM sodium acetate as per manufactures protocol.

### **Enterokinase cleavage:**

Plasmids ordered from Genscript contained an Enterokinase cleavage sequence up-stream of the N-terminus of the C1 or C1C2 constructs. Recombinant Enterokinase (rEK) was ordered from Sigma Aldrich (CAT: 69066-3) and optimized from the published protocol. Reactions occurred at room temp (RT) for 24 hours while rotating with the assumption that 1 U of rEK will cleave ~50 µg/day. Reactions were analyzed via SDS-PAGE before removal of rEK. Removal of rEK was accomplished with 0.22 µm spin filters and the resin was washed with 1X rEK Dilution buffer (200 mM NaCl, 20 mM Tris-HCl, 2 mM CaCl<sub>2</sub>, 50% (v/v) glycerol, pH 7.4).

### **Size exclusion chromatography.**

GE healthcare S75 was utilized to verify globular protein weight via size exclusion chromatography. The column was equilibrated in 50 mM MES pH 6.0, 150 mM NaCl at a flow rate of 0.3 mL/min and half milliliter injections of tagged and cleaved C1C2 or C1 constructs were performed. Peaks were collected in front and back half fractions and visualized on a 12.5% SDS page gel. The S75 column was stored in 20% ethanol and cleaned with 1M NaOH between runs.

### **Mammalian cell culturing:**

In a sterile hood, 9 mL of Hybridoma Medium E (MedE) from STEM Cell technologies (CAT# 03805) was placed into a sterile 15-mL conical centrifuge tube. Hybridoma cells stored at ~ 1 million cells/mL in MedE with 10% dimethyl sulfoxide (DMSO) were quickly thawed in a 37 °C water bath for approximately 45 seconds until almost completely thawed. Cells were pipetted

into the 9 mL MedE aliquot, capped, and gently inverted to ensure dilution of DMSO. Hybridoma cells were pelleted by centrifugation at 1000 rpm at RT for 5 minutes. The MedE-DMSO containing supernatant was carefully discarded and the hybridoma cells were gently resuspended in 2 mL of MedE and transferred to a T-75 flask containing 15 mL's of MedE. The T-75 flask was sealed with a vented cap and hybridoma cells were placed into a sterile water bath incubator at 5% Co2 and 37 ° C. Observations of cells were taken based on adherence to the T-75 flask, percent of confluence, and color of solution. Up to 25 mL's of additional MedE was added to the T-75 flask 48 hours after initial transfer. A hemocytometer was utilized to accurately assess cell density before cryopreservation. Hybridoma cells for cryopreservation or passaging were pelleted at 1000 rpm for 2 minutes at RT and diluted with 10 mL of MedE. Serial dilutions of 1:10, 1:100, and 1:1000 were made in 1 mL aliquots and 200 µL of each dilution was analyzed by counting across 5 large hemocytometer squares and averaging and multiplying by the dilution factor to calculate the cell density.

### **Expression of Antibodies in AOF Media:**

Expression of anti-fVIII antibodies was completed in AOF media (Cat#: 03835). Hybridoma cells were grown in MedE until 50% confluent and sluffed off using 2 mL of Versene solution. Viable was confirmed via hemocytometer and a few drops of cells were added to a sterile T-75 flask for containing 25 mL of AOF media. AOF media containing hybridoma cells were left for 10 days, at which time media was spun at 1100 rpm for 10 minutes at RT and 20% sodium azide was added to a final concentration of 0.1%. Antibody containing media was stored for 3 days at 4 °C or stored at -80 °C for long term storage.

### **Antibody purification with Protein A resin**

Collected antibodies were diluted at least 1:2 with HBS prior to purification. Diluted antibody media was run over 2-3 mL's of Protein A resin in a disposable gravity column. Antibody FT was collected and washed with 5 CV of 1x HBS. Elution was achieved using 10 CV 0.2 M glycine pH 2.8-3.0 and collected in a 50 mL centrifuge tube containing 2 CV of 0.5 M HEPES pH 7.4. Purity was analyzed via SDS-PAGE analysis using loading dye containing and in the absence of beta-mercaptoethanol (BME).

### **Enzyme Linked Immunosorbent Assays:**

Nunc-Immuno MicroWell PolySorp 96 well solid plates were coated with 80% 1,2-dioleoyl-sn-glycero-3-phosphocholine (DOPC) and 20% 1,2-dioleoyl-sn-glycero-3-phospho-L-serine sodium salt (DOPS) (Avanti Polar Lipids Inc.) at 10 µg/ml. Negative control wells were coated with 100% DOPC at 10 µg/ml. The wells were then blocked for 45 minutes with a 1% (w/v) bovine serum albumin (BSA), 50 mM Tris-HCl pH 7.5, 100 mM NaCl solution. Protein samples were prepared with serial dilutions of 1:2 in a 1% (w/v) BSA, 50 mM Tris-HCl pH 7.5, 100 mM NaCl solution with initial protein concentrations of 2000 nM for 12 samples total. Subsequently, Ni-NTA•HRP diluted to 1:1500 (in 1% (w/v) BSA, 50 mM Tris-HCl pH 7.5, 100 mM NaCl solution) was incubated for 30 minutes. Lastly, 2,2'-Azinobis (3-ethylbenzthiazoline-6-sulfonic acid) (ABTS) was used to detect binding at 405 nm. All incubation steps were shaken at 75 rpm in a 37°C incubator. Between each incubation, the wells were washed with a 1% (w/v) BSA, 50 mM Tris-HCl pH 7.5 solution using an automated plate washer. Salt gradient ELISA's were performed as above with blocking serial dilution steps being performed in 1:2 in 1% (w/v) BSA, 50 mM Tris-HCl pH 7.5, 50 mM, 100 mM, 150 mM, or 225 mM NaCl solution with an initial

protein concentration of 1000 nM. Following data collection, binding curves were normalized, and approximate equilibrium binding affinities were analyzed in a 1:1 nonlinear region with Graph Pad Prism.

### **Sedimentation assays:**

Unilamellar vesicles were adapted from the Morrisey lab at University of Michigan. A total of 2.6  $\mu$ mole of lipids in either 80:20 or 100:0 DOPC:DOPS molar ratios were dried under a stream of argon gas and resolubilized in 2.6 mL of 20 mM HEPES pH 7.4, 50 mM NaCl, 0.1% NaN<sub>3</sub>. Resolubilized lipids were allowed 1 hour to rehydrate with intermittent inverting. Post hydration, lipids were vigorously vortexed until a milky suspension was achieved. Lipids were submerged in liquid nitrogen and quickly thawed in a 37 °C water bath four times. Freeze-thawed lipids were subsequently extruded using Avantipolar lipids extruder 11 times. Lipids were stored for up to 2 months at 4 °C with a final concentration of 1 mM.

FVIII sedimentation assays were performed in 8x32mm microcentrifuge tubes in 300  $\mu$ L reactions. ET3i and C1C2 domain assays were performed at 200 nM whereas C1 and C2 were performed at 5  $\mu$ M. In an 8\*32 mm tube, 125  $\mu$ L of unilamellar vesicles were added to protein and buffer (20 mM HEPES pH 7.4, 50 mM NaCl) was added to final volume of 300  $\mu$ L. Reactions were flicked to mix and allowed to sit at room temp for 5 minutes. Reactions were spun at 168,000 g for 45 minutes at 4 °C. Protein supernatant was removed and precipitated in at least 5x volume of -20 °C acetone overnight. Gel samples were made of lipid sedimentation assay pellets and acetone precipitation pellets and were analyzed via SDS-PAGE gel. Controls were run as per above but with 100% PC vesicles.

### **Nanodisc Technology:**

MSP1D1 plasmid was ordered from Genscript and expressed in BL21 (DE3) cells in LB<sub>50</sub> broth. Soluble MSP1D1 was purified using Ni<sup>2+</sup>-affinity resin and dialyzed into TBS, concentrated to 10 mg/mL, frozen in liquid N<sub>2</sub>, and stored at -80 °C. Typical yield was around 30 mg per L of culture.

MSP1D1 cleaved nanodiscs (cND) were formed with 6 μmole of lipids at an 80:20 or 100:0 DOPC:DOPS molar ratio. Lipids, stored in chloroform, were evaporated under a stream of argon gas and resolubilized with 140 μl of 1x TBS containing 100 mM sodium cholate. Lipids were solubilized by running warm tap water (~40-50 °C) and vortexing until a clear solution was obtained. TBS was added along with MSP1D1 at a final 1:200 molar ratio for untagged MSP1D1. The lipid:MSP1D1:sodium cholate solution was incubated for one hour at 37 °C. Biobeads were equilibrated in TBS and 0.5 mL was added to each 500 μL reaction and let sit overnight. Biobeads were removed using a 0.22 μM spin filter. Samples were purified using size exclusion chromatography (S200, GE Healthcare) with TBS as the equilibration buffer. For untagged ND, a single peak was obtained with an 8-9 mL retention time and concentrations was calculated from MSP1D1 extinction coefficient (assuming 2 molecules per ND).

### **Crystallography:**

Crystals suitable for X-ray crystallographic structure determination were grown by hanging drop vapor diffusion in 0.1 M CHES (pH 10.4), 0.1 M magnesium acetate, and 10% (v/v) ethanol in a 2:1 ratio of crystallization buffer and 2 mg/mL porcine C2 (pC2) domain in storage buffer. Growth of crystals occurred overnight at 4 °C in the presences of 220 μL Al's oil. Crystals were soaked in a 5 mM solution containing phosphatidylserine headgroup (OPLS) and cryoprotected

with a 1:1 addition of 0.1 M CHES (pH 10.4), 0.1 M magnesium acetate, and 30% (v/v) glycerol. X-ray diffraction data were collected to 1.3 Å resolution the Advanced Light Source (ALS) Berkeley Center for Structural Biology (BCSB) beamline 5.0.1 (Berkeley, CA). Data collection and processing were performed with Adxv, XDS and Aimless. Phasing of pC2 crystal was accomplished using PHASER-MR with the previously determined 1.7 Å pC2 structure (PDB ID: 4MO3). Model building and refinement were performed with WinCoot and PHENIX, respectively. All structure figures and structural alignments were generated with PyMOL Molecular Graphics System, Version 2.0 (Schrödinger, LLC).

### Chapter 3: Results

#### *FVIII C domain construct expression and purification.*

Expression and purification of soluble WT hC1C2 and hC1 fusion proteins were successful in SHuffle K12 *E. coli* cells and yielded no protein in traditional BL21(DE3) or SHuffle B cells (Figure 16 A-C). WT C2, which was previously published, expressed excellent in BL21(DE3) cells with an approximately 5 mg/L of culture (Table 3). Protein expression of isolated WT C1 yielded similarly to WT C2, achieving 4 mg/L of culture. Post IMAC samples showed a 70 kD contaminant across K12 cell lines which could be removed using construct specific approaches. All C2 constructs were purified with a strong cation exchange resin (Capto S) while WT C1C2 and WT C1 were purified with ATP washes, respectively, but both methods were generally unsuccessful for the C1 mutants (Figure 16 D-E). Further purification of the C1C2 fusion constructs, including all mutants, were completed via IEC (Figure 16 F-G). C1C2 mutants (R2163S, R2320S, and R2163S/R2320S) were expressed and solubilized as mentioned previously, with yields ~3 fold lower, and needed to be purified on the FPLC to separate away contaminants (Figure 17).

**Table 3.** Approximate protein expression of fVIII C domain constructs per liter of expression. Values are based off 6 L growths in LB<sub>50</sub>.

Protein Construct	Average Yield Post IMAC	Purification scheme	Yield post purification
WT hC1	4 mg/L	IMAC -> SEC	4 mg/L
WT hC2	5 mg/L	IMAC -> S column	2 mg/L
WT C1C2	1 mg/L	IMAC -> S column/SEC	0.5mg/L
hC1 mutants	0.5 mg/L	IMAC -> SEC	Unsuccessful
hC1C2 mutants	0.3 mg/L	IMAC -> S column/SEC	0.125 mg/L

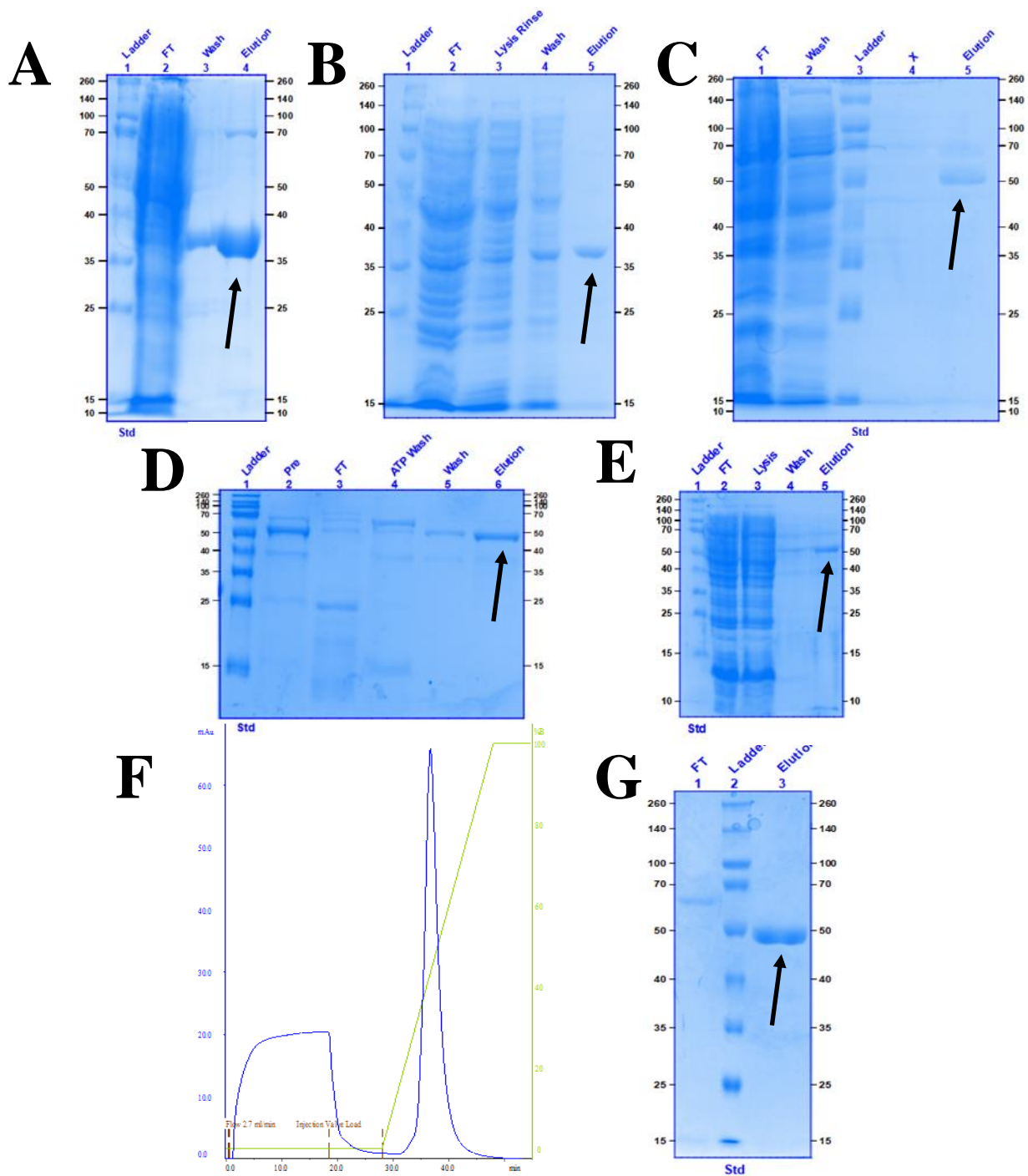


**Figure 16.** Purification and analysis of C1, C2 and C1C2 constructs. A.) WT C2 domain following TALON IMAC purification. B) WT C1 domain following TALON IMAC. C.) WT C1C2 purification with the dominant band at ~ 50 kDa. D.) Purification of C1C2 R2163S utilizing an ATP wash to remove the 70 kDa contaminant. E.) Purification of C1C2 R2320S using an ATP wash approach similar to R2163S. F.) Secondary purification with a Capto S column for WT C1C2. G.) SDS-PAGE gel following S column purification of WT C1C2. The elution in lane three corresponds to the gradient elution peak from F. Arrows indicate respective protein of interest depending on purification.

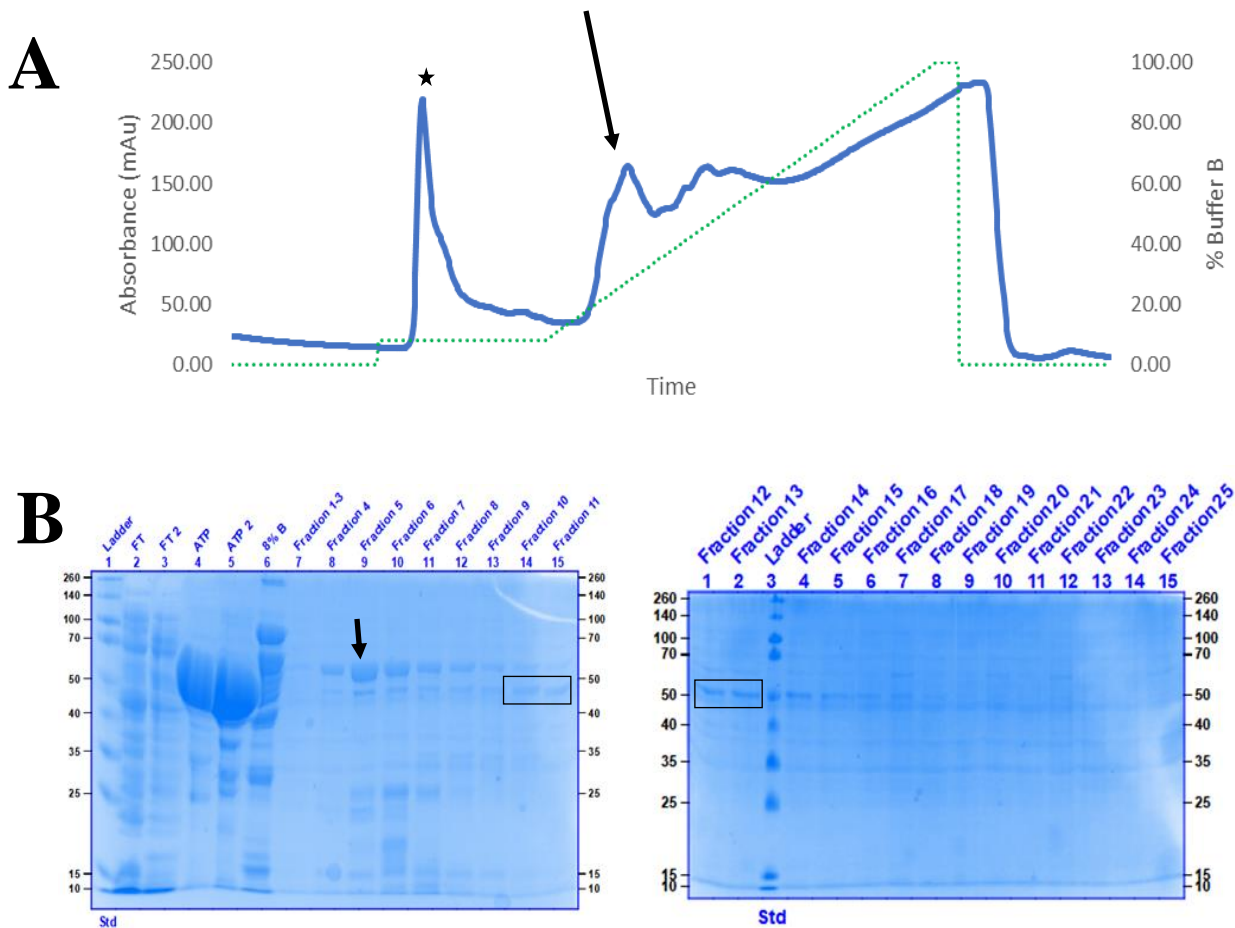


**Figure 17.** Purification of R2163S/R2320S C1C2 mutant via FPLC. A.) Post-lysis high speed supernatant was loaded onto a 5 mL Hi-trap Ni-NTA column and subjected to a 100 CV ATP wash (denoted by ★) and a gradient elution (indicated by the green dashed line). B.) SDS gel of FPLC purification. The arrow denotes the higher molecular weight contaminant and boxes denote fraction with >90% purity when pooled.

*Enterokinase cleavage of C1C2:*

To verify the protein of interest expressed, the N-terminal thioredoxin fusion tag and hexahistidine tag were removed from C1 and C1C2 using recombinant Enterokinase. Recombinant Enterokinase was generally successful in removing the thioredoxin-6His tag from C1C2, however, typical post cleavage IMAC purifications were unsuccessful in separating the cleaved C domain from the free thioredoxin. In turn, strong cation exchange (S column) was successful in removing all contaminants, as the theoretical isoelectric point (pI) of Enterokinase and thioredoxin-His<sub>6</sub>

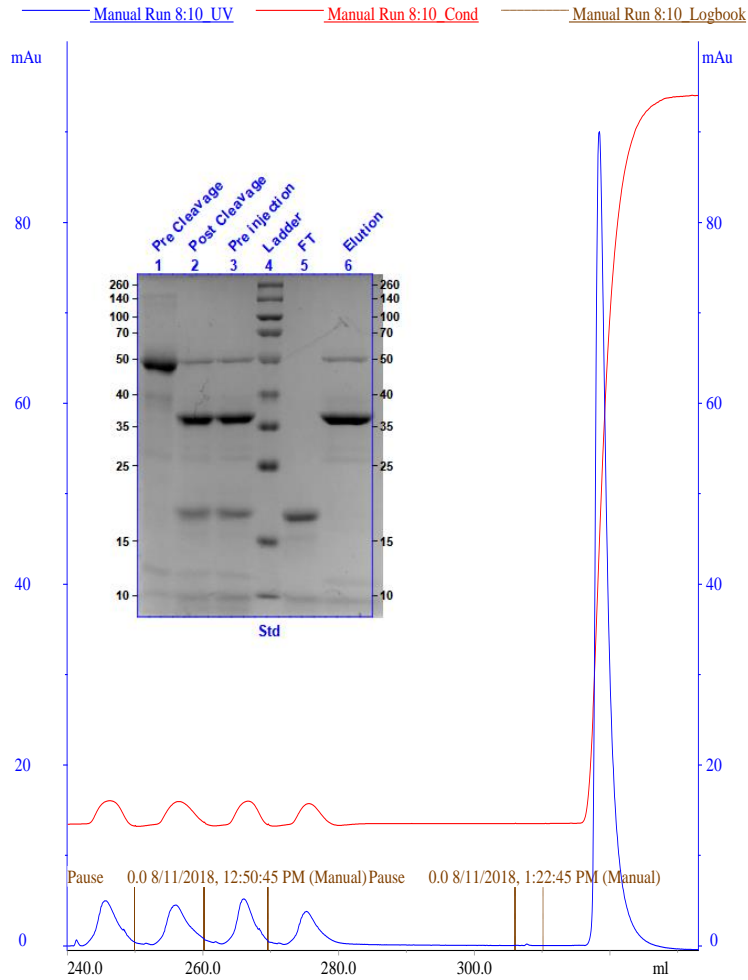


**Figure 18.** Post Cleavage Purification and Analysis. Lane 1-2 shows the emergence of a 35 and 17 kDa band from pre to post cleavage of C1C2. Post purification via S column retain both cleaved and uncleaved C1C2.

reactions. Subsequent purifications on the S-column showed high retention of cleaved and tagged C1C2 whereas the Trx tag was solely in the FT (Figure 18).

linker were lower than the MES pH 6.5 buffer utilized. C1C2 has an abnormally basic theoretical pI of 9.8, so utilizing a pH buffer around 6.5, the C1C2 cleaved protein was able to be retained on the column. Although successful, rEK was most efficient at cleaving over a 24-hour time frame at RT, which had negative effects on the solubility of C1 and C1C2, which tend to precipitate when left at RT. Thus, C1C2, C1, and mutants were ordered with TEV cleavage sites to circumvent this problem. TEV optimizations were completed for both C1C2 and C1, with equal success as rEK cleavage

### Antibody purification:



**Figure 19.** Pre and post AOE expression of B136 anti-C1 inhibitor. Development of a yellow solution is an indication of proper growth and expression of hybridoma cells.

highly pure antibodies (Figure 20).

Antibody production was attempted with anti-C1 mAbs 2A9, B136, and M6143. Hybridoma cells containing the murine IgG<sub>2ak</sub> “Group B” B136 and “Group A” 2A9 were successfully cultured and expressed. Murine hybridomas were cultured in Medium E, a fetal bovine serum (FBS) containing media, and passaged into a recombinantly derived AOE media which lacked antibody contamination from the FBS. Cells were retained in MedE until peak viability (>95%, 50-60% confluence) before being transferred to AOE. Expression was tracked by exhaustion of resources and production of acid byproduct, which turned the indicator from red/pink to a yellow/orange (Figure 19). Media was diluted with HBS to maintain ionic strength of media and purified with protein A resin, which binds to IgG<sub>2ak</sub> antibodies. 2A9, an inhibitory class II antibody, expressed extremely well, yielding around 5 mg per 45 mL expression prep whereas B136 expressed 10-fold lower per 45-mL prep. Purifications via ion exchange chromatography resulted in co-elution of impurities, whereas Protein A (or G) yielded

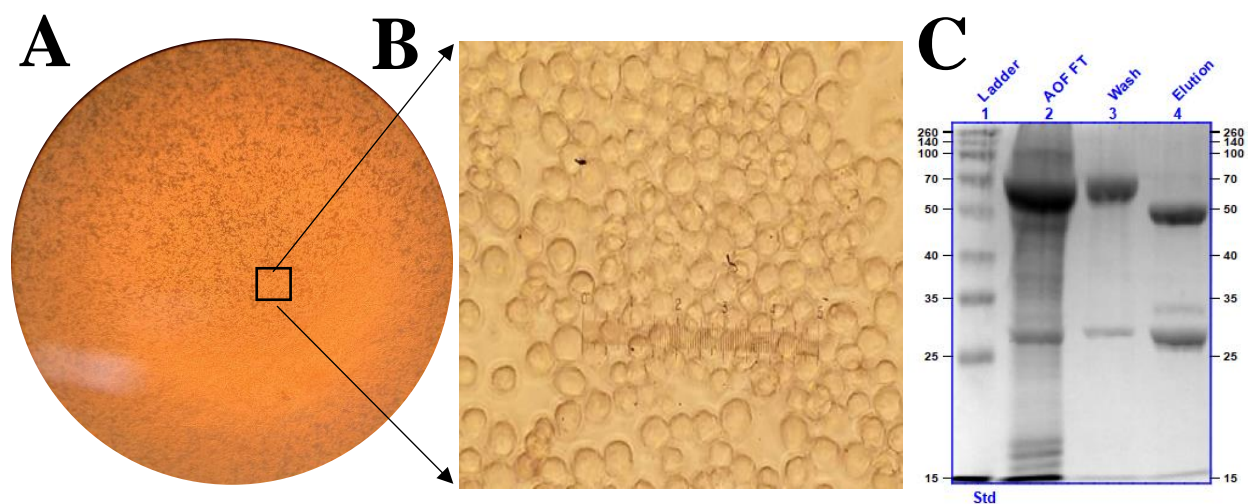


**Figure 20.** Hybridoma cells and expression verification. A.) Hybridoma cells viewed at 10x zoom. B.) Hybridoma cells viewed at 200x zoom (95%) confluence. C.) Purification of B136 by Protein A. Two bands at 50 and 25 kDa in Lane 4 are characteristic of antibodies in reducing denaturing conditions.

### *ELISA measurements*

Membrane-binding ELISA measurements with WT C1, C2, and C1C2 were accomplished to assess PS phospholipid binding. Hydrophobic plates were coated with an 80:20 molar composition of DOPC:DOPS lipids to mimic the activated platelet environment and performed in triplicate. HRP chelated to Ni-NTA was used to bind to the hexa-histidine linker and ABTS was added as the colorimetric agent. Apparent equilibrium dissociation constants ( $K_D$ ) for WT C1C2, C1, and C2 were  $80.91 \pm 18.58$  nM,  $3447 \pm 1330$  nM, and  $3327 \pm 2036$  nM, respectively, in HBS ( $R^2$ : 0.96, 0.97, 0.92, respectively) (Figure 21, A). The importance of electrostatic interactions had been previously documented in Novakovic et al. from 2011, which show that the C2 domain of fVIII lipid binding properties was disrupted with the addition of high salt. ELISA's of the C1 and C1C2 fusion constructs in increasing amounts of salt demonstrate a negative correlation between salt and  $K_D$ , which concur with previous studies (Figure 21, B).

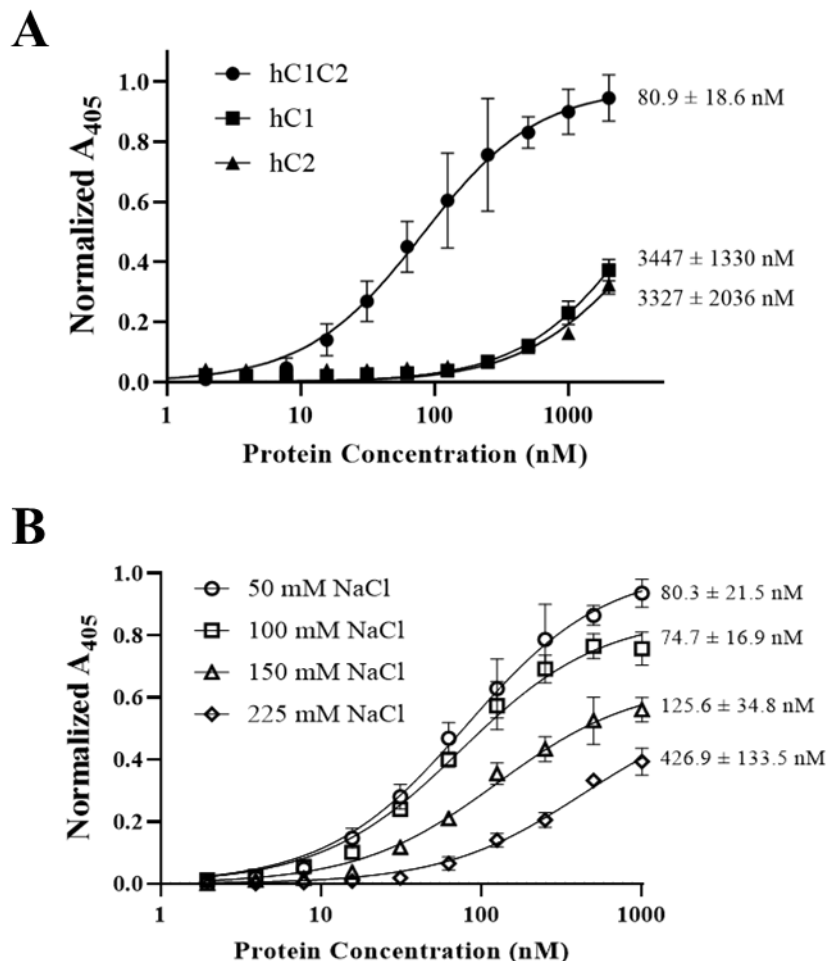


**Figure 21. ELISA results of fVIII C domain Trx-fusion constructs binding to phosphatidylserine coated plates.** A.) Comparison of hC1C2-Trx (closed circle), hC1-Trx (closed square), and hC2-Trx (closed triangle) to 20% PS/ 80% PC in TBS B.) Comparison of fVIII C1C2 construct affinity to phospholipids in 50 mM (open circle), 100 mM (open square), 150 mM (open triangle), and 225 mM (open diamond) sodium chloride. Bound Trx-C domains were detected with Ni-NTA-HRP, and bound HRP was probed with ABTS with color development detection completed at 410 nm.

### *Sedimentation assays*

Preparation of unilamellar vesicles (UV's) were properly formed following basic unilamellar extraction protocols. Initial tests of ET3i at 400 nM total protein concentration in HBS with 100 mM NaCl demonstrated complete retention in the pellet of 80:20 DOPC:DOPS

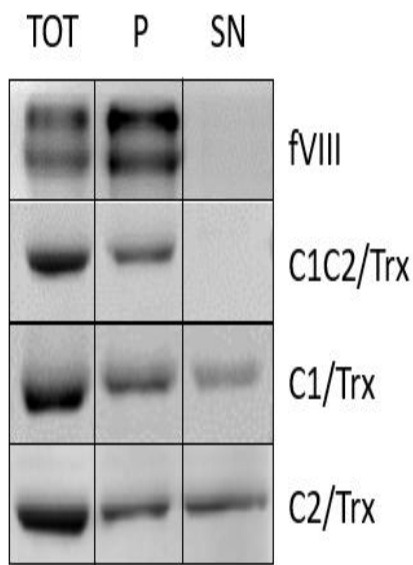


**Figure 22. Sedimentation of fVIII and isolated C domain constructs.** ET3i and C1, C2, and C1C2 were incubated with 80:20 DOPC:DOPS lipid vesicles, sedimented, and separated into Supernatant (SN) and pellet (P) fractions. Total corresponds to the 100:0 DOPC:DOPS control run concurrently with each construct.

UV's and zero retention with 100:0 DOPC:DOPS UV's (Figure 22). In similar conditions, complete retention on the 80:20 DOPC:DOPS UV was recorded for WT C1C2 construct with slight retention in the pellet of 100:0 DOPC:DOPS UV's. Both C1 and C2 fusion constructs demonstrated ~60% retention in the 80:20 DOPC:DOPS UV's at 5  $\mu$ M total protein concentration, which is expected based on the  $K_D$  of WT C1 and C2 ELISA data.

The power of this assay was probed by pre-incubating WT C1 and ET3i with anti-C1 and anti-C2 inhibitors, respectively, to replicate ELISA data that has been previously published (Figure 23). As previously, WT C1 demonstrated ~60% retention when incubated with DOPC:DOPS UVs compared to 100% retention of ET3i to DOPC:DOPS UVs.

Pre-complexing C1 or ET3i with B136 led to complete loss of binding and 50% reduction in binding, respectively (Figure 22). This relationship was similarly observed for 3E6 and ET3i, which had been previously demonstrated to completely disrupt phospholipid binding properties of C2. Antibodies 2A9 and G99, both which are classified as non-classical inhibitors, showed near identical sedimentation retention results as WT.

Mutational sedimentation assays were performed at 4  $\mu$ M for C2 domain containing mutations at 100 mM NaCl to mimic physiological conditions. Residues of interest were based on the working binding model of C2 to platelets derived from the C2:G99:3E6 ternary complex and

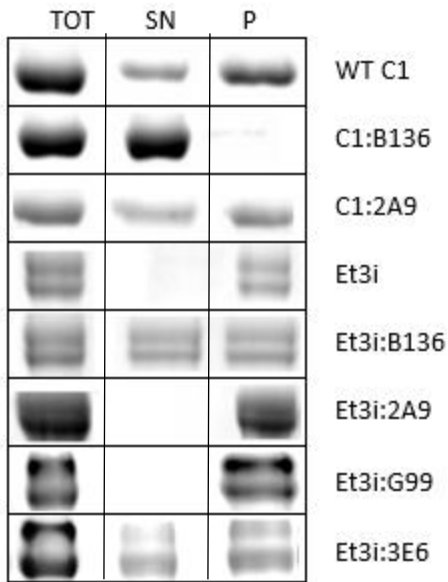


**Figure 23.** Inhibitor disruption of phospholipid binding using isolated C1 and E3ti. Isolated C1 and ET3i were pre-incubated with classical (3E6 and B136) and non-classical (2A9 and G99) inhibitors and sedimented in the presence of 100:0 and 80:20 DOPC:DOPS lipid vesicles. Total corresponds to the complete DOPC control.

mutations correlated with hemophilia A from the CHAMP database. Namely, basic residues K2183, D2187, R2215, and R2320 are postulated to interact with the negatively charged PS head groups of activated platelet membranes, while residue K2227 was a control mutation made as K2227 does not interact with lipid membranes as it sits within the G99 epitope. A2201P has been reported to have a detrimental effect on lipid binding, and sedimentation assays compared to WT C2 demonstrate a reduction in pellet retention from 70% to 18% (Figure 24). Mutations to R2215 and R2320 significantly reduced binding to 22.8% and 14%, respectively, with P-values of 0.001 and <0.001, respectively ( $\alpha = 0.05$ ). The D2187A mutation was significant in reducing binding compared to WT (P-

value: 0.041) whereas control mutation K2227A and K2183A showed similar retention as WT C2.

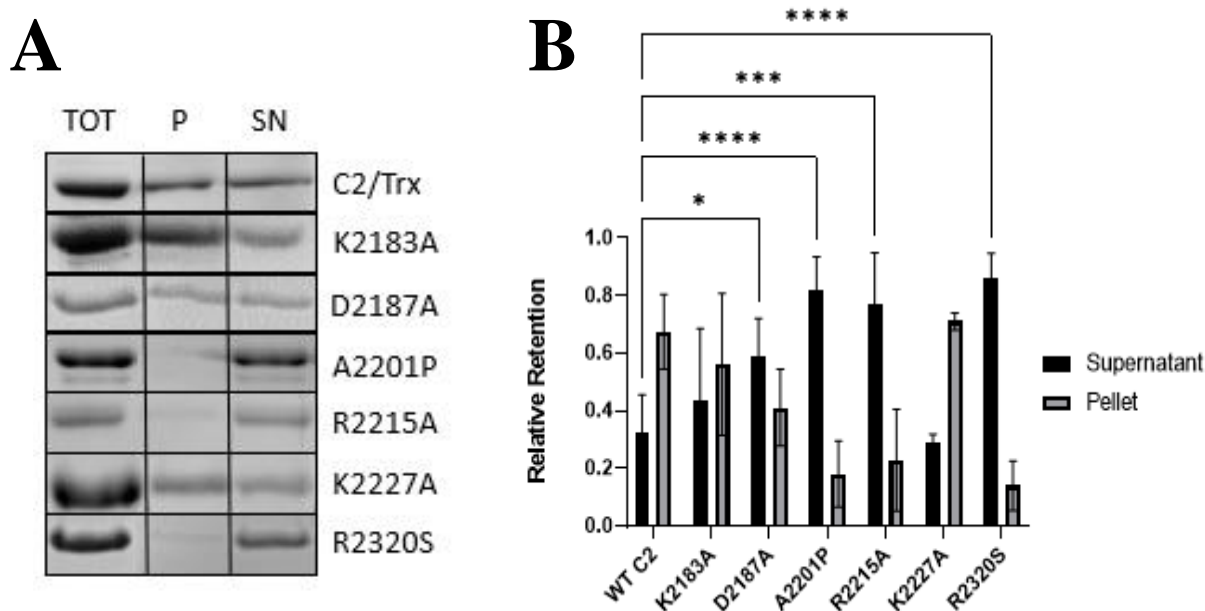


**Figure 24. C2 mutational sedimentation assay and analysis. A.) C2 domain point mutations binding to 100:0 and 80:20 DOPC:DOPS lipid vesicles. B.) Sedimentation assays of C2-Trx and various C2 domain point mutations with 80:20 DOPC:DOPS lipid vesicles. Total corresponds to the SN of 100% PC vesicles. C.) Quantitation of liposome binding assay from Panel B. SN denotes the supernatant and P the pellet. A two-way ANOVA comparing each mutant to WT C2 was performed using GraphPad Prism 9.1.2, with three or more independent trials, and Dunnett's posttest. \* $p < 0.05$ , \*\*\* $p < 0.001$ , \*\*\*\* $p < 0.0001$ .**

### *Formation and Optimization of Lipid Nanodiscs*

Preparations of nanodiscs underwent numerous screening and optimizations. First, tagged-MSP1D1 and tagged-MSP2N2 were attempted to be formed following a Stoilova, et al. protocol.<sup>59</sup> Post formation SEC of MSP1D1 nanodiscs was successful with retention time shift from a 15 mL retention time for native MSP1D1 protein to a 13 mL retention time shift for formed ND. Formation of ND with tagged-MSP2N2 were unsuccessful due to impurities and little to no formation of larger peaks post gel filtration. Thus, tagged-MSP1D1 was further optimized by

varying MSP:lipid molar ratios of 1:47, 1:100, 1:200, and 1:400 (Figure 25). Single point binding of the 4 ratios was probed using anti-His<sub>5</sub> BLI tips by loading 800 nM ND and associating 800 nM ET3i (Table 4). The 1:200 molar ratio peak demonstrated the lowest  $K_D$  at 83.5 nM and was utilized as the MSP1D1:lipid ratio for further optimizations.

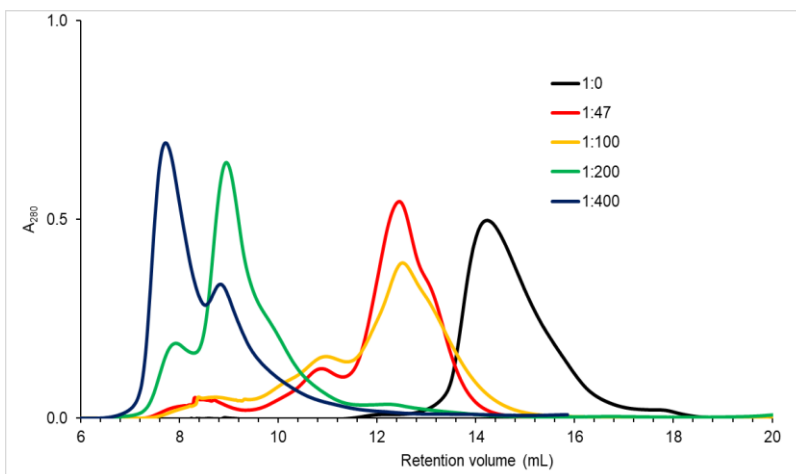


**Figure 25. MSP1D1 SEC chromatograms of nanodisc formation at varying MSP:lipid ratios.** MSP1D1 ND were injected in 0.5 mL samples volumes onto a S75 SEC at 0.3 mL/min. Peaks before 8 mL are within the “dead volume” and are not separated.

Further optimizations were investigated by changing the lipid composition to include various DOPS:DOPC:DOPE ratios. The 20:80:0 ratio reported the lowest single point  $K_D$  when compared to 60:30:10 and 70:15:15 ratios (Table 5). After optimizations with tagged ND revealed that 1:200 and 80:20 DOPC:DOPS ratio was the optimal combination, MSP1D1 was cleaved by the addition of TEV and purified according to established methods. The cleaved MSP1D1 was

**Table 4. Binding kinetics of ET3i to different MSP1D1 ND lipid ratios.** All molar compositions were 80:20 DOPC:DOPS.

Sample	$k_a$ (1/M*s)	$k_d$ (1/s)	$K_D$ (nM)
1:0	ND	ND	ND
1:47	$1.61 \times 10^5$	$1.64 \times 10^{-2}$	102
1:100	$2.53 \times 10^5$	$4.62 \times 10^{-2}$	183
1:200	$1.00 \times 10^5$	$8.37 \times 10^{-3}$	83.5
1:400	$1.04 \times 10^5$	ND	ND

formed and subjected to SEC purification, where a single, monodisperse peak of 9 mL retention time was observed. Large scale nanodiscs formation was attempted in 2 mL reactions compared to 0.5 mL reactions, but noticeable heterogeneity was observed (Figure 26).

**Table 5. Binding kinetics of ET3i to 1:200 MSP1D1 ND with varying phospholipid compositions.** Peaks 1 and 2 refer to Figure 25.

Sample	$k_a$ (1/Ms)	$k_d$ (1/s)	$K_D$ (nM)
20:80:0 (Peak 1)	$1.7 \times 10^5$	$8.6 \times 10^{-3}$	50
20:80:0 (Peak 2)	$1.6 \times 10^5$	$9.5 \times 10^{-3}$	58
15:70:15 (Peak 1)	$1.7 \times 10^5$	$1.1 \times 10^{-3}$	67
15:70:15 (Peak 2)	$1.2 \times 10^5$	$1.5 \times 10^{-2}$	132
30:60:10 (Peak 1)	$1.5 \times 10^5$	$1.8 \times 10^{-2}$	128
30:60:10 (Peak 2)	$1.0 \times 10^5$	$1.8 \times 10^{-2}$	182

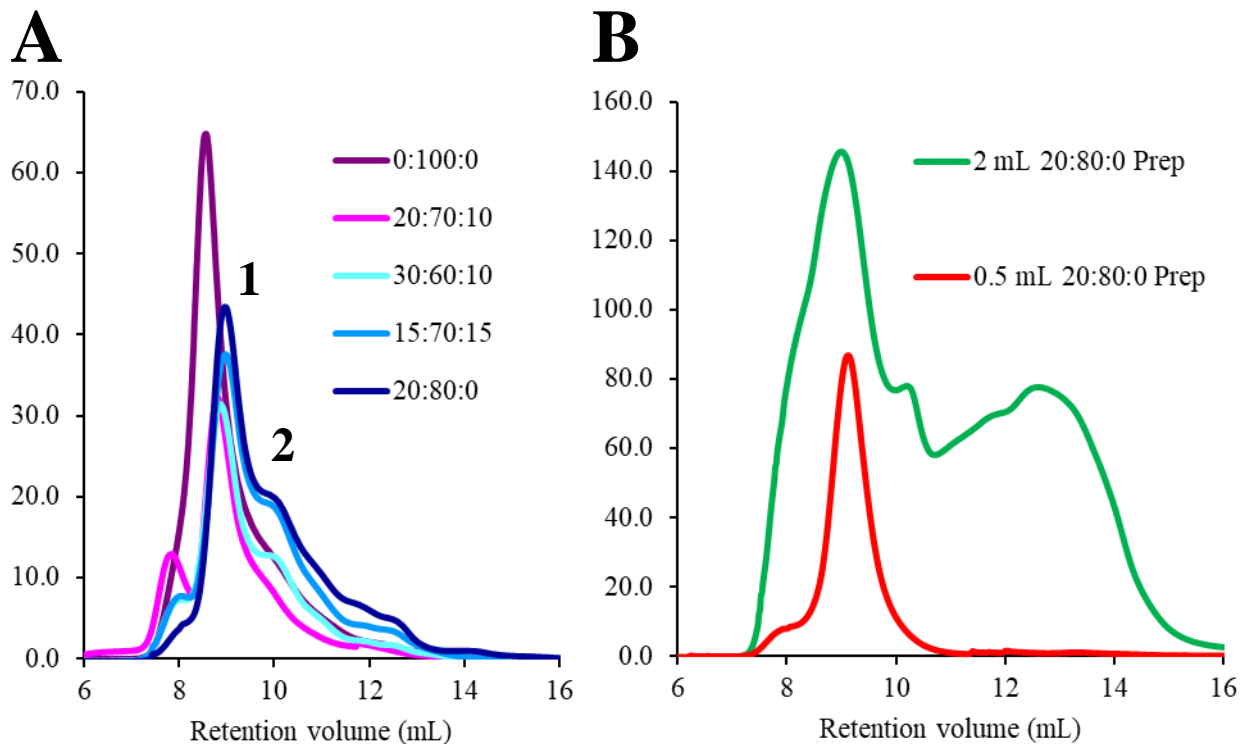


**Figure 26. SEC chromatograms of Nanodiscs formation optimization.** A.) SEC chromatograms of MSP1D1 ND formed at varying DOPS:DOPC:DOPE ratios. Peaks 1 and 2 correspond to fractions tested for optimal fVIII binding. B.) Volume trials for improving ND yield. Increasing the volume of ND preps lead to the emergence of numerous peaks.

Binding to cND was verified utilizing a mouse derived anti-human A2 domain mAb 1D4 pre-complexed with ET3i. The A2 domain is the most distally positioned fVIII domain in relation to the C domains. Binding of ET3i to an anti-A2 domain inhibitor immobilized on a BLI sensor would position the C domains away from the biosensor tip, maximally exposing the two lipid binding domains. Anti-A2 inhibitor 1D4 and ET3i were pre-complexed, loaded onto anti-mouse antibody capture biosensors (AMC) and associated to cleaved ND at 800 nM. Binding extrapolated from a triplicate; single concentration trial yielded a  $K_D$  of 50 nM (Figure 27). When 100% DOPC containing cND was tested against the ET3i:1D4 complex, no association was measured.

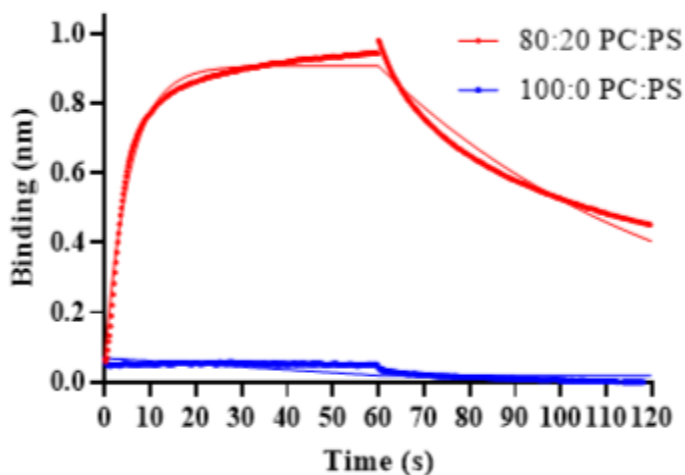


**Figure 27. Cleaved MSP1D1 binding verification via BLI.** ET3i was pre-complexed with A2-inhibitor 1D4, bound to AMC tips, and incubated with cND at 800 nM. Triplicate association and dissociation trials were normalized and reveal minimal binding to 100% DOPC cND and nanomolar affinity to 80:20 DOPC:DOPS cND.

$\text{min}^{-1}$ , respectively, for a  $K_D$  of  $8.9 \pm 7.2$  nm. The  $K_D$  for R2163S and R2320S were  $1.4 \pm 0.031$   $\mu\text{M}$  and  $2.9 \pm 0.015$   $\mu\text{M}$ , respectively. The apparent affinity of both R2163S and R2320S was 160-fold and 326-fold lower, largely in part to a faster dissociation rate ( $0.055 \pm 0.0042$   $\text{min}^{-1}$  and  $0.24$

Binding kinetics for WT C1C2, R2163S, R2320S, and R2163S\_R2320S were calculated by loading 800 nM C1C2 complex onto an anti-His<sub>5</sub> biosensor and associated against serially diluted cND from 4500 nM to 6.25 nM (Table 6). Association and dissociation rate constants for WT C1C2 were  $1.5 \times 10^5 \pm 1.6 \times 10^3$   $\text{min}^{-1}\text{M}^{-1}$  and  $1.3 \times 10^{-3} \pm 5.6 \times 10^{-4}$

$\pm 0.012 \text{ min}^{-1}$ , respectively). This indicated that mutations to R2163 or R2320 not only disrupted binding to cND compared to WT, but that single point mutations resulted in  $K_D$  values identical to WT isolated C1 and C2 ( $3.4 \pm 1.3 \text{ }\mu\text{M}$  and  $3.3 \pm 2.0 \text{ }\mu\text{M}$ , respectively). Point mutations at both R2163 and R2320 in the same construct were accomplished with minimal above background binding observed at the highest ND concentration attempted (Figure 28).

**Table 6. Apparent binding kinetics and affinities of fVIII C1C2 mutations with lipid nanodiscs.** Data represents the average of three or more independent experiments with a 95% confidence interval. WT C1C2, R2163S, R2320S, and R2163S/R2320S double mutant were associated to an anti-His5 BLI sensor and associated to cleaved nanodiscs.  $k_{on}$ - rate of association,  $k_{off}$ - rate of dissociation,  $K_D$ -dissociation constant ( $k_{off}/k_{on}$ ).

	$k_{on}$ ( $\times 10^4 \text{ M}^{-1}\text{s}^{-1}$ )	$k_{off}$ ( $\times 10^{-3} \text{ s}^{-1}$ )	$K_D$ (nM)
<b>WT</b>	$14.7 \pm 0.16$	$1.31 \pm 0.56$	$8.93 \pm 7.2$
<b>R2163S</b>	$3.81 \pm 0.21$	$54.8 \pm 4.2$	$1,440 \pm 31$
<b>R2320S</b>	$8.23 \pm 0.38$	$241 \pm 12$	$2,900 \pm 15$
<b>R2163S/R2320S</b>	ND	ND	ND

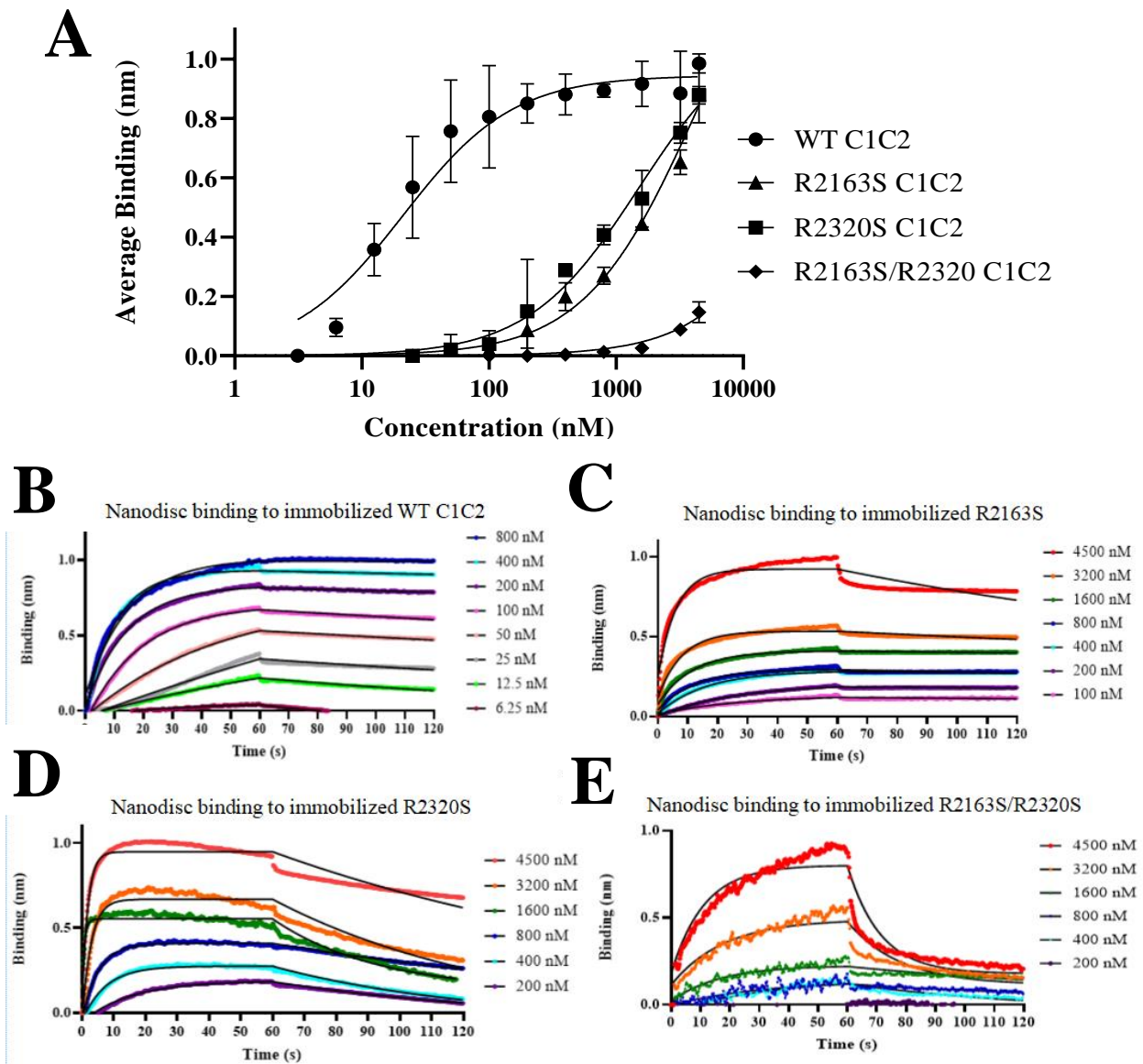


**Figure 28.) Bio-Layer interferometry binding measurements of fVIII C1C2 domain mutations to cleaved nanodiscs.** A.) Average association binding for bound WT C1C2 (closed circle), R2163S C1C2 (closed triangle), R2320S C1C2 (closed square), and R2163S/R2320S C1C2 (closed diamond) with cleaved 80:20 PC/PS 1:200 MSP1D1 ND and baseline was established from 100% PC 1:200 cleaved MSP1D1 ND. C domain loading onto the tips was step-corrected, normalized using Excel, and graphed on GraphPad Prism 9.1.2. Raw normalized binding curves for B.) WT C1C2, C.) R2163S, D.) R2320S, E.) R2163S/R2320S.

## OPS:C2 crystal structure

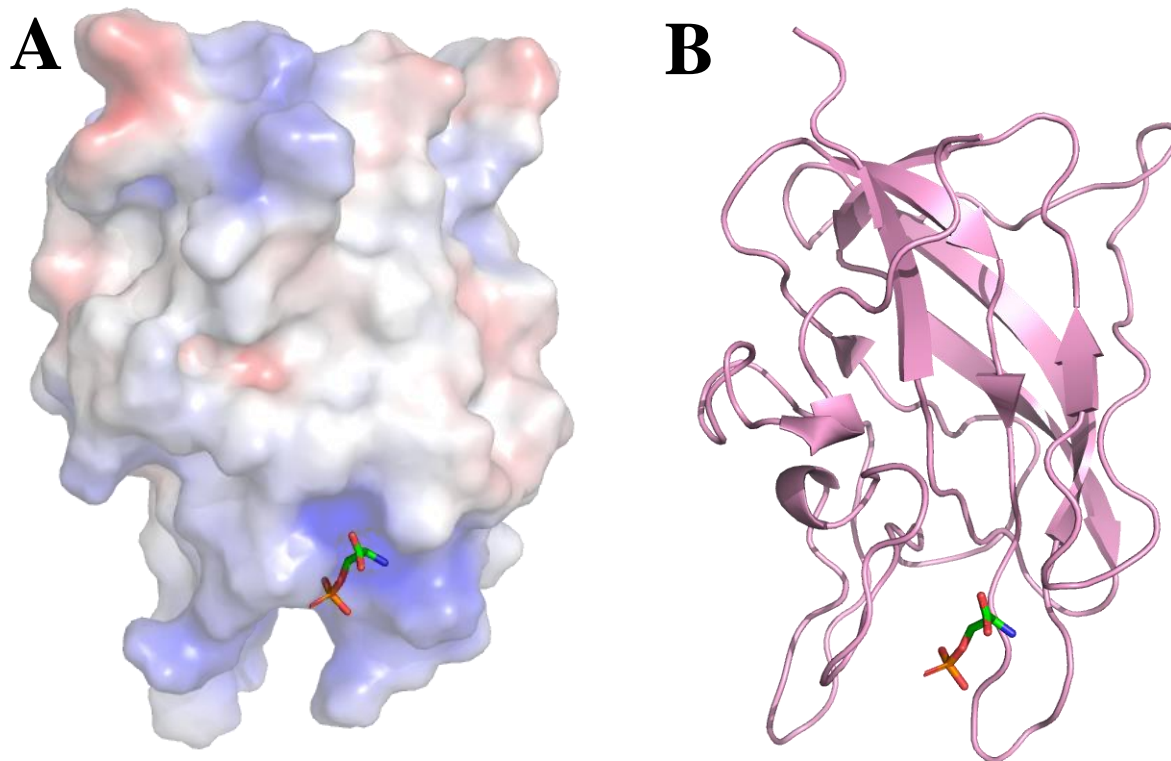
The porcine fVIII C2 domain was crystallized, soaked with the headgroup of phosphatidylserine (OPLS), and X-ray diffraction data was collected at the ALS beamline by previous Spiegel lab members. The structure of pC2 bound to OPLS was phased and refined to 1.3Å resolution, which provides high resolution insight into the basic residues that may interact with phosphatidylserine containing lipids on activated platelet membranes (Table 7). Alternate conformation modeling was done by modeling two hydrophobic loops separately and manually modifying the PDB file to incorporate two distinct conformations, which was then subjected to multiple rounds of refinement (Figure 29). OPLS was placed into the pC2 crystal using Ligand fit and refined in real space until the correlation coefficient could not be improved. Final refinements with water molecule, OPLS, and multiple conformations resulted in a final pC2 crystal with model refinement statistics of  $R_{\text{factor}}$  ( $R_{\text{work}}$ ) and  $R_{\text{Free}}$  of 0.1354 and 0.1570, respectively.  $R_{\text{factor}}$  values below 0.2 confers a high-quality model (Brunger 1992) and a  $R_{\text{work}}/R_{\text{free}}$  ratio less than one indicates a non-biased model based on x-ray fitting. The C2:OPS structure was submitted and deposited into the protein data bank (PDB) under the code S70P.

**Table 7. X-ray data collection and model refinement statistics.**

---

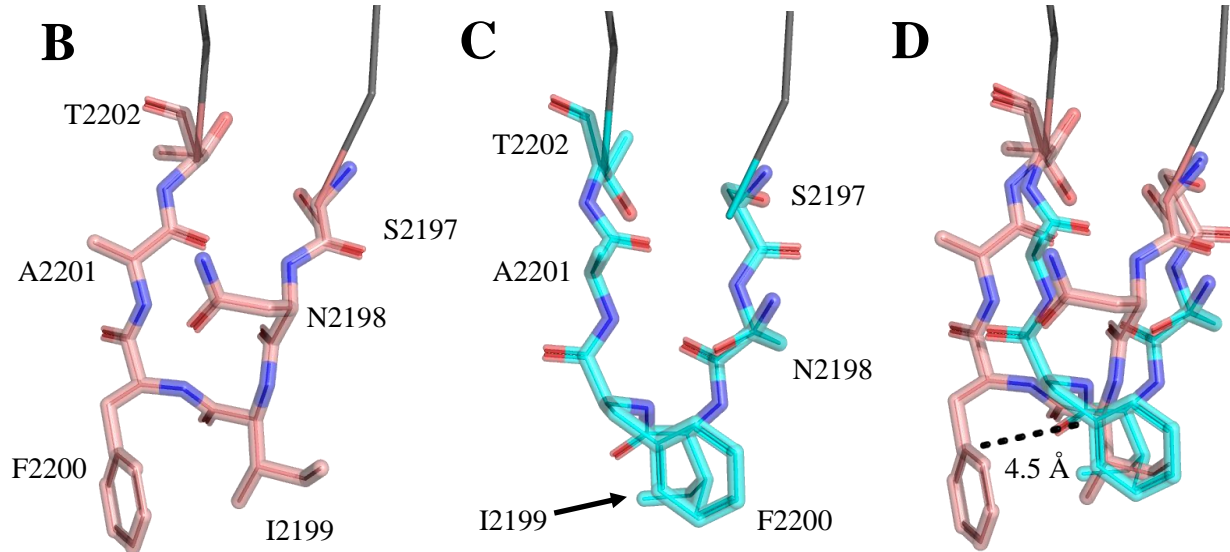
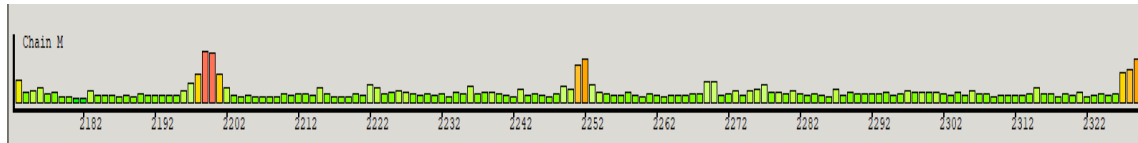
<b>X-ray data statistics</b>	
Wavelength (Å)	1.00 Å
Resolution range (Å)	44.53 - 1.3 (1.346 - 1.3)
Space group	I 2 2 2
Unit cell (Å)	a = 49.1, b = 68.3, c = 106.0
Total reflections	85226 (6517)
Unique reflections	42675 (3297)
Completeness (%)	96.54 (75.65)
Mean I/sigma (I)	18.77 (2.33)
R <sub>pin</sub>	0.01354 (0.2791)
<b>Model refinement statistics</b>	
R <sub>factor</sub>	0.1354 (0.2106)
R <sub>free</sub>	0.1570 (0.2308)
<b>Number of Atoms</b>	
Protein	1544
Water	182
Protein residues	157
RMS bonds (Å)	0.007
RMS angles (°)	1.07
Ramachandran favored (%)	93.55
Ramachandran outliers (%)	0.00
Rotamer outliers (%)	1.95
<b>Average B-factor (Å<sup>2</sup>)</b>	
Protein	20.25
Solvent	30.17

---



**Figure 29. Porcine C2:OPS crystal structure.** C2 crystals were grown via hanging drop vapor diffusion and soaked in 10 mM OPS. A.) Electrostatic surface map of the C2:OPS crystal structure. OPS is situated within the most basic cleft on the C2 domain. B.) Ribbon diagram of C2:OPS. PDB (S70P).

The structure of C2 aligns with previously published structures of the C2 domain, containing 2 solvent exposed hydrophobic loops and a  $\beta$ -barrel motif. Previous literature mentions inherent flexibility of the solvent exposed hydrophobic loops on the basal surface of the C2 domain.<sup>60</sup> Within this data set, poor density was observed within the N-terminal, C-terminal, and two solvent exposed, hydrophobic loops of C2 (Figure 30, A). The loops pertain to S2197/T2202 and L2251/L2252, which have both been corroborated as loops involved in phospholipid binding. Despite the poor density, two loop conformations were manually modeled for the S2197/T2202 loop. Refinement placed equal weight between the two conformations, resulting in a 4.5 Å shift between both present F2200 sidechains (Figure 30, B-D).

**A**

**Figure 30. Flexibility of fVIII C2 domain solvent exposed loop.** A.) Density fit validation of the C2:OPS structure in WinCoot. Green indicates excellent fit of the structure into diffraction density and red indicates poor density fit B.) Alternate conformation 1 of the 2197-2202 loop. C.) Alternate conformation 2 of the 2197-2202 loop. D.) Overlay of the 2197-2202 loop conformations.

Modeling of the OPLS residue was utilized to investigate basic residues involved in binding to PS head groups during clotting. Placement of OPLS into positive density positioned it within 3.2 Å of R2320, 3.3 Å of S2289, 3.1 Å of N2217, and 3.4 Å within Q2213 (Figure 31). In this structure, the R2320 and Q2213 residues contact the carboxylate of OPLS whereas N2217 seems to bind to the phosphoric acid moiety. Placement of OPLS extends distally between protruding hydrophobic loops L2209-G2214 and S2250/S2253. This offers structural evidence to support the working binding based on the classical epitope. Along with mutational data, structural data suggests the R2320 resides makes an essential contact with PS headgroups and is critical to factor fVIII function.

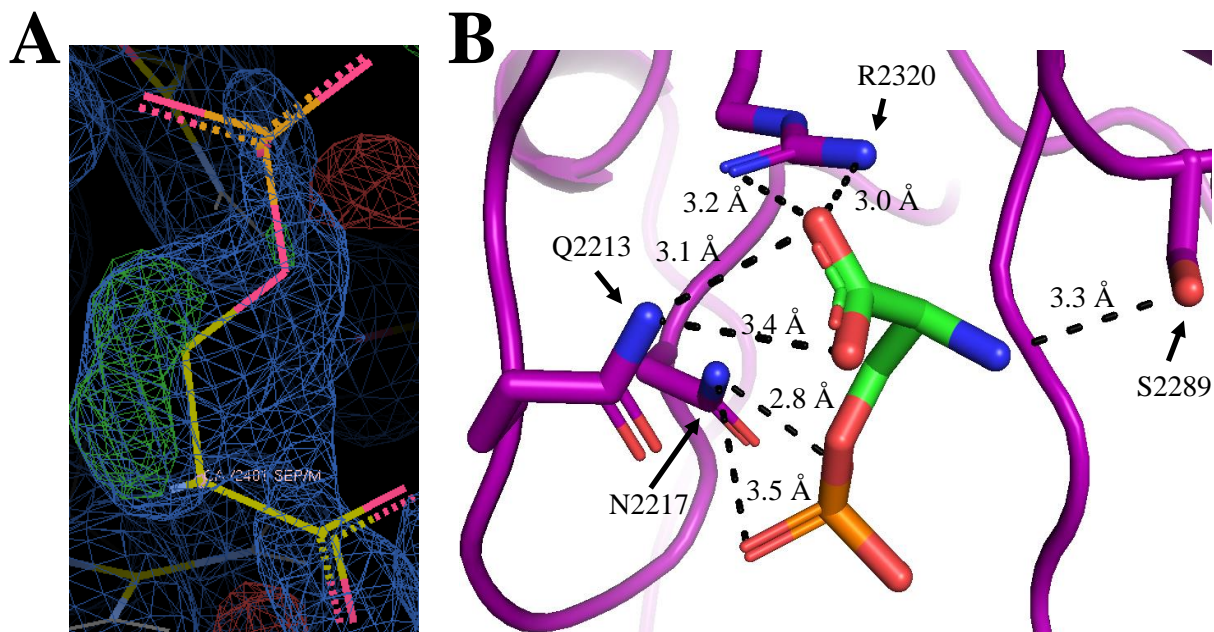


**Figure 31. OPLS fitting and crystal contacts.** A.) WinCoot density placement of OPLS within the C2 crystal structure. Blue density represents accounted for density within the density map. B.) Intermolecular contact between OPS and C2. R2320, S2289, N2217, and Q2213 make ionic interactions with the OPS molecule.

## Chapter 4: Discussion

The C domains of fVIII facilitate membrane binding onto activated platelet surfaces during the formation of key coagulation complexes. Initial binding models proposed for the C domains to platelet membranes focused on the C2 domain due to the ample amount of structural information present. Within the C2 domain, two hydrophobic, solvent exposed loops imbed into the anhydrous interior of the platelet bilayer, anchoring C2 to the surface. This observation has been corroborated through mutational and structural studies from numerous labs.<sup>54,60-62</sup> Although these interactions have been supported, hydrophobic fVIII membrane association is proposed to have a complementary role with basic residues surrounding the hydrophobic loops. Phosphatidylserine concentration is upregulated during platelet activation and studies have suggested that fVIII contains an OPLS specific binding region that mediates tight association.<sup>53</sup>

C2 domain binding models collectively support the embedding of two hydrophobic loops into the anhydrous interior of lipid membrane, but models deviate on which basic residues interact with the platelet surface. The first detailed model proposed K2227 as an important basic residue contact for lipid binding.<sup>45,46</sup> This complementary interaction, however, was brought into question after structural information placed the K2227 residue within the “non-classical” epitope, which disrupts Tenase complex formation by preventing the formation of the fVIIIa:fIXa interface but not phospholipid binding.<sup>63</sup> This data suggested that the “non-classical” epitope must face away from the lipid surface and K2227 could not be involved in lipid binding. The “classical” epitope face was resolved within the same structure and subsequently utilized to modify the orientation of C2 within the binding model. Within this inhibitor informed model, the C2 domain was rotated ~130 degrees around a central axis, placing the “classical” epitope within contact of the negatively

charged platelet surface. The updated binding model was centered upon C2 domain residue 2320, which is the most basic residue of the C2 domain based on electrostatic surface calculations (Figure 32). This updated model provided an avenue to structural and mutationally verify the binding model.

The crystallization of C2

with OPLS revealed a high-resolution snapshot of basic residues involved in lipid binding. The conserved R2320 residue made direct contact with OPLS at 3.0 and 3.2 Å, forming the main salt bridge interaction with the head group of phosphatidylserine. Based on the orientation of the OPLS moiety, interactions with Q2213 and N2217 appear to be involved but are hypothesized to play a stabilization role in binding to the PS headgroup. This binding of R2320 to OPLS provides direct structural confirmation of the inhibitor influenced model detailed in Brison et al. Compared to previous crystal structures of porcine C2 domain (PDB: 4MO3), there are minimal differences between structures with an RMSD of 0.052, with difference between structures present in highly flexible regions of C2: the N-terminus, C-terminus, and hydrophobic solvent exposed loops.

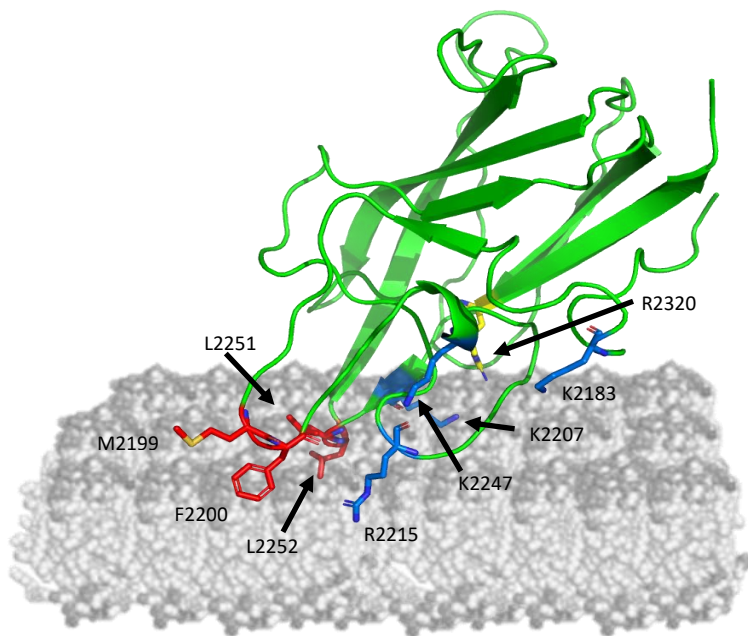


**Figure 32. Updated activated platelet binding model of the fVIII C2 domain.** The model situates hydrophobic residues inside the anhydrous interior of the platelet bilayer and positions solvent exposed basic residues in proximity to phospholipid head groups. The model was centered around R2320 (yellow) as the principal residue. PDB: 6MF0.

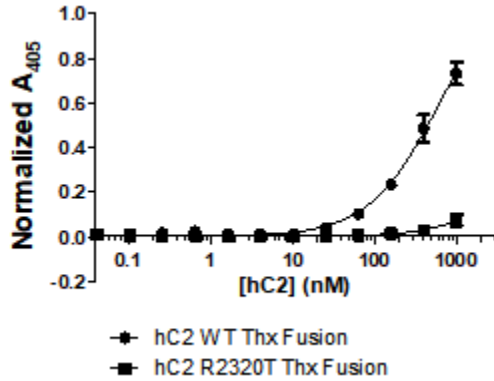


**Figure 33. ELISA of WT C2 and R2320S binding to phospholipid coated surfaces.** Non-linear fit was accomplished using GraphPad Pro.

Preliminary mutational data was completed for C2 residues R2320 and R2215, which both were proposed to make direct interactions with the phospholipid surface. ELISA assays completed for C2 R2320S inhibited binding to phospholipid coated plate compared to WT C2 with no detectable  $K_D$  and 1600 nM, respectively (Figure 33). Intrinsic fluorescence of the R2320S mutation was accomplished by a previous graduate student, which demonstrated a slight decrease (2.3 kJ/mol) in stability compared to WT. This  $\Delta G_{H20}$ , although different, is likely not significant and suggests that WT and R2320S may have similar tertiary structures. Even though this data suggested the relationship of R2320, it is difficult to completely presume the relationship as both C domains of fVIII have been postulated to have similar roles in phospholipid binding. Even so, models generated utilize the C2 domain alone. Expression of fVIII is troublesome because it contains three heavily glycosylated A domains that require mammalian cell vectors for proper folding and expression to occur. Thus, to circumvent this problem, the C1C2 construct was pursued to obtain an *E. coli* expressible construct that mimics fVIII physiological binding affinities.

Previous attempts at the expression of a C1C2 construct have been attempted by other labs.<sup>64</sup> Published expression of C1C2 has exclusively occurred in the insoluble fraction during *E. coli* preparations. This data supports previous attempts to express the isolated C1 domain, which was unsuccessful to achieve outside of the insoluble fraction. Circumvention of this problem was achieved by expressing the C1C2 and C1 domains with a Trx solubility tag in a modified SHuffle

T7 cell line optimized to promote slow expression and proper folding of disulfide containing proteins.<sup>65</sup> Expression of C1C2 and C1 in SHuffle K12 cells allowed soluble expression of 50 kDa and 36 kDa proteins that bound to lipid membranes as expected, with  $K_D$ 's similar to fVIII and C2, respectively. Affinity of C1C2 to phospholipid treated ELISA plates in physiological conditions was 10-fold higher than literature and of the same magnitude when measured with BLI and ND. ELISA assays utilizing treatment with lipids have high background and can possibly explain the difference between current and published values. Research focusing on C2 lipid binding have demonstrated a inversely correlated relationship between C2 domain lipid affinity and salt concentration.<sup>66</sup> Utilizing the C1C2 domain, we were able to confirm this relationship with ELISA, further cementing the importance of electrostatic interactions between the C domains and PS containing surfaces.

Purification of the C1C2 and C1 domains proved to be problematic. During expression, a 70-kD contaminant co-eluted during IMAC purification regardless of stringent washes of over 50 CV. Based on the size and frequency of the 60-70 kD band, it was presumed that the impurity was most likely a chaperone. One of the most prevalent chaperones in *E. coli* is Hsp70, which is a heterodimer of 60 and 10 kDa bands. Hsp70 is presumed to bind via hydrophobic interactions, which may bind to the 1200 Å hydrophobic C1 domain interface normally sequestered by the A3 domain of fVIII. Chaperone-C1C2 containing complexes were separated and purified by addition of ATP/MgCl<sub>2</sub> or IEC at low ionic strength. Literature of the Hsp70 chaperone details how chaperone bound proteins can be released from the chaperone due to an ATP-induced conformational change within Hsp70 upon binding of ATP.<sup>67</sup> Moreover, hydrophobic interactions have a correlated relationship with salinity of solution, where hydrophobic interactions are strengthened in high salt conditions. Thus, removal of salt by IEC may have reduced the strength

of chaperone binding in hydrophobic areas and allowed purification of C1 and C1C2 constructs. Furthermore, the presence of a 6-fold greater hydrophobic region on C1 compared to C2 might explain the amount of precipitation witnessed for C1 contain constructs versus C2.

In support of the crystallographic finding that R2320 is the central residue involved in negatively charged phospholipid binding, mutational data of C1C2 R2320S, R2163S, and R2320S/R2163S demonstrate disruption of phospholipid binding. As previously mentioned, the C1 and C2 domain are believed to have a complimentary binding interaction, as WT isolated C1 and C2 domains bind with ~100-1000 fold lower affinity compared to WT fVIII.<sup>66,68,69</sup> Disruption of either R2163 or R2320 resulted in binding comparable to isolated C domain bindings, and mutation within the same C1C2 construct led to minimal binding above background. This interaction not only implicates the importance of this arginine at this position within each domain but also that hydrophobic loops alone cannot rescue binding. There appears to be no current publications that inquire about the stability and potential structural implications of mutations to different fVIII C2 domain residues. Although intrinsic fluorescence was completed for the isolated C2 R2320S mutation, no trials were completed for any C1 domain containing construct. Even so, the R2163 and R2320 residues are conserved between species and within the fV homolog, which implies the importance of these residues. In support of this OPLS interaction with both R2163 and R2320, membrane binding simulations predicted that C2 basic residues nonspecifically interact with the negatively charged lipid membrane with the exception of R2320 and R2220.<sup>57</sup> This study postulated that although there are two interactions possible, they are mutually exclusive. For the interaction of R2320 to occur with OPLS, the interaction with R2220 cannot occur. A study with full length BDD-fVIII with a R2220A mutation demonstrated that the relative specific activity of this mutation was greater than that of WT fVIII.<sup>54</sup> Moreover, simulation conducted on the C1

domain resulted with the only direct interaction corresponding to R2163. The residue in the same position of R2220 in the C1 domain is S2063, further supporting the robustness of the conserved nature of the R2320/R2163 binding interaction.

Recent improvement in full length fVIII structures has provided improved atomic structural insight into how the C1 and C2 domains are positioned relative to another.<sup>33,70,71</sup> Within one of these crystallographic data sets, two molecules of fVIII were resolved per unit cell.<sup>33</sup> Interestingly, the C2 domain in model A was oriented as previously described in literature, but model B was rotated and tilted compared to previous structures. This contrast in C2 conformations suggested that the C2 domain has inter-domain conformational states as well as the previously described intradomain conformational movement of the solvent exposed, hydrophobic loops.<sup>60,72</sup> Although suggested, no detailed model has been proposed utilizing this conformational state. Employing the 6MF0 model A and B, alignment to the C1 and A domains results in a single C1 conformation and two C2 conformations. Given that mutations to R2163 and R2320 result in abrogation of binding, the platelet surface is hypothesized to sit within contact of both of the residues. By aligning the C2:OPS structure to both C2 domains, the OPLS headgroup was utilized to create a planar orientation of the C domains to lipids that extends perpendicular to the OPLS moiety. Since the C2 domain R2320 residue shifts 9.0 Å between model A and B, two different planar models were generated to account for the possible conformations (Figure 34).

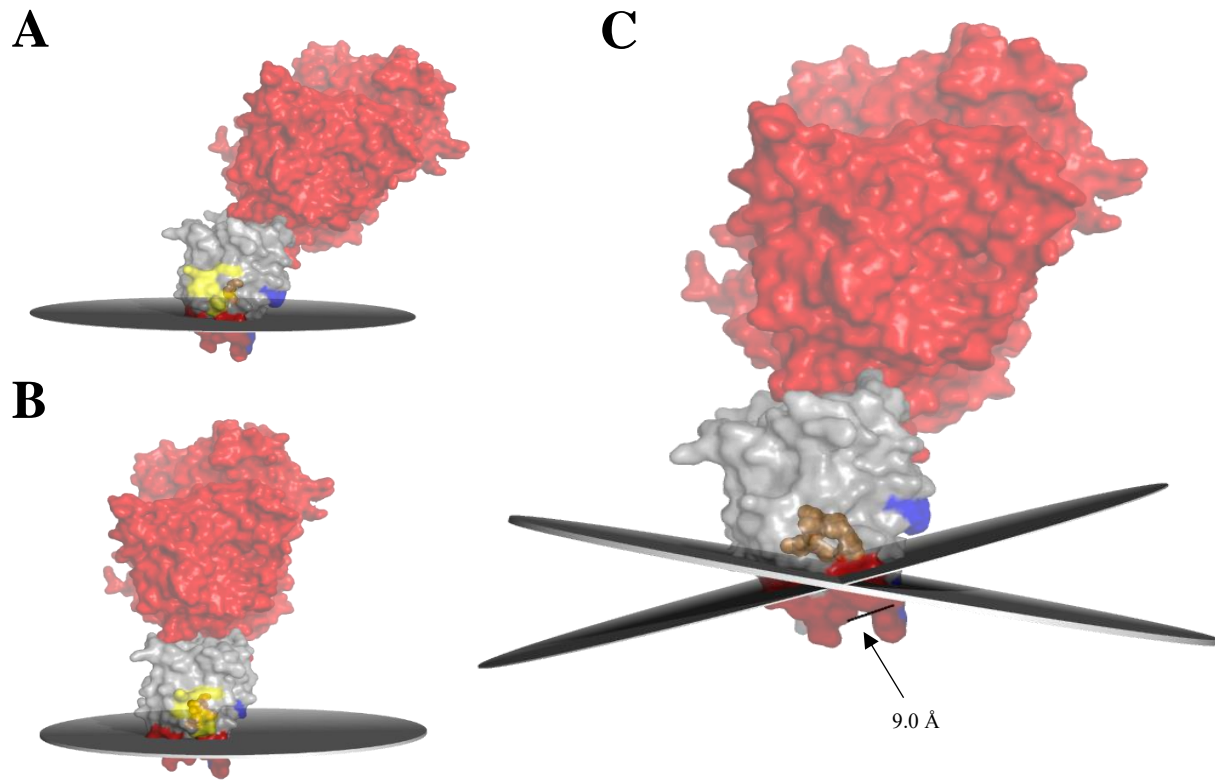


**Figure 34. Planar modeling of the fVIII Model A and Model B C2 domain orientations.** PyMOL script was used to generate a free-floating plane that passes 3.0 Å below R2320 and R2163. A.) Horizontal planar orientation of Model A. B.) Horizontal planar orientation of Model B. C.) Aligned Model A and B planar orientations. Surface coloration of fVIII domains (red: A domains, gray: C domains) and structurally defined epitopes G99, 3e6, and B02C11 (yellow, blue, dark red, respectively).

To investigate the possibility of a “correct” membrane model, epitope mapping of inhibitory C2 antibodies were utilized to reveal regions of both domains that are involved in platelet binding as well as offer insight into regions that do not interfere with platelet binding.<sup>62-64,73</sup> Alignment of G99 and 3E6, which were used in generation of the current proposed membrane model, resulted in similar orientations for both models A and B (Figure 35). Within the B model, placement of 3E6 protrudes between the C domains and appears to make contacts with the C1 domain, which has not been alluded to in literature. Regardless of the model, the G99 inhibitor extends away from the planar membrane which is expected of a “non-classical” C2 inhibitor. The 3E6 epitope itself, comprised of K2183, D2187, R2209, H2211, Q2213, and R2215, is widely

speculated to make direct contact with negatively charged lipid headgroups. Mutational data, however, indicates alanine mutations to these residues retains fVIII activity.<sup>54,74</sup> Additional hypotheses surrounding 3E6 binding disruption revolve around charge neutralization during complex formation and spatial disruption.<sup>63</sup> Within this newly proposed model, the 3E6 inhibitor extends deep into the planar membrane model, indicating that 3E6 might truly spatially displace fVIII from lipid membranes. Point mutations identified with disruption of PL binding were also

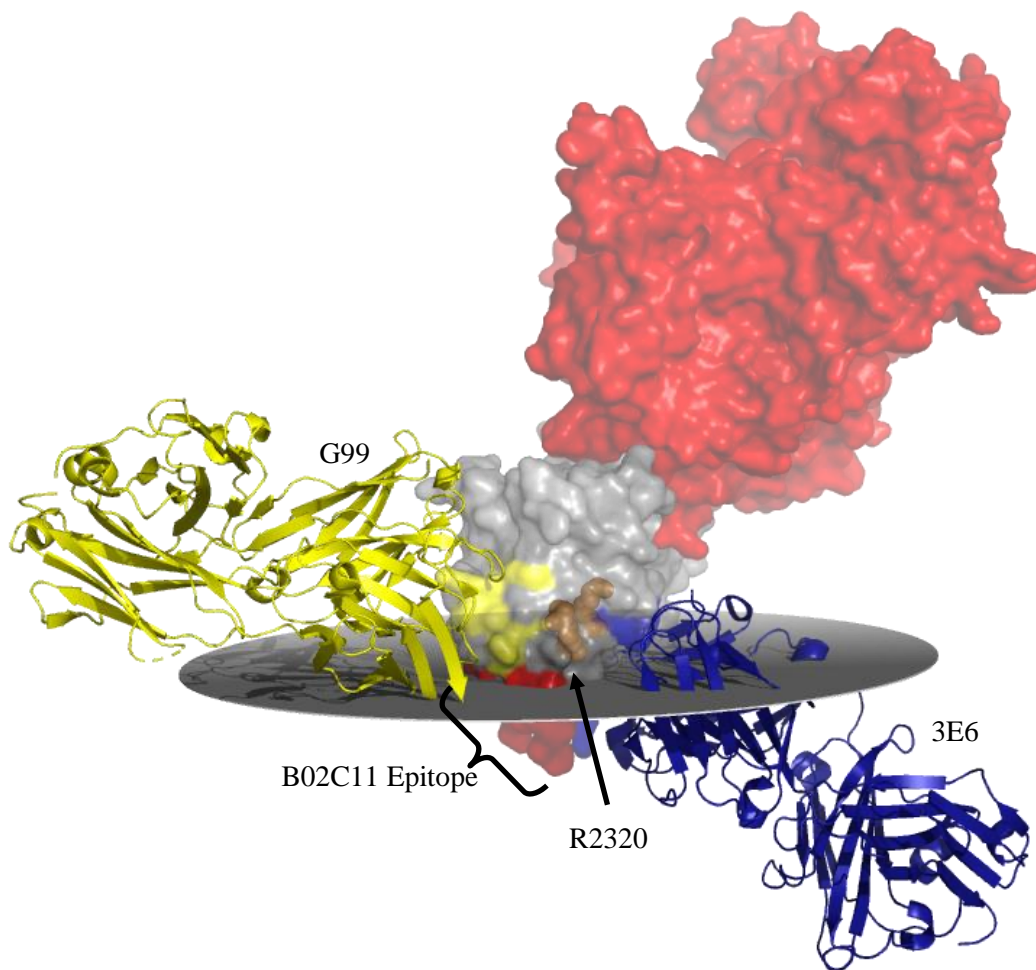


**Figure 35. Structural modeling of anti-C2 inhibitors based on fVIII planar model.** Structural depiction of Model A with anti-C2 antibodies 3E6 and G99 (blue and yellow, respectively). A domains of fVIII are shown in red, yellow: G99 F<sub>AB</sub>, blue: 3E6 F<sub>AB</sub>, orange: R2163/R2320, gray: C domains. The G99 non-classical inhibitor extends away from the surface while classical inhibitor protrudes well within the membrane surface.

highlighted within each model to validate the placement of the new model. (Figure 36). Residues W2313-H2315 are positioned at or slightly above the proposed planar membrane, justifying the proposed interaction given the high flexibility of the given region.<sup>60</sup> The two hydrophobic loops containing M2199, F2200, L2251, and L2252 are positioned well below the surface. The synonymous C1 hydrophobic loop containing K2092 and F2093 are additionally positioned below the mock membrane surface. Basic residues of interest (Q2213 and R2215), which are main contacts within the 3E6 epitope, are positioned at and well below the membrane surface, respectively. Given the highly flexible nature of the C2 domain loops and multiple conformers of arginine, it seems plausible that the R2215 residue may undergo a local conformational change in the presence of lipid membranes. Mutations documented at the 2215 position are more hydrophobic in nature (S and T) and allude to this plausibility.

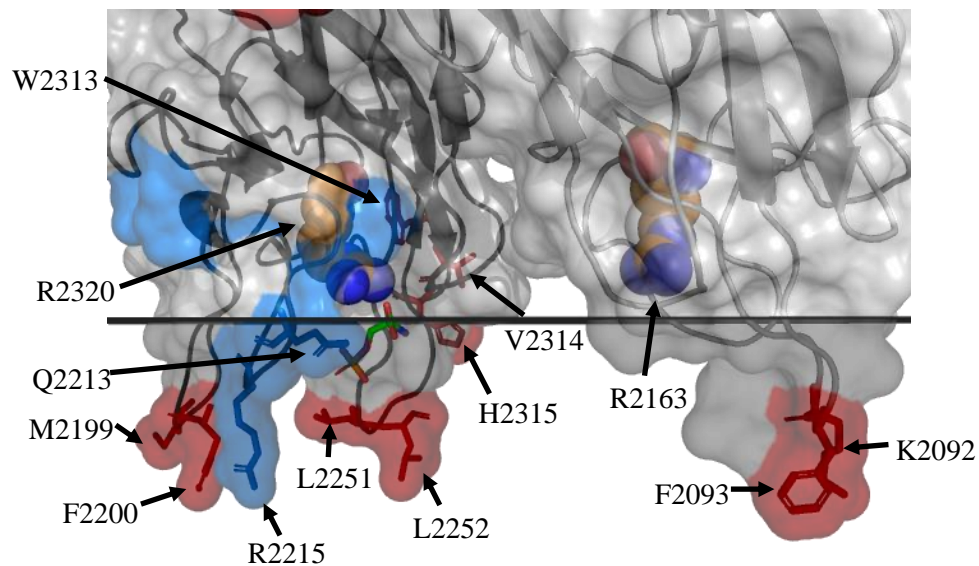


**Figure 36. Updated fVIII C domain lipid model based on mutational data.** A) Superposition of the C2:OPS structure with the A model of ET3i. Hydrophobic residues and 3E6 residues shown to impact phospholipid binding are shown as red sticks and blue sticks, respectively. The 3E6 epitope (marine) is oriented towards the phospholipid bilayer.

The main structural deviations between model A and B are the orientation of A domains in relation to the C domains and the overall tilt of the molecule. Models of fVIII lipid binding portray fVIII as a vertically ascending molecule that has the A domains stacked directly above the two C domains. This model is demonstrated in papers from Wakabayashi et al 2013, Dalm et al 2015, and Lu et al 2010. Contrary to this orientation, Model A of fVIII has the A domains shifted and tilted away from a central axis at approximately 45°. Fluorescence resonance energy transfer (FRET) studies indicate that fVIII associated to membranes tilts with an angle of 36-46 degree in relation to the membrane surface.<sup>75</sup> Based on this observation and that both C domains are oriented perpendicular to the lipid surface when modeled to interact with the two conserved R2320/R2163, the model A of fVIII seems to best portray how fVIII is oriented on lipid membranes. This model does deviate from previous models, where the C domains themselves are tilted in relation to the platelet membrane. Previous models do not take into consideration the collective placement of both C domains, as binding models are historically based on high-resolution structures of isolated C2.<sup>60,61,63,75,76</sup> Additional, both models may provide insight into a conformational shift of the C2 domain when associating to fIXa during hemostasis. Association of the fVIII C2 domain to the fIXa Gla domain is well established, occurring between residues 2228-2240 while interactions at 484-509, 558-565, 1790-1798, and 1811-1818 have been predicted for A2 and A3 domains.<sup>77</sup> Model B rotates the C2 domain inwards, decreasing the distance between the 2228-2240 region and putative residues on the A domains (Figure 37). This suggests that although model A best corroborates previous findings for generalized lipid binding, both models may be informative when binding to fIXa, lipids, or both.

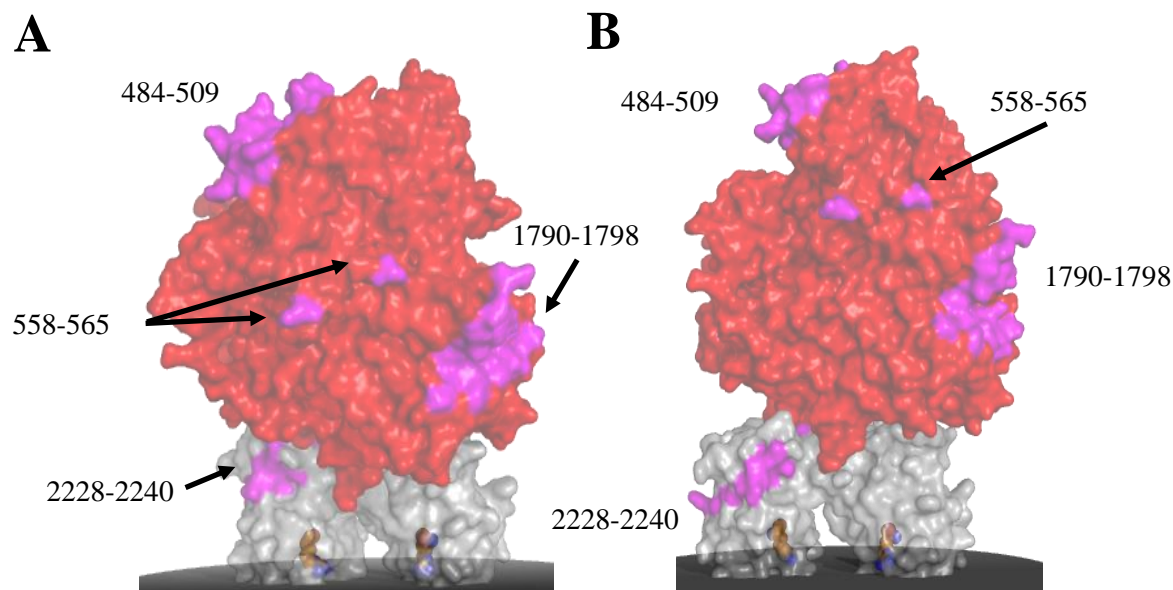


**Figure 37. fIXa epitope mapping on fVIII.** A.) Epitope mapping of the putative fIXa binding region (purple) onto model A. C.) Model B epitope mapping of fIXa epitope. The C2 domain swings the C2 interaction face towards the front of the structure.

In this study, we used mutational and structural information to improve a full fVIII lipid binding model. Mainly, the orientation of the C domains revolves around a conserved R2320/2163 motif at the classical epitope face. Specific interactions observed for the OPLS molecule occur with R2320 but observed interactions at Q2213 and N2217 appear to be non-essential as previously determined. Overall, it is hypothesized that two hydrophobic, solvent exposed feet protrude into lipid membranes, orienting the R2320/2163 motif at the lipid interface, and position other basic residues to be involved in complementary roles. Further research with fVIII and lipid nanodiscs could allow a higher resolution structure containing a full lipid surface to corroborate the electrostatic interactions that may take place.

## Works Cited

1. Versteeg, H. H., Heemskerk, J. W. M., Levi, M. & Reitsma, P. H. New Fundamentals in hemostasis. *Physiol. Rev.* 93, 327–358 (2013).
2. Periyah MH, Halim AS & Saad AZM. Mechanism action of platelets and crucial blood coagulation pathways in Hemostasis. *Int. J. Hematol. Stem Cell Res.* 11, 319–327 (2017).
3. Gordan, R., Gwathmey, J. K. & Xie, L.-H. Autonomic and endocrine control of cardiovascular function. *World J. Cardiol.* 7, 204 (2015).
4. Michael G Franz, Robson, M. C. & Steed, D. L. Current Understanding of Hemostasis. *Curr. Probl. Surg.* 38, 273–280 (2001).
5. Palta, S., Saroa, R. & Palta, A. Overview of the coagulation system. *Indian J. Anaesth.* 58, 515–523 (2014).
6. Farndale, R. W. Collagen-induced platelet activation. *Blood Cells, Mol. Dis.* 36, 162–165 (2006).
7. Peyvandi, F., Garagiola, I. & Baronciani, L. Role of von Willebrand factor in the haemostasis. *Blood Transfus.* 9, 3–8 (2011).
8. Eric G Huizinga<sup>1</sup>, R Martijn van der Plas<sup>1</sup>, Jan Kroon<sup>2</sup>, J. J. S. and P. G. Crystal structure of the A3 domain of human von Willebrand factor: implications for collagen binding. *Structure* 5, 1147–1156 (1997).
9. Zilla, P., Fasol, R. & Hammerle, A. Scanning electron microscopy of circulating platelets reveals new aspects of platelet alteration during cardiopulmonary bypass operations. *Texas Hear. Inst. J.* 14, 13–21 (1987).
10. Bevers, E. M., Comfurius, P. & Zwaal, R. F. A. Changes in membrane phospholipid distribution during platelet activation. *BBA - Biomembr.* 736, 57–66 (1983).
11. Grover, S. P. & Mackman, N. Intrinsic pathway of coagulation and thrombosis: Insights from animal models. *Arterioscler. Thromb. Vasc. Biol.* 39, 331–338 (2019).
12. HAMER, R. J., KOEDAM, J. A., BEESER-VISSER, N. H. & SIXMA, J. J. The effect of thrombin on the complex between factor VIII and von Willebrand factor. *Eur. J. Biochem.* 167, 253–259 (1987).
13. Turner, N. A. & Moake, J. L. Factor VIII is synthesized in human endothelial cells, packaged in weibel-palade bodies and secreted bound to ULVWF strings. *PLoS One* 10, 1–28 (2015).
14. Shen, B. W. *et al.* The tertiary structure and domain organization of coagulation factor VIII. *Blood* 111, 1240–1247 (2008).
15. Stoilova-Mcphie, S., Lynch, G. C., Ludtke, S. & Pettitt, B. M. Domain organization of membrane-bound factor VIII. *Biopolymers* 99, 448–459 (2013).

16. Toole, J. J., Pittman, D. D. & Orr, E. C. A large region ( $\approx$ 95 kDa) of human factor VIII is dispensable for in vitro procoagulant activity. *Proc. Natl. Acad. Sci. U. S. A.* 83, 5939–5942 (1986).
17. Eaton, D., Rodriguez, H. & Vehar, G. A. Proteolytic Processing of Human Factor VIII. Correlation of Specific Cleavages by Thrombin, Factor Xa, and Activated Protein C with Activation And Inactivation of Factor VIII Coagulant Activity. *Biochemistry* 25, 505–512 (1986).
18. Lollar, P., Hill-Eubanks, D. C. & Parker, C. G. Association of the factor VIII light chain with von Willebrand factor. *J. Biol. Chem.* 263, 10451–10455 (1988).
19. Fay, P. J. Activation of factor VIII and mechanisms of cofactor action. *Blood Rev.* 18, 1–15 (2004).
20. Ngo, J. C. K., Huang, M., Roth, D. A., Furie, B. C. & Furie, B. Crystal Structure of Human Factor VIII: Implications for the Formation of the Factor IXa-Factor VIIIa Complex. *Structure* 16, 597–606 (2008).
21. Gilbert, G. E., Novakovic, V. A., Kaufman, R. J., Miao, H. & Pipe, S. W. Conservative mutations in the C2 domains of factor VIII and factor V alter phospholipid binding and cofactor activity. *Blood* 120, 1923–1932 (2012).
22. Neufeld, E. J. *et al.* Cost analysis of plasma-derived factor VIII/von Willebrand factor versus recombinant factor VIII for treatment of previously untreated patients with severe hemophilia A in the United States. *J. Med. Econ.* 21, 762–769 (2018).
23. Srivastava, A. *et al.* Guidelines for the management of hemophilia. *Haemophilia* 19, (2013).
24. Rocino, A., Santagostino, E., Mancuso, M. E. & Mannucci, P. M. Immune tolerance induction with recombinant factor inhibitors. *Haematologica* 91, 558–561 (2006).
25. Leissinger, C. A. Prevention of bleeds in hemophilia patients with inhibitors: Emerging data and clinical direction. *Am. J. Hematol.* 77, 187–193 (2004).
26. Christopher E. Walsh<sup>1</sup>, J. Michael Soucie<sup>2</sup>, C. H. M. and the U. S. H. T. C. N. Impact of Inhibitors on Hemophilia A Mortality in the United States. *Cell* (2006).
27. Franchini, M. & Lippi, G. The use of desmopressin in acquired haemophilia A: A systematic review. *Blood Transfus.* 9, 377–382 (2011).
28. Antunes, S. V. *et al.* Randomized comparison of prophylaxis and on-demand regimens with FEIBA NF in the treatment of haemophilia A and B with inhibitors. *Haemophilia* 20, 65–72 (2014).
29. Konkle, B. A. *et al.* Randomized, prospective clinical trial of recombinant factor VIIa for secondary prophylaxis in hemophilia patients with inhibitors. *J. Thromb. Haemost.* 5, 1904–1913 (2007).

30. Waters, E. K., Sigh, J., Friedrich, U., Hilden, I. & Sørensen, B. B. Concizumab, an anti-tissue factor pathway inhibitor antibody, induces increased thrombin generation in plasma from haemophilia patients and healthy subjects measured by the thrombin generation assay. *Haemophilia* 23, 769–776 (2017).
31. Schep, S. J., Schutgens, R. E. G., Fischer, K. & Boes, M. L. Review of immune tolerance induction in hemophilia A. *Blood Rev.* 32, 326–338 (2018).
32. Doering, C. B., Healey, J. F., Parker, E. T., Barrow, R. T. & Lollar, P. High level expression of recombinant porcine coagulation factor VIII. *J. Biol. Chem.* 277, 38345–38349 (2002).
33. Smith, I. W. *et al.* The 3.2 Å structure of a bioengineered variant of blood coagulation factor VIII indicates two conformations of the C2 domain. *J. Thromb. Haemost.* 18, 57–69 (2020).
34. Doering, C. B., Healey, J. F., Parker, E. T., Barrow, R. T. & Lollar, P. Identification of Porcine Coagulation Factor VIII Domains Responsible for High Level Expression via Enhanced Secretion. *J. Biol. Chem.* 279, 6546–6552 (2004).
35. Schroeder, H. W. J. & Cavacini, L. Structure and Function of Immunoglobulins (author manuscript). *J. Allergy Clin. Immunol.* 125, S41–S52 (2010).
36. Arai, M., Scandella, D. & Hoyer, L. W. Molecular basis of factor VIII inhibition by human antibodies. Antibodies that bind to the factor VIII light chain prevent the interaction of factor VIII with phospholipid. *J. Clin. Invest.* 83, 1978–1984 (1989).
37. Lollar, P. *et al.* Inhibition of human factor VIIIa by anti-A2 subunit antibodies. *J. Clin. Invest.* 93, 2497–2504 (1994).
38. Meeks, S. L., Healey, J. F., Parker, E. T., Barrow, R. T. & Lollar, P. Nonclassical anti-C2 domain antibodies are present in patients with factor VIII inhibitors. *Blood* 112, 1151–1153 (2008).
39. Hartholt, R. B. *et al.* To serve and protect: The modulatory role of von Willebrand factor on factor VIII immunogenicity. *Blood Rev.* 31, 339–347 (2017).
40. Meeks, S. L., Healey, J. F., Parker, E. T., Barrow, R. T. & Lollar, P. Antihuman factor VIII C2 domain antibodies in hemophilia A mice recognize a functionally complex continuous spectrum of epitopes dominated by inhibitors of factor VIII activation. *Blood* 110, 4234–4242 (2007).
41. Kahle, J. *et al.* Frequency and epitope specificity of anti-factor VIII C1 domain antibodies in acquired and congenital hemophilia A. *Blood* 130, 808–816 (2017).
42. Jacquemin, M. *et al.* A human antibody directed to the factor VIII C1 domain inhibits factor VIII cofactor activity and binding to von Willebrand factor. *Blood* 95, 156–163 (1999).
43. Batsuli, G. *et al.* Anti-C1 domain antibodies that accelerate factor VIII clearance

- contribute to antibody pathogenicity in a murine hemophilia A model. *J. Thromb. Haemost.* 16, 1779–1788 (2018).
44. Batsuli, G. *et al.* High-affinity, noninhibitory pathogenic C1 domain antibodies are present in patients with hemophilia A and inhibitors. *Blood* 128, 2055–2067 (2016).
  45. Pratt, K. P. *et al.* Structure of the C2 domain of human factor VIII at 1.5 Å resolution. *Nature* 402, 439–442 (1999).
  46. Stoilova-McPhie, S., Villoutreix, B. O., Mertens, K., Kemball-Cook, G. & Holzenburg, A. 3-Dimensional structure of membrane-bound coagulation factor VIII: Modeling of the factor VIII heterodimer within a 3-dimensional density map derived by electron crystallography. *Blood* 99, 1215–1223 (2002).
  47. Meems, H., Meijer, A. B., Cullinan, D. B., Mertens, K. & Gilbert, G. E. Factor VIII C1 domain residues Lys 2092 and Phe 2093 contribute to membrane binding and cofactor activity. *Blood* 114, 3938–3946 (2009).
  48. Walter, J. D. *et al.* Thrombosis and hemostasis: Structure of the factor VIII C2 domain in a ternary complex with 2 inhibitor antibodies reveals classical and nonclassical epitopes. *Blood* 122, 4270–4278 (2013).
  49. Meeks, S. L., Healey, J. F., Parker, E. T., Barrow, R. T. & Lollar, P. Non-classical anti-factor VIII C2 domain antibodies are pathogenic in a murine in vivo bleeding model. *J. Thromb. Haemost.* 7, 658–664 (2009).
  50. Brison, C. M., Mullen, S. M., Wuerth, M. E., Podolsky, K. & Spiegel, P. C. The 1.7 Å X-Ray Crystal Structure of the Porcine Factor VIII C2 Domain and Binding Analysis to Anti-Human C2 Domain Antibodies and Phospholipid Surfaces. 1–17 (2015) doi:10.1371/journal.pone.0122447.
  51. Giles, A. R., Mann, K. G. & Nesheim, M. E. A combination of factor Xa and phosphatidylcholine-phosphatidylserine vesicles bypasses factor VIII in vivo. *Br. J. Haematol.* 69, 491–497 (1988).
  52. Gilbert, G. E., Furie, B. C. & Furie, B. Binding of human factor VIII to phospholipid vesicles. *J. Biol. Chem.* 265, 815–822 (1990).
  53. Gilbert, G. E. & Drinkwater, D. Specific Membrane Binding of Factor VIII Is Mediated by O-Phospho-L-serine, a Moiety of Phosphatidylserine. *Biochemistry* 32, 9577–9585 (1993).
  54. Gilbert, G. E., Kaufman, R. J., Arena, A. A., Miao, H. & Pipe, S. W. Four hydrophobic amino acids of the factor VIII C2 domain are constituents of both the membrane-binding and von Willebrand factor-binding motifs. *J. Biol. Chem.* 277, 6374–6381 (2002).
  55. Foster, B. P. A., Fulcher, C. A., Houghten, R. A. & Zimmermant, T. S. Synthetic Factor VIII Peptides With Amino Acid Sequences Contained Within the C2 Domain of Factor VIII Inhibit Factor VIII Binding to Phosphatidylserine. (1990).

56. Schatz, S. M. *et al.* Mutation of the surface-exposed amino acid Trp2313 to Ala in the FVIII C2 domain results in defective secretion of the otherwise functional protein. *Br. J. Haematol.* 125, 629–637 (2004).
57. Jesper J. Madsen, Y. Zenmei Ohkubo, Günther H. Peters, Johan H. Faber, E. & Tajkhorshid, and O. H. O. Membrane interaction of the factor VIIIa discoidin domains in atomistic detail. *Biochemistry* 54, 6123–6131 (2015).
58. Liu, M. L. *et al.* Hemophilic factor VIII C1- and C2-domain missense mutations and their modeling to the 1.5-angstrom human C2-domain crystal structure. *Blood* 96, 979–987 (2000).
59. Grushin, K., Miller, J., Dalm, D. & Stoilova-McPhie, S. Factor VIII organisation on nanodiscs with different lipid composition. *Thromb. Haemost.* 113, 741–749 (2015).
60. Liu, Z. *et al.* Trp2313-his2315 of factor VIII C2 domain is involved in membrane binding: Structure of a complex between the C2 domain and an inhibitor of membrane binding. *J. Biol. Chem.* 285, 8824–8829 (2010).
61. Spiegel, P. C., Murphy, P. & Stoddard, B. L. Surface-exposed hemophilic mutations across the factor VIII C2 domain have variable effects on stability and binding activities. *J. Biol. Chem.* (2004) doi:10.1074/jbc.M409389200.
62. Spiegel, P. C., Jacquemin, M., Saint-Remy, J. M. R., Stoddard, B. L. & Pratt, K. P. Structure of a factor VIII C2 domain-immunoglobulin G4κ Fab complex: Identification of an inhibitory antibody epitope on the surface of factor VIII. *Blood* 98, 13–19 (2001).
63. Walter, J. D. *et al.* Structure of the factor VIII C2 domain in a ternary complex with 2 inhibitor antibodies reveals classical and nonclassical epitopes. *Blood* 122, 4270–4278 (2013).
64. Hsu, T. C., Pratt, K. P. & Thompson, A. R. The factor VIII C1 domain contributes to platelet binding. *Blood* 111, 200–208 (2008).
65. Lobstein, J. *et al.* SHuffle, a novel Escherichia coli protein expression strain capable of correctly folding disulfide bonded proteins in its cytoplasm. *Microb. Cell Fact.* 11, 1 (2012).
66. Novakovic, V. A. *et al.* Membrane-binding properties of the Factor VIII C2 domain. *Biochem. J.* 435, 187–196 (2011).
67. Morales, E. S., Parcerisa, I. L. & Ceccarelli, E. A. A novel method for removing contaminant Hsp70 molecular chaperones from recombinant proteins. *Protein Sci.* 28, 800–807 (2019).
68. Keri Csencsits-Smith<sup>1</sup>, Krill Grushin<sup>2</sup>, and S. S.-M. Binding of Factor VIII to Lipid Nanodiscs Increases its Clotting Function in a Mouse Model of Hemophilia A. 1, 1–19 (2018).
69. Dalm, D. *et al.* Dimeric organization of blood coagulation factor VIII bound to lipid

- nanotubes. *Sci. Rep.* 5, 1–14 (2015).
70. Gish, J. S. *et al.* Structure of Blood Coagulation Factor VIII in Complex with an Anti-C1 Domain Pathogenic Antibody Inhibitor. *Blood* 137, 2981–2986 (2021).
  71. Ronayne, E. K. *et al.* Structure of Blood Coagulation Factor VIII in Complex With an Anti-C2 Domain Non-Classical, Pathogenic Antibody Inhibitor. *Front. Immunol.* 12, 1–9 (2021).
  72. Spiegel, P. C. & Stoddard, B. L. Optimization of factor VIII replacement therapy: Can structural studies help in evading antibody inhibitors? *Br. J. Haematol.* 119, 310–322 (2002).
  73. Lü, J., Pipe, S. W., Miao, H., Jacquemin, M. & Gilbert, G. E. A membrane-interactive surface on the factor VIII C1 domain cooperates with the C2 domain for cofactor function. *Blood* 117, 3181–3189 (2011).
  74. Pellequer, J. L. *et al.* Functional mapping of factor VIII C2 domain. *Thromb. Haemost.* 106, 121–131 (2011).
  75. Wakabayashi, H. & Fay, P. J. Molecular orientation of Factor VIIIa on the phospholipid membrane surface determined by fluorescence resonance energy transfer. *Biochem. J.* 452, 293–301 (2013).
  76. Lü, J., Pipe, S. W., Miao, H., Jacquemin, M. & Gilbert, G. E. A membrane-interactive surface on the factor VIII C1 domain cooperates with the C2 domain for cofactor function. *Blood* 117, 3181–3189 (2011).
  77. Soeda, T. *et al.* The Factor VIIIa C2 domain (residues 2228-2240) interacts with the factor IXa Gla domain in the factor Xase complex. *J. Biol. Chem.* 284, 3379–3388 (2009).
  78. Parker, E. T., Doering, C. B. & Lollar, P. A1 subunit-mediated regulation of thrombin-activated factor VIII A2 subunit dissociation. *J. Biol. Chem.* 281, 13922–13930 (2006).
  79. Doering, C. B. *et al.* Directed engineering of a high-expression chimeric transgene as a strategy for gene therapy of hemophilia A. *Mol. Ther.* 17, 1145–1154 (2009).
  80. Brown, H. C. *et al.* Bioengineered coagulation factor VIII enables long-term correction of murine hemophilia A following liver-directed adeno-associated viral vector delivery. *Mol. Ther. - Methods Clin. Dev.* 1, 14036 (2014).
  81. Leinøe, E. *et al.* Application of whole-exome sequencing to direct the specific functional testing and diagnosis of rare inherited bleeding disorders in patients from the Öresund Region, Scandinavia. *Br. J. Haematol.* 179, 308–322 (2017).
  82. Lhermusier, T., Chap, H. & Payrastre, B. Platelet membrane phospholipid asymmetry: From the characterization of a scramblase activity to the identification of an essential protein mutated in Scott syndrome. *J. Thromb. Haemost.* 9, 1883–1891 (2011).
  83. Paul, D. & Kulkarni, S. N. Trauma and Coagulopathy: Findings of the Last Decade. *Eur.*

*J. Pharm. Med. Res.* 3, 171–176 (2016).

## Appendix

### Factor VIII C1C2\_pET-32a(+):

MSDKIIHLTDDSFDTDLKADGAILVDFWAIEWCGPCKMIAPILDEIADEYQGKLTVAKLNIDQNPGTAPKYGIRGIPTLLLFKNGEVAAT  
KVGALSKGQLKEFLDANLAGSGSGHM~~MHHHHHH~~SSGLVPRGSGMKETAAAKFERQHMDSPDLGTDDDDKAMADIGSENLYFQSNNSNK  
CQTPLGMASGHIRDFQITASGQYQGWAPKLARLHYSGSINAWSTKEPFSWIKVDLLAPMIIHGIKTQGARQKFSSLYISQFIIMYSLDGKK  
WQTYRGNSTGTLMVFFGNVDSSGIKHNIFNPPIAR YIRLHPHYSIRSTLRMELMGCDLNCSMPLGMESKAISDAQITASSYFTNMFAT  
WSPSKARLHLQGRSNAWRPQVNNPKEWLQVDFOKTMTKVTGVTQGVKSLLTSMYVKEFLISSQDGHQWTLFFQNGKVKVFQGNQD  
SFTPVVNSLDPPLLTRYLRIHPQSVVHQIALRMEVLGCEAQDLY

### Factor VIII C1C2\_R2163S\_pET-32a(+):

MSDKIIHLTDDSFDTDLKADGAILVDFWAIEWCGPCKMIAPILDEIADEYQGKLTVAKLNIDQNPGTAPKYGIRGIPTLLLFKNGEVAAT  
KVGALSKGQLKEFLDANLAGSGSGHM~~HHHHHH~~SSGLVPRGSGMKETAAAKFERQHMDSPDLGTDDDDKAMADIGSENLYFQSNNSNK  
CQTPLGMASGHIRDFQITASGQYQGWAPKLARLHYSGSINAWSTKEPFSWIKVDLLAPMIIHGIKTQGARQKFSSLYISQFIIMYSLDGKK  
WQTYRGNSTGTLMVFFGNVDSSGIKHNIFNPPIAR YIRLHPHYSIRSTL~~S~~MELMGCDLNCSMPLGMESKAISDAQITASSYFTNMFAT  
WSPSKARLHLQGRSNAWRPQVNNPKEWLQVDFOKTMTKVTGVTQGVKSLLTSMYVKEFLISSQDGHQWTLFFQNGKVKVFQGNQD  
SFTPVVNSLDPPLLTRYLRIHPQSVVHQIALRMEVLGCEAQDLY

### Factor VIII C1C2\_R2320S\_pET-32a(+):

MSDKIIHLTDDSFDTDLKADGAILVDFWAIEWCGPCKMIAPILDEIADEYQGKLTVAKLNIDQNPGTAPKYGIRGIPTLLLFKNGEVAAT  
KVGALSKGQLKEFLDANLAGSGSGHM~~HHHHHH~~SSGLVPRGSGMKETAAAKFERQHMDSPDLGTDDDDKAMADIGSENLYFQSNNSNK  
CQTPLGMASGHIRDFQITASGQYQGWAPKLARLHYSGSINAWSTKEPFSWIKVDLLAPMIIHGIKTQGARQKFSSLYISQFIIMYSLDGKK  
WQTYRGNSTGTLMVFFGNVDSSGIKHNIFNPPIAR YIRLHPHYSIRSTLRMELMGCDLNCSMPLGMESKAISDAQITASSYFTNMFAT  
WSPSKARLHLQGRSNAWRPQVNNPKEWLQVDFOKTMTKVTGVTQGVKSLLTSMYVKEFLISSQDGHQWTLFFQNGKVKVFQGNQD  
SFTPVVNSLDPPLLTRYLRIHPQSVVHQIAL~~S~~MEVLGCEAQDLY

### Factor VIII C1C2\_R2163S\_R2320S\_pET-32a(+):

MSDKIIHLTDDSFDTDLKADGAILVDFWAIEWCGPCKMIAPILDEIADEYQGKLTVAKLNIDQNPGTAPKYGIRGIPTLLLFKNGEVAAT  
KVGALSKGQLKEFLDANLAGSGSGHM~~HHHHHH~~SSGLVPRGSGMKETAAAKFERQHMDSPDLGTDDDDKAMADIGSENLYFQSNNSNK  
CQTPLGMASGHIRDFQITASGQYQGWAPKLARLHYSGSINAWSTKEPFSWIKVDLLAPMIIHGIKTQGARQKFSSLYISQFIIMYSLDGKK  
WQTYRGNSTGTLMVFFGNVDSSGIKHNIFNPPIAR YIRLHPHYSIRSTL~~S~~MELMGCDLNCSMPLGMESKAISDAQITASSYFTNMFAT  
WSPSKARLHLQGRSNAWRPQVNNPKEWLQVDFOKTMTKVTGVTQGVKSLLTSMYVKEFLISSQDGHQWTLFFQNGKVKVFQGNQD  
SFTPVVNSLDPPLLTRYLRIHPQSVVHQIAL~~S~~MEVLGCEAQDLY

### Factor VIII C1\_pET-32a(+):

MSDKIIHLTDDSFDTDLKADGAILVDFWAIEWCGPCKMIAPILDEIADEYQGKLTVAKLNIDQNPGTAPKYGIRGIPTLLLFKNGEVAAT  
KVGALSKGQLKEFLDANLAGSGSGHM~~HHHHHH~~SSGLVPRGSGMKETAAAKFERQHMDSPDLGTDDDDKAMADIGSENLYFQSNNSNK  
CQTPLGMASGHIRDFQITASGQYQGWAPKLARLHYSGSINAWSTKEPFSWIKVDLLAPMIIHGIKTQGARQKFSSLYISQFIIMYSLDGKK  
WQTYRGNSTGTLMVFFGNVDSSGIKHNIFNPPIAR YIRLHPHYSIRSTLRMELMGCDLNS

**Appendix Figure 1. Complete Construct Sequences for factor VIII C1 and C1C2.** Sequences were ordered from Genscript, verified, and translated to amino acid codes using Expsy through ProtParam. Factor VIII C domain sequences are highlighted in green, thioredoxin in yellow, 6x-His tag in cyan, and mutations in red.